ISSN 1949-8470 (online)

World Journal of Radiology

World J Radiol 2010 January 28; 2(1): 1-54

A peer-reviewed, online, open-access journal of Radiology

WJR World Journal of Radiology

A peer-reviewed, online, open-access journal of Radiology

Editorial Board

2009-2013

The *World Journal of Radiology* Editorial Board consists of 304 members, representing a team of worldwide experts in radiology. They are from 38 countries, including Australia (3), Austria (4), Belgium (4), Brazil (2), Canada (9), Chile (1), China (23), Denmark (1), Egypt (4), Estonia (1), Finland (1), France (6), Germany (17), Greece (8), Hungary (1), India (9), Iran (5), Ireland (1), Israel (4), Italy (28), Japan (14), Lebanon (1), Libya (1), Malaysia (2), Mexico (1), Netherlands (4), New Zealand (1), Norway (1), Saudi Arabia (3), Serbia (1), Singapore (2), Slovakia (1), South Korea (16), Spain (8), Switzerland (5), Turkey (20), United Kingdom (15), and United States (76).

Youlia M Kirova, *Paris*
Géraldine Le Duc, *Grenoble Cedex*
Laurent Pierot, *Reims*
Frank Pilleul, *Lyon*
Pascal Pommier, *Lyon*

Germany

Ambros J Beer, *München*
Thomas Deserno, *Aachen*
Frederik L Giesel, *Heidelberg*
Ulf Jensen, *Kiel*
Markus Sebastian Juchems, *Ulm*
Kai U Juergens, *Bremen*
Melanie Kettering, *Jena*
Jennifer Linn, *Munich*
Christian Lohrmann, *Freiburg*
David Maintz, *Münster*
Henrik J Michaely, *Mannheim*
Oliver Micke, *Bielefeld*
Thoralf Niendorf, *Berlin-Buch*
Silvia Obenauer, *Duesseldorf*
Steffen Rickes, *Halberstadt*
Lars V Baron von Engelhardt, *Bochum*
Goetz H Welsch, *Erlangen*

Greece

Panagiotis Antoniou, *Alexandroupolis*
George C Kagadis, *Rion*
Dimitris Karacostas, *Thessaloniki*
George Panayiotakis, *Patras*
Alexander D Rapidis, *Athens*
Ioannis Tsalafoutas, *Athens*
Virginia Tsapaki, *Anixi*
Ioannis Valais, *Athens*

Hungary

Peter Laszlo Lakatos, *Budapest*

India

Anil Kumar Anand, *New Delhi*
Surendra Babu, *Tamilnadu*
Sandip Basu, *Bombay*
Kundan Singh Chufal, *New Delhi*
Shivanand Gamanagatti, *New Delhi*
Vimoj J Nair, *Haryana*
R Prabhakar, *New Delhi*
Sanjeeb Kumar Sahoo, *Orissa*

Iran

Vahid Reza Dabbagh Kakhki, *Mashhad*
Mehran Karimi, *Shiraz*
Farideh Nejat, *Tehran*
Alireza Shirazi, *Tehran*
Hadi Rokni Yazdi, *Tehran*

Ireland

Joseph Simon Butler, *Dublin*

Israel

Amit Gefen, *Tel Aviv*
Eyal Sheiner, *Be'er-Sheva*
Jacob Sosna, *Jerusalem*
Simcha Yagel, *Jerusalem*

Italy

Mohssen Ansarin, *Milan*
Stefano Arcangeli, *Rome*
Tommaso Bartalena, *Imola*
Filippo Cademartiri, *Parma*
Sergio Casciaro, *Lecce*
Laura Crocetti, *Pisa*
Alberto Cuocolo, *Napoli*
Mirko D'Onofrio, *Verona*
Massimo Filippi, *Milan*
Claudio Fiorino, *Milano*
Alessandro Franchello, *Turin*
Roberto Grassi, *Naples*
Stefano Guerriero, *Cagliari*
Francesco Lassandro, *Napoli*
Nicola Limbucci, *L'Aquila*
Raffaele Lodi, *Bologna*
Francesca Maccioni, *Rome*
Laura Martincich, *Candiolo*
Mario Mascalchi, *Florence*
Roberto Miraglia, *Palermo*
Eugenio Picano, *Pisa*
Antonio Pinto, *Naples*
Stefania Romano, *Naples*
Luca Saba, *Cagliari*
Sergio Sartori, *Ferrara*
Mariano Scaglione, *Castel Volturno*
Lidia Strigari, *Rome*
Vincenzo Valentini, *Rome*

Japan

Shigeru Ehara, *Morioka*
Nobuyuki Hamada, *Chiba*
Takao Hiraki, *Okayama*
Akio Hiwatashi, *Fukuoka*
Masahiro Jinzaki, *Tokyo*
Hiroshi Matsuda, *Saitama*
Yasunori Minami, *Osaka*
Jun-Ichi Nishizawa, *Tokyo*
Tetsu Niwa, *Yokohama*
Kazushi Numata, *Kanagawa*
Kazuhiko Ogawa, *Okinawa*
Hitoshi Shibuya, *Tokyo*
Akira Uchino, *Saitama*
Haiquan Yang, *Kanagawa*

Lebanon

Aghiad Al-Kutoubi, *Beirut*

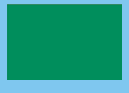

Libya

Anuj Mishra, *Tripoli*

Malaysia

R Logeswaran, *Cyberjaya*
Kwan-Hoong Ng, *Kuala Lumpur*

Mexico

Heriberto Medina-Franco, *Mexico City*

Netherlands

Jurgen J Fütterer, *Nijmegen*
Raffaella Rossin, *Eindhoven*
Paul E Sijens, *Groningen*
Willem Jan van Rooij, *Tilburg*

New Zealand

W Howell Round, *Hamilton*

Norway

Arne Sigmund Borthne, *Lørenskog*

Saudi Arabia

Mohammed Al-Omran, *Riyadh*
Ragab Hani Donkol, *Abha*
Volker Rudat, *Al Khobar*

Serbia

Djordjije Saranovic, *Belgrade*

Singapore

Uei Pua, *Singapore*
Lim CC Tchoyoson, *Singapore*

Slovakia

František Dubecký, *Bratislava*

South Korea

Bo-Young Choe, *Seoul*
Joon Koo Han, *Seoul*
Seung Jae Huh, *Seoul*
Chan Kyo Kim, *Seoul*
Myeong-Jin Kim, *Seoul*
Seung Hyup Kim, *Seoul*
Kyoung Ho Lee, *Gyeonggi-do*
Won-Jin Moon, *Seoul*
Wazir Muhammad, *Daegu*
Jai Soung Park, *Bucheon*
Noh Hyuck Park, *Kyunggi*
Sang-Hyun Park, *Daejeon*
Joon Beom Seo, *Seoul*
Ji-Hoon Shin, *Seoul*
Jin-Suck Suh, *Seoul*
Hong-Gyun Wu, *Seoul*

Spain

Eduardo J Aguilar, *Valencia*

Miguel Alcaraz, *Murcia*
Juan Luis Alcazar, *Pamplona*
Gorka Bastarrika, *Pamplona*
Rafael Martínez-Monge, *Pamplona*
Alberto Muñoz, *Madrid*
Joan C Vilanova, *Girona*

Switzerland

Nicolau Beckmann, *Basel*
Silke Grabherr, *Lausanne*
Karl-Olof Lövblad, *Geneva*
Tilo Niemann, *Basel*
Martin A Walter, *Basel*

Turkey

Olus Api, *Istanbul*
Kubilay Aydin, *İstanbul*
Işıl Bilgen, *Izmir*
Zulkif Bozgeyik, *Elazig*
Barbaros E Çil, *Ankara*
Gulgun Engin, *Istanbul*
M Fatih Evcimik, *Malatya*
Ahmet Kaan Gündüz, *Ankara*
Tayfun Hakan, *Istanbul*
Adnan Kabaalioglu, *Antalya*
Fehmi Kaçmaz, *Ankara*
Musturay Karcaaltincaba, *Ankara*
Osman Kizilkilic, *Istanbul*
Zafer Koc, *Adana*
Cem Onal, *Adana*
Yahya Paksoy, *Konya*
Bunyamin Sahin, *Samsun*
Ercument Unlu, *Edirne*
Ahmet Tuncay Turgut, *Ankara*
Ender Uysal, *Istanbul*

United Kingdom

K Faulkner, *Wallsend*
Peter Gaines, *Sheffield*
Balaji Ganeshan, *Brighton*
Nagy Habib, *London*
Alan Jackson, *Manchester*
Pradesh Kumar, *Portsmouth*
Tarik F Massoud, *Cambridge*
Igor Meglinski, *Bedfordshire*
Ian Negus, *Bristol*
Georgios A Plataniotis, *Aberdeen*
N J Raine-Fenning, *Nottingham*
Manuchehr Soleimani, *Bath*
MY Tseng, *Nottingham*
Edwin JR van Beek, *Edinburgh*
Feng Wu, *Oxford*

United States

Athanassios Argiris, *Pittsburgh*
Stephen R Baker, *Newark*
Lia Bartella, *New York*
Charles Bellows, *New Orleans*
Walter L Biffl, *Denver*
Homer S Black, *Houston*
Wessam Bou-Assaly, *Ann Arbor*
Owen Carmichael, *Davis*
Shelton D Caruthers, *St Louis*
Yuhchyau Chen, *Rochester*
Melvin E Clouse, *Boston*
Ezra Eddy Wyssam Cohen, *Chicago*
Aaron Cohen-Gadol, *Indianapolis*
Patrick M Colletti, *Los Angeles*
Kassa Darge, *Philadelphia*
Abhijit P Datir, *Miami*
Delia C DeBuc, *Miami*
Russell L Deter, *Houston*
Adam P Dicker, *Phil*
Khaled M Elsayes, *Ann Arbor*
Steven Feigenberg, *Baltimore*
Christopher G Filippi, *Burlington*
Victor Frenkel, *Bethesda*
Thomas J George Jr, *Gainesville*
Patrick K Ha, *Baltimore*
Robert I Haddad, *Boston*
Walter A Hall, *Syracuse*
Mary S Hammes, *Chicago*
John Hart Jr, *Dallas*
Randall T Higashida, *San Francisco*
Juebin Huang, *Jackson*
Andrei Iagaru, *Stanford*
Craig Johnson, *Milwaukee*
Ella F Jones, *San Francisco*
Csaba Juhasz, *Detroit*
Mannudeep K Kalra, *Boston*
Riyad Karmy-Jones, *Vancouver*
Daniel J Kelley, *Madison*
Amir Khan, *Longview*
Vikas Kundra, *Houston*
Kennith F Layton, *Dallas*
Rui Liao, *Princeton*
CM Charlie Ma, *Philadelphia*
Nina A Mayr, *Columbus*
Thomas J Meade, *Evanston*
Steven R Messé, *Philadelphia*
Feroze B Mohamed, *Philadelphia*
Koenraad J Mortele, *Boston*
Mohan Natarajan, *San Antonio*
John L Nosher, *New Brunswick*
Chong-Xian Pan, *Sacramento*
Dipanjan Pan, *St Louis*
Martin R Prince, *New York*
Reza Rahbar, *Boston*
Carlos S Restrepo, *San Antonio*
Veronica Rooks, *Honolulu*
Maythem Saeed, *San Francisco*
Edgar A Samaniego, *Palo Alto*
Jason P Sheehan, *Charlottesville*
William P Sheehan, *Willmar*
Charles Jeffrey Smith, *Columbia*
Dan Stoianovici, *Baltimore*
Dian Wang, *Milwaukee*
Jian Z Wang, *Columbus*
Liang Wang, *New York*
Shougang Wang, *Santa Clara*
Wenbao Wang, *New York*
Aaron H Wolfson, *Miami*
Ying Xiao, *Philadelphia*
Juan Xu, *Pittsburgh*
Benjamin M Yeh, *San Francisco*
Terry T Yoshizumi, *Durham*
Jinxing Yu, *Richmond*
Jianhui Zhong, *Rochester*

WJR World Journal of Radiology

Contents

Monthly Volume 2 Number 1 January 28, 2010

World Journal of Radiology
Volume 2 Number 1 January 28, 2010

Contents

NAME OF JOURNAL
World Journal of Radiology

LAUNCH DATE
December 31, 2009

SPONSOR
Beijing Baishideng BioMed Scientific Co., Ltd.,
Room 903, Building D, Ocean International Center,
No. 62 Dongsihuan Zhonglu, Chaoyang District,
Beijing 100025, China
Telephone: 0086-10-8538-1892
Fax: 0086-10-8538-1893
E-mail: baishideng@wjgnet.com
http://www.wjgnet.com

EDITING
Editorial Board of *World Journal of Radiology*,
Room 903, Building D, Ocean International Center,
No. 62 Dongsihuan Zhonglu, Chaoyang District,
Beijing 100025, China
Telephone: 0086-10-5908-0036
Fax: 0086-10-8538-1893
E-mail: wjr@wjgnet.com
http://www.wjgnet.com

PUBLISHING
Beijing Baishideng BioMed Scientific Co., Ltd.,
Room 903, Building D, Ocean International Center,
No. 62 Dongsihuan Zhonglu, Chaoyang District,
Beijing 100025, China
Telephone: 0086-10-8538-1892
Fax: 0086-10-8538-1893
E-mail: baishideng@wjgnet.com
http://www.wjgnet.com

SUBSCRIPTION
Beijing Baishideng BioMed Scientific Co., Ltd.,
Room 903, Building D, Ocean International Center,
No. 62 Dongsihuan Zhonglu, Chaoyang District,
Beijing 100025, China
Telephone: 0086-10-8538-1892
Fax: 0086-10-8538-1893
E-mail: baishideng@wjgnet.com
http://www.wjgnet.com

ONLINE SUBSCRIPTION
One-Year Price 216.00 USD

PUBLICATION DATE
January 28, 2010

CSSN
ISSN 1949-8470 (online)

EDITORIAL OFFICE
Na Ma, Director
World Journal of Radiology
Room 903, Building D, Ocean International Center,
No. 62 Dongsihuan Zhonglu, Chaoyang District,
Beijing 100025, China
Telephone: 0086-10-5908-0036
Fax: 0086-10-8538-1893
E-mail: wjr@wjgnet.com
http://www.wjgnet.com

INSTRUCTIONS TO AUTHORS
Full instructions are available online at http://www.wjgnet.com/1949-8470/index.htm. If you do not have web access please contact the editorial office.

ONLINE SUBMISSION
http://www.wjgnet.com/1949-8470office

World Journal of Radiology

Online Submissions: http://www.wjgnet.com/1949-8470office
wjr@wjgnet.com
doi:10.4329/wjr.v2.i1.1

World J Radiol 2010 January 28; 2(1): 1-14
ISSN 1949-8470 (online)

EDITORIAL

Reperfusion injury components and manifestations determined by cardiovascular MR and MDCT imaging

Maythem Saeed, Steve Hetts, Mark Wilson

Maythem Saeed, Steve Hetts, Mark Wilson, Department of Radiology and Biomedical Imaging, University of California San Francisco, 185 Berry Street, Suite 350, San Francisco, CA 94107-5705, United States
Author contributions: Saeed M contributed to conception and design of study, as well as acquisition of data, and analysis and interpretation of data, manuscript writing, including drafting the article, and revising it critically for important intellectual content; Hetts S and Wilson M reviewed it critically for important intellectual content.
Correspondence to: Maythem Saeed, Professor, Department of Radiology and Biomedical Imaging, University of California San Francisco, 185 Berry Street, Suite 350, San Francisco, CA 94107-5705, United States. maythem.saeed@radiology.ucsf.edu
Telephone: +1-415-5146221 Fax: +1-415-3539423
Received: November 26, 2009 Revised: January 6, 2010
Accepted: January 13, 2010
Published online: January 28, 2010

Abstract

Advances in magnetic resonance (MR) and computed tomography (CT) imaging have improved visualization of acute and scar infarct. Over the past decade, there have been and continues to be many significant technical advancements in cardiac MR and multi-detector computed tomography (MDCT) technologies. The strength of MR imaging relies on a variety of pulse sequences and the ability to noninvasively provide information on myocardial structure, function and perfusion in a single imaging session. The recent technical developments may also allow CT technologies to rise to the forefront for evaluating clinical ischemic heart disease. Components of reperfusion injury including myocardial edema, hemorrhage, calcium deposition and microvascular obstruction (MO) have been demonstrated using MR and CT technologies. MR imaging can be used serially and noninvasively in assessing acute and chronic consequences of reperfusion injury because there is no radiation exposure or administration of radioactive materials. MDCT is better suited for assessing coronary artery stenosis and as an alternative technique for assessing viability in patients where MR imaging is contraindicated. Changes in left ventricular (LV) volumes and function measured on cine MR are directly related to infarct size measured on delayed contrast enhanced images. Recent MR studies found that transmural infarct, MO and peri-infarct zone are excellent predictors of poor post-infarct recovery and mortality. Recent MR studies provided ample evidence that growth factor genes and stem cells delivered locally have beneficial effects on myocardial viability, perfusion and function. The significance of deposited calcium in acute infarct detected on MDCT requires further studies. Cardiac MR and MDCT imaging have the potential for assessing reperfusion injury components and manifestations.

Key words: Calcium deposits in myocardium; Magnetic resonance imaging; Multi-detector computed tomography; Myocardial micro and macro-infarct; Reperfusion injury; Vascular injury

Peer reviewers: Yahya Paksoy, MD, Professor, Department of Radiology, Selcuk University Meram Chool of Medicine, 42085 Konya, Turkey; Patrick M Colletti, MD, Professor of Radiology and Medicine, Director Nuclear Medicine Fellowship, USC Keck School of Medicine, Professor of Biokinesiology, Professor of Pharmacology and Pharmaceutical Sciences, Chief of MRI, LAC+USC Imaging Science Center, University of Southern California, 1200 N State Street Room 3566, Los Angeles, CA 90033, United States

Saeed M, Hetts S, Wilson M. Reperfusion injury components and manifestations determined by cardiovascular MR and MDCT imaging. *World J Radiol* 2010; 2(1): 1-14 Available from: URL: http://www.wjgnet.com/1949-8470/full/v2/i1/1.htm DOI: http://dx.doi.org/10.4329/wjr.v2.i1.1

INTRODUCTION

Ischemic heart disease remains the leading cause of

death worldwide and accounts for the majority (almost 70%) of congestive heart failure cases. Reperfusion therapy, which includes thrombolytic therapy, angioplasty and stent placement, is the greatest advancement in the treatment of acute myocardial infarction. On the other hand, reperfusion therapy induces myocardial injury. Recent studies have shown that interstitial edema, infarct dimensions (size, circumferential extent and transmurality), peri-infarct zone, microvascular obstruction (MO), interstitial hemorrhage and calcium deposition are major components of reperfusion injury and these components predict the short and long term survival.

The common denominator magnetic resonance (MR) sequences used in clinical viability protocols involves evaluating left ventricular (LV) function on cine techniques and myocardial infarct size on delayed contrast enhancement (DE) imaging. Other pulse sequences, such as first pass perfusion, tagged, velocity encoded cine, T2-weighted turbo spin echo and T2*-susceptibility MR imaging have also been used for assessment of the consequences of post-infarct reperfusion. MR imaging has also been useful in defining the etiology of non-ischemic diseases, such as amyloidosis[1], viral myocarditis[2] and hypertrophic cardiomyopathy[3]. DE-MR imaging also eliminates the exposure of patients to ionizing radiation used in computed tomography (CT) imaging[4].

On the other hand, the clinical indications for implantable cardiac defibrillators and biventricular pacing therapy continue to expand, and the development and validation of alternative imaging modalities with similar abilities for assessing LV function, perfusion and viability, are needed to accommodate such a growing population of patients who are unfavorable candidates for MR imaging. The application of multi-detector computed tomography (MDCT) does not suffer from relative contraindications (such as implanted active permanent pacemakers or defibrillators (or retained components of either, due to their potential to become dysfunctional) and/or unwanted conductors (e.g. induction of ectopy or heating capable of burning) within the rapidly changing magnetic and radiofrequency environments during imaging commonly confronting MR imaging in routine clinical cardiac imaging. Furthermore, there is no limitation of basic life-support and physiologic-monitoring equipment in the vicinity of the CT scanner. MR and MDCT imaging have been used to assess cardiac anatomy[5], measure left and right ventricular volumes and function[6], regional perfusion[7,8] and myocardial viability[9,10]. The focus of this review is on the manifestations of reperfusion injury using MR and MDCT imaging.

COMPONENTS OF REPERFUSION INJURY

Myocardial edema

Reperfusion of previously ischemic myocardium causes edema related to the leakage of blood macromolecules into interstitium. Edema is one of the features of the salvageable area at risk[11,12]. The increase in mobile water content (edema) within the ischemic region causes a prolongation of T2 relaxation time[13]. The salvaged area at risk in reperfused infarct has been visualized on T2-weighted turbo spin echo MR imaging as a hyperintense area (Figure 1)[14-18].

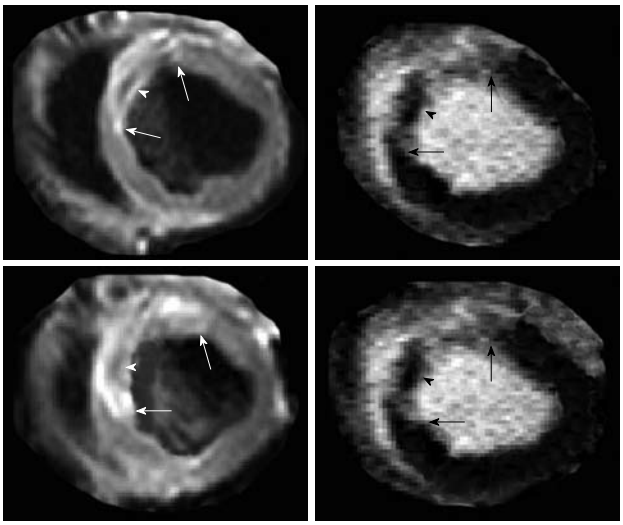

Figure 1 Multi-slice T2-weighted turbo spin echo imaging demonstrates the hyperintense edematous area at risk (white arrows in the left images) with hypoenhanced zone, which may represent microvascular and/or interstitial hemorrhage zone (arrowhead in the left images). Delayed contrast enhancement magnetic resonance (DE-MR) imaging confirmed the presence of microvascular and/or interstitial hemorrhage zone in the core (black arrowhead in the right images) of hyperenhanced infarcted myocardium (black arrows in the right images).

Accurate assessment of the area at risk is required to compare different revascularization techniques or for studies aimed at improving myocardial salvage[19-22] as an end point. MR imaging has documented regional myocardial edema in patients with normal coronary angiograms[23] and stunning[24]. Kwong *et al*[25] combined the assessment of LV function, myocardial perfusion and infarct in patients who presented to the emergency room with chest pain. The investigators found that MR imaging is the strongest predictor for the diagnosis of acute coronary syndrome compared with a standard workup. The sensitivity and specificity of MR imaging for detecting acute coronary syndrome was 84% and 85%, respectively. Moreover, multiple logistic regression analysis revealed that MR imaging had independent diagnostic value over clinical parameters, including ECG and initial troponin I levels. In another adenosine perfusion MR study, Ingkanisorn *et al*[26] evaluated the diagnostic value of adenosine in 135 patients who presented to the emergency room with chest pain with no elevation in troponin levels. MR imaging data indicated that there was no evidence of significant ischemic heart disease in these patients. Patients were contacted 1 year later to determine the incidence of coronary artery stenosis (> 50%) on invasive coronary angiography, abnormal correlative stress test, new infarct, or death. Based on this survey, MR perfusion imaging showed 100% sensitivity and 93% specificity for the detection of myocardial ischemia. It was concluded that MR imaging had significant prog-

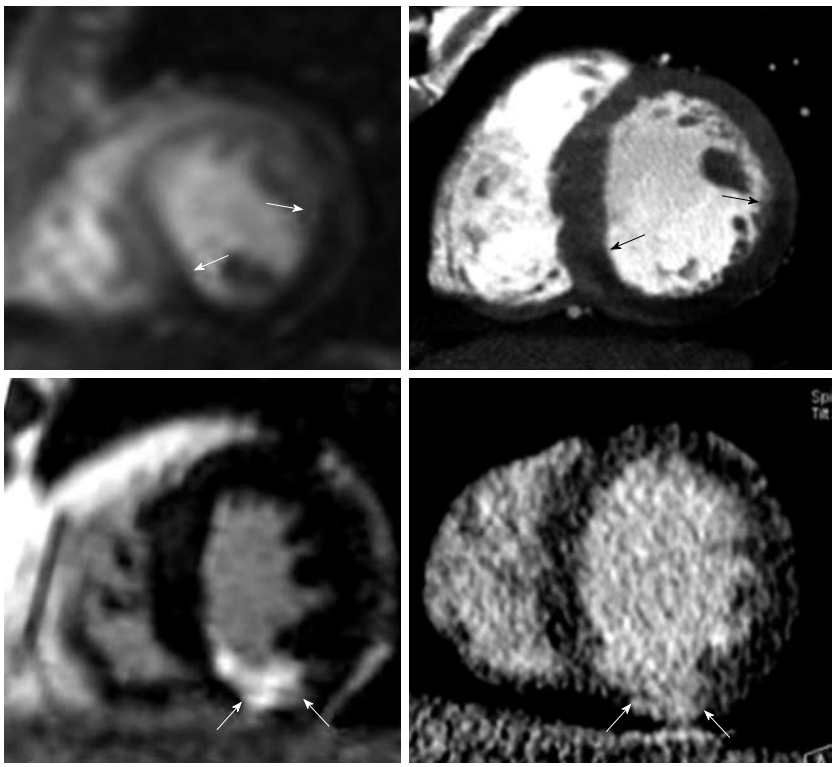

Figure 2 Head-to-head comparison between first pass perfusion MR (top left) and first pass multidetector computed tomography (MDCT) imaging (top right) in a 42-year-old man with acute reperfused infarct. Ischemic myocardium (arrows) appears as a hypoenhanced region with comparable extent on both imaging modalities. Bottom: Head-to-head comparison of DE-MR (bottom left) and DE-MDCT imaging (bottom right) shows a bright region comparable in size to enhanced inferior infarct (arrows). Note that the enhanced infarct on DE-imaging is substantially smaller than ischemic myocardium[38].

nostic value in predicting a future diagnosis of ischemia, infarct, or death. First pass perfusion imaging can be used to discriminate ischemic myocardium. A recent MR-impact study in 234 patients reported improved detection of ischemic myocardium distal to coronary stenosis compared to single photon emission computed tomography in a multicenter and multivendor randomized trial[27].

MDCT imaging has also been used in the evaluation of cardiac function, myocardial viability and plaque morphology[28-30]. A preclinical study demonstrated that this modality has the potential to detect infarct heterogeneity in the peri-infarct zone[31]. Recent experimental studies using modern MDCT technology confirmed the potential of the technique in depicting ischemic myocardium during the first pass perfusion of iodinated contrast media[10,32].

HOMOGENEOUS MYOCARDIAL INFARCT

Several studies indicated that there is a close correlation between homogeneous myocardial infarct size, dimensions (size, circumferential extent and transmurality) and LV remodeling. Inversion-recovery low-angle-shot MR imaging and helical MDCT imaging have been recently introduced and performed following the intravenous administration of contrast media with a delay of 5-10 min to define myocardial infarct dimensions[7,9,10,33-39] (Figure 2). Investigators found that differentially contrast enhanced regions on MR and MDCT imaging correlate well with areas of decreased flow[32,40] and dobutamine stress on echocardiography[41]. Furthermore, the combined use of cine and DE-MR imaging are able to differentiate regional transitional dysfunction in stunned and hibernating myocardium from permanent dysfunction on contrast enhanced infarct[42,43]. A recent study showed multicontrast MR imaging enables simultaneous assessment of wall motion, MO and viability[44].

Cine and DE-MR imaging have been used to determine contractile reserve in transmural and non-transmural infarct[45,46]. These studies have also indicated the substantial improvement in regional function in segments with 50% transmural enhancement and global LV improvement in transmural enhancement of less than 25% of LV wall thickness[45-47]. Others found that 75% of the patients with transmural enhancement died within 26-36 mo of diagnosis[48]. Tarantini *et al*[49] demonstrated in 76 patients with reperfused infarct that transmural enhancement using DE-MR imaging is associated with LV remodeling. These findings were confirmed by Roes *et al*[50] who showed that the size of the infarct scar in 231 patients is a stronger predictor of all-cause mortality than LV ejection fraction and LV volumes. Thus, extensive transmural enhancement is an excellent predictor of poor recovery.

Contrast enhanced T1-weighted and non-contrast T2-weighted MR imaging is useful in discriminating acute from chronic myocardial infarct[51]. In a study of 73 patients with acute and chronic infarct by Abdel-Aty *et al*[51] MR imaging was effective (96% sensitive) in discriminating acute from chronic infarct. In a preclinical study, Saeed *et al*[52] observed lack of deferential enhancement of chronic infarct after administration of blood pool MR contrast media, but not after clinically approved extracellular MR contrast media. Unlike acute reperfused infarct, chronic infarct lacks edema, MO or hemorrhage because they are resorbed.

Expanding the use of coronary MDCT into clinical

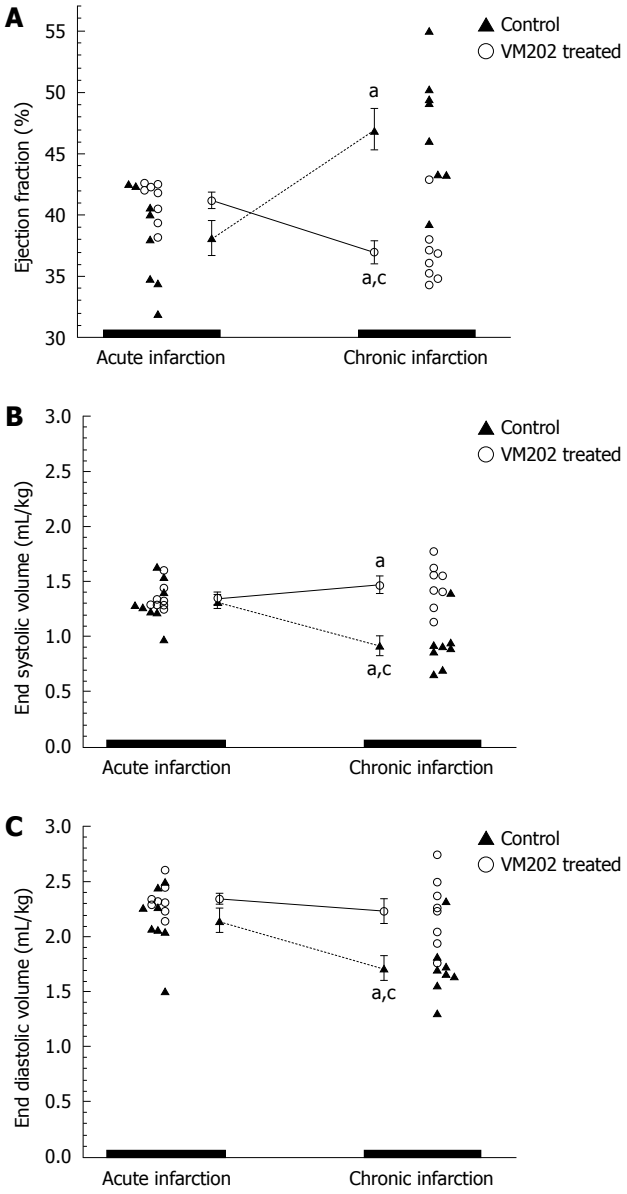

Figure 3 The ejection fraction (A), end systolic volumes (B) and end diastolic volumes (C) are shown for control and hepatocyte growth factor gene (VM202) treated animals. The hepatocyte growth factor gene administered at 3 d after reperfusion significantly decreased end diastolic (mL/kg) and end systolic volumes at 8 wk compared to 3 d infarct ($^{a}P < 0.05$) and control group ($^{c}P < 0.05$). Control animals at 8 wk showed a significant decrease in ejection fraction and significant increase in end systolic and end diastolic volumes compared with 3 d infarct[59].

practice has sparked interest in using the modality for assessing myocardial viability[53]. Gerber *et al*[9] showed the similarity between infarct size measured on DE-MDCT and DE-MR imaging in a series of patients. The investigators demonstrated good agreement (82%, $k = 0.61$, $P < 0.001$) between the two measurements (Figure 2). Nikolaou *et al*[54] demonstrated the diagnostic power of MDCT in assessing the presence, age, and size of myocardial infarct in 106 patients. Myocardial infarct was found in 27 of 106 patients. MDCT detected 23 of 27 patients with infarct with a sensitivity of 85%, specificity of 91% and accuracy of 90%.

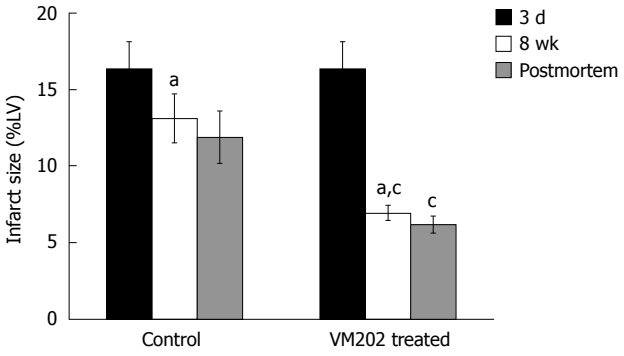

Figure 4 Histogram shows the difference in infarct size prior to intramyocardial gene delivery at 3 d and 8 wk after infarction in control animals (left block) and animals treated with hepatocyte growth factor gene (VM202) (right block) measured on DE-MR imaging (black and white bars) and postmortem (gray bars). Note the decline in infarct size was greater in gene treated animals compared with control animals. $^{a}P < 0.05$ compared with 3 d acute infarction. $^{c}P < 0.05$ compared with 8 wk chronic infarction in control animals. %LV: Percentage of LV mass[59].

Transfer of angiogenic genes to ischemic myocardium is a promising approach under development for the treatment of myocardial infarct. MR and CT imaging may be a useful tool for defining myocardial infarct and for use in targeting the infarct for gene and stem cell therapies[55-60]. Catheter-based fluoroscopic MR and MDCT imaging has been recently used for delivering these therapies transendocardially[37,58]. Sequential cine and DE-MR imaging showed great sensitivity in detecting improvement in ejection fraction, reduction of LV volumes and infarct size (Figures 3 and 4) after intramyocardial delivery of different angiogenic genes[58-60]. Figure 5 demonstrates the increase in vascular density of infarcted myocardium 8 wk after intramyocardial delivery of vascular growth factor gene. Thus, MR imaging provides great promise in evaluating gene and cell therapies[58,61-63].

A preliminary experimental study investigated MDCT for the assessment of the efficacy of stem cells in infarcted myocardium and showed that this technique has the capability to elucidate new therapies[37]. The radiation doses in MDCT may limit such application in patients because therapeutic studies need a minimum of two imaging sessions. The potential advantages of using MDCT in assessing myocardial viability may be related to faster acquisition time compared with cardiac MR imaging and the ability to scan claustrophobic or uncooperative patients. Additionally, MDCT angiography is the method of choice for direct visualization of the coronary arteries, coronary calcium and atherosclerosis in its earliest stages; when treatment can be most effective in preventing subsequent heart attacks or sudden death. On the other hand, MR imaging has other advantages over MDCT including: (1) the absence of radiation exposure; (2) the lack of nephrotoxic iodinated contrast media; and (3) it allows for repeated scans, particularly in pediatric patients. It should be noted that MR contrast media cause nephrogenic systemic fibrosis in patients with compromised renal function[64].

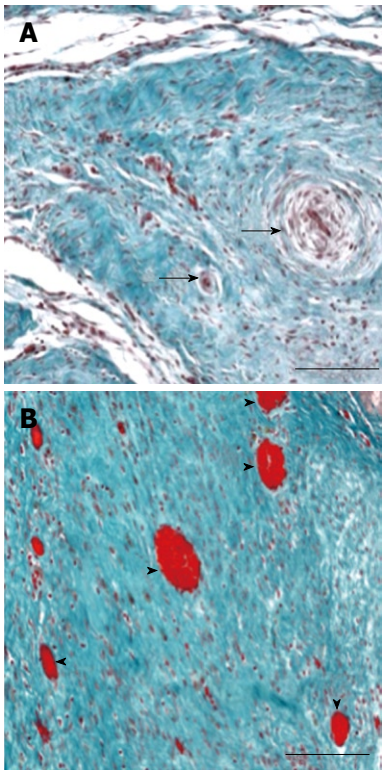

Figure 5 Micrographs of representative infarcts in control and VEGF-gene treated swine. A: The infarct in the control animal shows no appreciable angiogenesis and residual blood vessels have been remodeled, as shown by the thick vascular wall and small lumen (black arrows). B: VEGF-gene treated animal contains numerous blood vessels (arrowheads) in linear array representing injection track (calibration bar = 200 μm)[60].

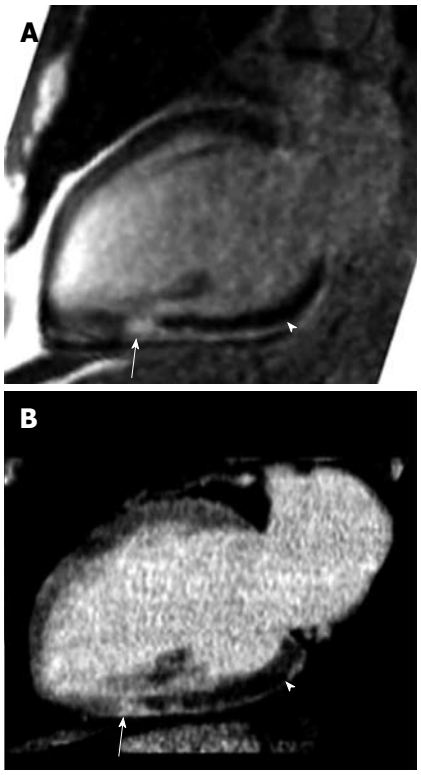

Figure 6 Head-to-head comparison of DE-MR (A) and DE-MDCT images (B) showing the dark MO zone (arrowheads) surrounded by a bright enhanced infarct in a reperfused patient (arrows)[38].

MANIFESTATIONS OF REPERFUSION INJURY

MO zone

In the setting of an acute myocardial infarction, treatment strategies have primarily focused on the management of culprit occlusions in the epicardial coronary arteries[65]. Interventional cardiologists, however, found that the benefits of revascularization of the epicardial coronary artery is limited and later discovered that MO is a major component of infarction, which is frequently seen after revascularization of the epicardial coronary artery. Investigators found that the formation of MO is related to plaque emboli, endothelial swelling, inflammation, extravascular edema and microvascular spasm[66].

How best to measure MO in terms of predictive values is an important question. A variety of techniques, flow or frame count[67,68], myocardial blush grade[69] coronary Doppler imaging[70], contrast echocardiography[68], contrast-enhanced MR imaging[71,72] and contrast enhanced MDCT[32,38], have been used to detect MO zone in patients with TIMI (thrombosis in myocardial infarction). The quality of some of these techniques, however, is suboptimal due to poor spatial resolution.

MR and MDCT imaging delineated MO as a hypoenhanced zone in the core of acutely reperfused infarct (Figure 6). The delineation is attributed to inadequate contrast media delivery during first pass perfusion (17 s blood recirculation time)[46], early (1-2 min; equilibrium phase of contrast medium in the blood and tissue interstitium)[72] and delayed (10 min; peak enhancement of myocardial infarct) MR imaging[73]. The extent of MO after bolus administration of contrast media is time dependent and varies between first pass, early contrast enhancement and DE-imaging because it is governed by 2 processes namely: perfusion and passive diffusion. Figure 6 illustrates the comparable MO extent measured on DE-MR and DE-MDCT imaging in a patient subjected to reperfusion.

Both early and delayed persistent MO has been shown to predict post-infarct LV remodeling and outcome in patients with ST-elevation myocardial infarction (STEMI)[72-76]. A recent study showed that MO detected on DE-MR imaging is more frequently observed in patients with the most severe LV dyfunction[77]. A clinical study in 25 patients demonstrated that delayed persistent MO is also high (32%) in the No-STEMI population after successful percutaneous coronary intervention[78], but less than that observed in STEMI patients[73,79]. Recent studies indicated that MO is predictive of increasing recurrent myocardial infarct, congestive heart failure, stroke and death up to 16 mo after the event[72,73,75].

Preclinical studies showed that the extent of MO in reperfused infarct is less variable in the first 10 min after administration of blood pool MR contrast media, which may be attributed to slow convection of the contrast medium in the interstitium and its retention in the blood pool[80].

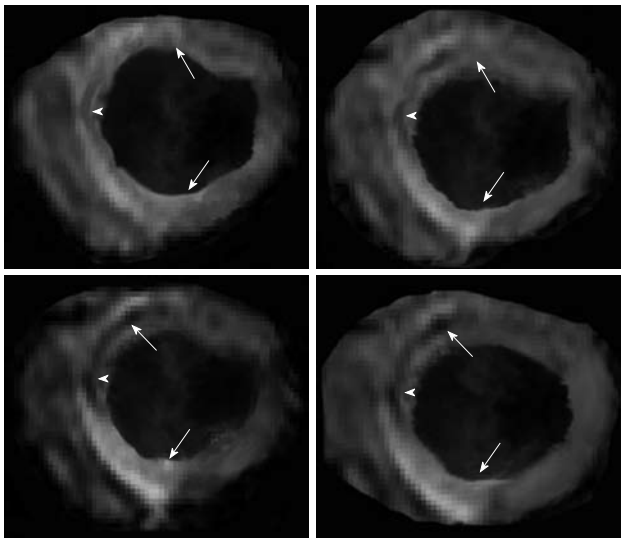

Figure 7 Multislice T2*-weighted (susceptibility) turbo spin echo images show severe interstitial hemorrhage in the core (arrowheads) of the hyperintense edematous area at risk (arrows) 3 d after reperfusion.

INTERSTITIAL HEMORRHAGE

Interstitial hemorrhage is another component of reperfusion injury in patients with ST-segment elevation due to acute infarct. Its presence is an important marker for myocardial and microvascular damage. Interstitial hemorrhage causes signal loss on T2*-weighted images, which depends on the status of hemoglobin (oxyhemoglobin, deoxyhemoglobin, or methemoglobin) and the presence of blood products such as ferritin and hemosiderin[15,81]. Figure 7 demonstrates intensive hypointense interstitial hemorrhage 3 d after reperfusion in a swine model on T2*-weighted (susceptibility) turbo spin echo MR imaging. O'Regan *et al*[82] quantified the extent of interstitial hemorrhage on T2*-weighted mapping and compared it with other indices of ischemic injury, such as area at risk and infarct size.

Although non-enhancing myocardium within the infarct is thought to represent MO[46], it is possible that the presence of blood products may also contribute to its low signal seen on MR images[15]. Ganame *et al*[83] also used T2-weighted MR imaging to measure the extent of hemorrhage and area at risk in 98 patients with a large reperfused infarct. Based on this technique, the investigators demonstrated a high prevalence of myocardial hemorrhage of 25% in this patient cohort, more common amongst patients with large transmural infarct and severe LV global and regional dysfunction.

PERI-INFARCT ZONE

A mixed population of viable and non-viable myocytes has been found around acutely infarcted myocardium, a territory previously described as the peri-infarct zone[84,85]. Microscopic studies indicated that the peri-infarct zone has leaky microvessels[84-88]. The peri-infarct zone has consistently been substantiated by a variety of modalities, including echocardiography[89], radiopaque bead arrays[90] and MR imaging[82]. The physiological correlates of the peri-infarct zone using MR imaging have been described[91].

MR or CT contrast media have been used to define the peri-infarct zone[31,88], identify patients who are susceptible to ventricular arrhythmias[92] and predict post-infarct mortality[93]. Using preclinical necrosis-specific (mesoporphyrin) and extracellular MR contrast medium in a seminal animal study, Saeed *et al*[94] demonstrated MR characterization of the peri-infarct zone. They found that the enhanced region on DE-MR imaging is larger than the true infarct delineated on TTC staining, which was identical to regions enhanced by the necrosis-specific contrast medium. The difference in enhancement regions demarcated by the 2 contrast media was considered the peri-infarct zone. At that time our findings were in contrast to other groups who demonstrated that differentially enhanced myocardium represents necrotic tissue. Recent clinical MR studies confirmed our findings[31,92,95] and went further to report the associations between infarct size, the peri-infarct zone and inducible ventricular arrhythmias[31,92,93,95]. Yan *et al*[93] found that the extent of the peri-infarct provides prognostic value for mortality incremental to that offered by ejection fraction and LV end-diastolic volume. On the other hand, the existence of viable myocytes in a large peri-infarct zone may raise an interesting hypothesis that reperfusion could be beneficial by reducing arrhythmogenic triggers, despite the apparent lack of measurable improvement in contractile function. Furthermore, implantable cardioverter-defibrillator therapy may be warranted in such high-risk patients identified by MR due to the creation of multiple action potential circuits derived from the peri-infarct zone.

CALCIUM DEPOSIT

Considering the deleterious effects of calcium overload in reperfused myocardium[96,97], the development of a noninvasive technique to visualize calcium deposits in infarcted myocardium may have clinical value. Noninvasive imaging techniques that directly incorporate the spatial distribution of calcium in infarcted myocardium may help our understanding of the relationship between calcium deposits in the myocardium, the rate of infarct resorption, and LV function[98].

Calcium deposited in infarcted myocardium has previously been used as a target for 99m-Tc pyrophosphate scintigraphy to delineate reperfused myocardial infarcts in patients[99,100]. For over a decade, electron-beam CT has been clinically used for calcium scoring in the coronary arteries of patients. In addition to calcium scoring and detection of coronary stenosis, modern MDCT scanners have been used to assess the extent of acute and chronic infarct[10,101].

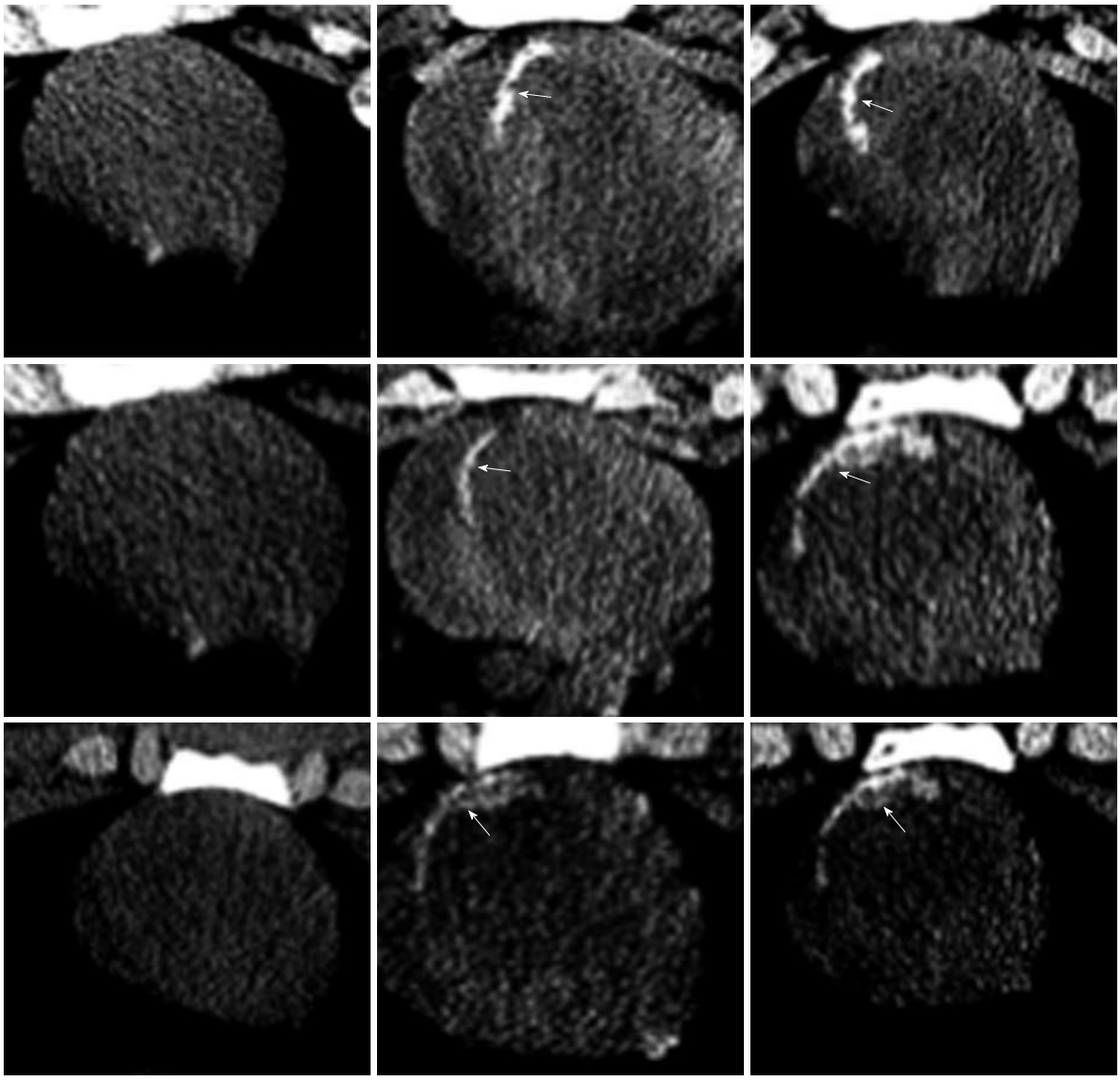

Figure 8 Non-contrast enhanced MDCT imaging demonstrates deposited calcium 7 d after reperfusion (right block arrows). In all 3 animals (the 3 rows) the deposited calcium was not evident at 2-3 h after reperfusion on non-contrast enhanced MDCT (left block)[102].

In a recent animal study, non-contrast MDCT images depicted calcium deposits as "hot-spots" 1 wk after reperfusion (Figure 8). The presence of calcium deposits on non-contrast MDCT images, however, was transient and specific to acute infarct because the calcium was resorbed from the infarct scar at 8 wk as shown on CT imaging and histopathology (Figure 9). Histopathology confirmed the engulfment of the deposited calcium by macrophages[102]. Noninvasive evaluation of the beneficial administration of calcium channel blockers on calcium overload during reperfusion may be possible using MDCT.

HETEROGENOUS MICROINFARCT

Heterogeneous microinfarct results from showers of microemboli shed following coronary intervention. Clinical studies showed that 42% of patients experience major cardiac problems, such as heart failure and sudden death, after percutaneous coronary angioplasty[103,104]. High incidences (30%-50%) of defects on myocardial perfusion scintigraphy have also been detected soon after coronary balloon angioplasty and with optimally implanted stents[105,106] and these events continued during follow-up[107-109]. The emboli sizes, collected by distal protection devices during percutaneous coronary intervention, differ widely (47-2503 μm)[110] and the size and number of ruptured atherosclerotic plaques is a key event in the pathogenesis of heterogeneous microinfarct[111]. A recent clinical study demonstrated that the volume of embolized material relates directly to the volume of new necrosis detected by delayed-enhancement MR imaging[112]. The American College of Cardiology and the European Society of Cardiology recently recognized the detrimental consequences of coronary microembolization in patients in their 2007 guidelines[113].

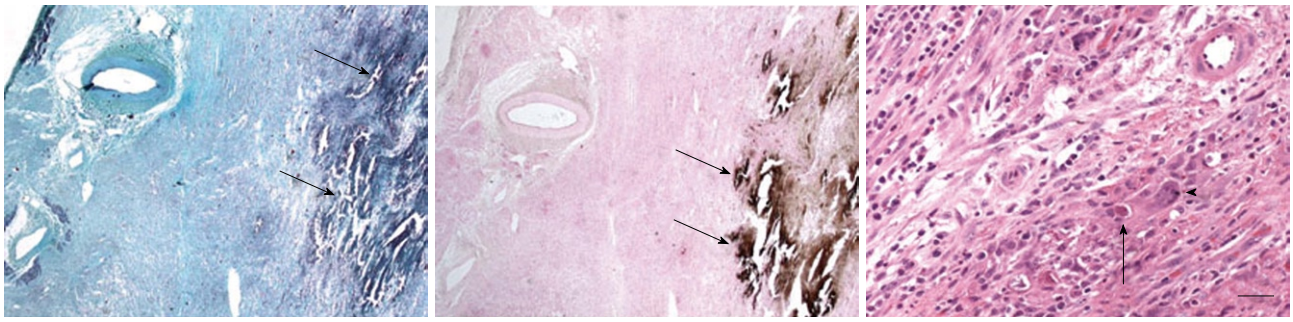

Figure 9 Histopathology from at 1-wk-old reperfused infarct shows calcium deposits as a black-brown precipitation product (arrows) on Masson trichrome (A) and the special calcium stain (von Kossa stain) (B). At 8 wk the stain shows traces of calcium deposits (C, arrow) surrounded by giant cell (arrowhead). Apparently the giant macrophages digest deposited calcium (calibration bars = 20 mm)[102].

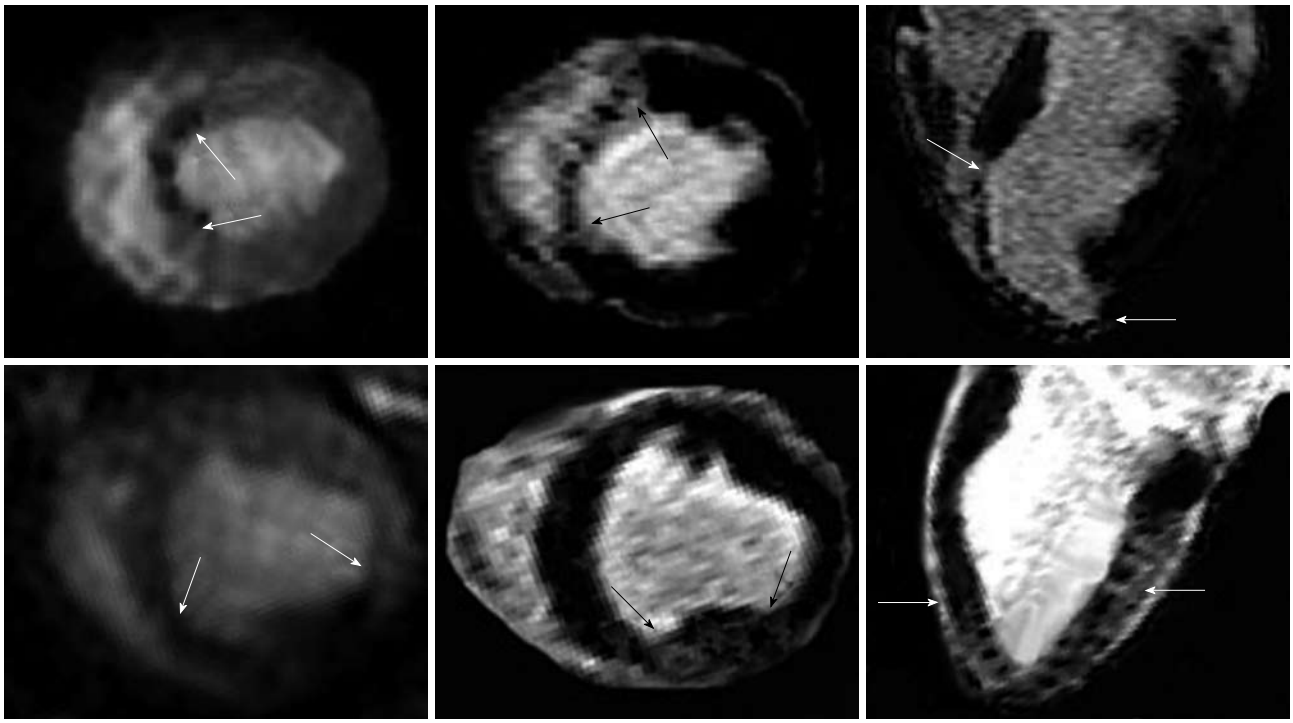

Figure 10 Preclinical study shows the patchy enhanced embolized region in two animals after delivery of embolic materials (7200 microsphere count, 100-300 μm diameters). Animal one received the embolic materials in the left anterior descending coronary artery causing perfusion deficit in the antero-septal wall 2-3 h after delivery of the embolic materials (top left, arrows), while animal two received the embolic materials in the left circumflex coronary artery causing perfusion deficit in the inferior wall (bottom left, arrows). Short (center images) and long (right images) axis views of DE-MR imaging illustrates the microinfarct of the same ischemic territory 7 d after embolization[114].

In a preclinical study, a microinfarcted region was detected on first pass perfusion imaging 2-3 h as well as 7 d after embolization[114]. DE-MR imaging failed to define microinfarct early but at 7 d it was clearly visible. Microinfarct was visualized as bright heterogeneous subregions on DE-MR imaging (Figure 8). Furthermore, DE-MR and DE-MDCT imaging is sensitive in detecting the direction of embolized vessels in experimental animals (Figure 9).

Several studies demonstrated the potential of DE-MR imaging in visualizing heterogeneous microinfarct in patients[102,112,114-118]. Ricciardi *et al*[118] and Choi *et al*[119] have demonstrated heterogeneous microinfarct in patients on DE-MR imaging. The investigators found a link between MR visualization of microinfarct and impaired myocardial perfusion (Figure 10)[119]. Selvanayagam *et al*[120] demonstrated that the extent of elevated troponin I levels 24 h after coronary intervention is directly related to the extent of microinfarct on DE-MR imaging. More recently, they examined myocardial perfusion and microinfarct serially after percutaneous coronary intervention using MR technique[117]. They found that myocardial perfusion is reduced in myocardial segments with new microinfarct 24 h after percutaneous coronary intervention. It has been shown that microinfarct causes severe and persistent LV dysfunction and in some cases sudden death[40]. Investigators concluded that even small amounts of infarct (microinfarct) detected on

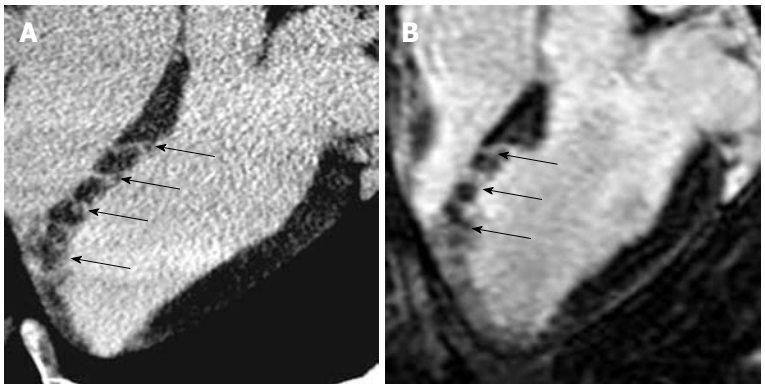

Figure 11 DE-multi-slice MDCT (A) and DE-MR (B) images from experimentally embolized LAD coronary artery show good correspondence between the modalities in defining heterogenous microinfarct. Both modalities show enhanced stripes (arrows) of microinfarct extending from the epicardium to the endocardium mapping occluded microvessels.

DE-images provides prognostic value beyond the routine clinical, angiographic and functional predictors[25].

Heterogeneous microinfarct is not limited to percutaneous coronary intervention for atherosclerosis but include a wide range of diseases, such as valvular disease, prosthetic valve, endocarditis, cardiomyopathy with mural thrombus, arrhythmias and during heart-lung-bypass[121-125]. This pathology has also been reported in patients with hypertension, diabetes[126], systemic lupus erythematosus[127] and sickle cell disease, where abnormally shaped erythrocytes obstructing the capillaries and small arterioles may cause myocardial fibrosis[128]. Therefore, early detection and subsequent effects of microinfarct need highly sensitive imaging modalities.

CONCLUSION

The clinical role of MR and MDCT imaging continues to expand supported by the advances in software and hardware. The strength of MR imaging relies on the variety of pulse sequences and the ability to noninvasively provide information on myocardial structure, function and perfusion in a single imaging session. The complementary use of both MR and MDCT imaging allows the components and manifestations of reperfusion injury including myocardial edema, interstitial hemorrhage, calcium deposition and MO to be visualized. MR imaging can be used serially and noninvasively in assessing the consequences of reperfusion injury because there is no radiation exposure or administration of radioactive materials. MDCT is better suited for assessing coronary artery stenosis and as an alternative technique for assessing viability in patients where MR imaging is contraindicated. Clinical MR studies found that the presence of transmural infarct, MO and peri-infarct are excellent predictor of poor post-infarct recovery and mortality[31,92,93,95,129]. Heterogeneous cardiac microinfarct detected on contrast enhanced MR and MDCT imaging has a prolonged effect on LV function and perfusion (Figure 11)[130]. The clinical significance of deposited calcium, detected on MDCT, in acute homogeneous infarct requires further studies. Recent preclinical MR studies provided ample evidence that angiogenic genes and stem cells, delivered transendocardially under MR-guidance, have beneficial effects on myocardial function, perfusion and viability. Imaging protocols are in progress to monitor the long-term efficacy of such therapeutic agents. Cardiac MR and MDCT imaging can characterize reperfusion injury components and manifestations.

REFERENCES

1 **Maceira AM**, Joshi J, Prasad SK, Moon JC, Perugini E, Harding I, Sheppard MN, Poole-Wilson PA, Hawkins PN, Pennell DJ. Cardiovascular magnetic resonance in cardiac amyloidosis. *Circulation* 2005; **111**: 186-193

2 **Friedrich MG**, Strohm O, Schulz-Menger J, Marciniak H, Luft FC, Dietz R. Contrast media-enhanced magnetic resonance imaging visualizes myocardial changes in the course of viral myocarditis. *Circulation* 1998; **97**: 1802-1809

3 **Amano Y**, Takayama M, Kumita S. Contrast-enhanced myocardial T1-weighted scout (Look-Locker) imaging for the detection of myocardial damages in hypertrophic cardiomyopathy. *J Magn Reson Imaging* 2009; **30**: 778-784

4 **Sakuma H**, Suzawa N, Ichikawa Y, Makino K, Hirano T, Kitagawa K, Takeda K. Diagnostic accuracy of stress first-pass contrast-enhanced myocardial perfusion MRI compared with stress myocardial perfusion scintigraphy. *AJR Am J Roentgenol* 2005; **185**: 95-102

5 **Hendel RC**, Patel MR, Kramer CM, Poon M, Hendel RC, Carr JC, Gerstad NA, Gillam LD, Hodgson JM, Kim RJ, Kramer CM, Lesser JR, Martin ET, Messer JV, Redberg RF, Rubin GD, Rumsfeld JS, Taylor AJ, Weigold WG, Woodard PK, Brindis RG, Hendel RC, Douglas PS, Peterson ED, Wolk MJ, Allen JM, Patel MR. ACCF/ACR/SCCT/SCMR/ASNC/NASCI/SCAI/SIR 2006 appropriateness criteria for cardiac computed tomography and cardiac magnetic resonance imaging: a report of the American College of Cardiology Foundation Quality Strategic Directions Committee Appropriateness Criteria Working Group, American College of Radiology, Society of Cardiovascular Computed Tomography, Society for Cardiovascular Magnetic Resonance, American Society of Nuclear Cardiology, North American Society for Cardiac Imaging, Society for Cardiovascular Angiography and Interventions, and Society of Interventional Radiology. *J Am Coll Cardiol* 2006; **48**: 1475-1497

6 **van der Vleuten PA**, Willems TP, Götte MJ, Tio RA, Greuter MJ, Zijlstra F, Oudkerk M. Quantification of global left ventricular function: comparison of multidetector computed tomography and magnetic resonance imaging. a meta-analysis and review of the current literature. *Acta Radiol* 2006; **47**: 1049-1057

7 **George RT**, Silva C, Cordeiro MA, DiPaula A, Thompson DR, McCarthy WF, Ichihara T, Lima JA, Lardo AC. Multidetector computed tomography myocardial perfusion imaging during adenosine stress. *J Am Coll Cardiol* 2006; **48**: 153-160

8 **Mahnken AH**, Bruners P, Katoh M, Wildberger JE, Günther RW, Buecker A. Dynamic multi-section CT imaging in acute myocardial infarction: preliminary animal experience. *Eur Radiol* 2006; **16**: 746-752

9 **Gerber BL**, Belge B, Legros GJ, Lim P, Poncelet A, Pasquet A, Gisellu G, Coche E, Vanoverschelde JL. Characterization of acute and chronic myocardial infarcts by multidetector computed tomography: comparison with contrast-enhanced magnetic resonance. *Circulation* 2006; **113**: 823-833

10 **Lardo AC**, Cordeiro MA, Silva C, Amado LC, George RT, Saliaris AP, Schuleri KH, Fernandes VR, Zviman M, Nazarian S, Halperin HR, Wu KC, Hare JM, Lima JA. Contrast-enhanced multidetector computed tomography viability imaging after myocardial infarction: characterization of myocyte death, microvascular obstruction, and chronic scar. *Circulation* 2006; **113**: 394-404

11 **Garcia-Dorado D**, Oliveras J. Myocardial oedema: a preventable cause of reperfusion injury? *Cardiovasc Res* 1993; **27**: 1555-1563

12 **García-Dorado D**, Oliveras J, Gili J, Sanz E, Pérez-Villa F, Barrabés J, Carreras MJ, Solares J, Soler-Soler J. Analysis of myocardial oedema by magnetic resonance imaging early after coronary artery occlusion with or without reperfusion. *Cardiovasc Res* 1993; **27**: 1462-1469

13 **Boxt LM**, Hsu D, Katz J, Detweiler P, Mclaughlin S, Kolb TJ, Spotnitz HM. Estimation of myocardial water content using transverse relaxation time from dual spin-echo magnetic resonance imaging. *Magn Reson Imaging* 1993; **11**: 375-383

14 **Arai AE**. Using magnetic resonance imaging to characterize recent myocardial injury: utility in acute coronary syndrome and other clinical scenarios. *Circulation* 2008; **118**: 795-796

15 **Basso C**, Corbetti F, Silva C, Abudureheman A, Lacognata C, Cacciavillani L, Tarantini G, Marra MP, Ramondo A, Thiene G, Iliceto S. Morphologic validation of reperfused hemorrhagic myocardial infarction by cardiovascular magnetic resonance. *Am J Cardiol* 2007; **100**: 1322-1327

16 **Friedrich MG**, Abdel-Aty H, Taylor A, Schulz-Menger J, Messroghli D, Dietz R. The salvaged area at risk in reperfused acute myocardial infarction as visualized by cardiovascular magnetic resonance. *J Am Coll Cardiol* 2008; **51**: 1581-1587

17 **Stork A**, Lund GK, Muellerleile K, Bansmann PM, Nolte-Ernsting C, Kemper J, Begemann PG, Adam G. Characterization of the peri-infarction zone using T2-weighted MRI and delayed-enhancement MRI in patients with acute myocardial infarction. *Eur Radiol* 2006; **16**: 2350-2357

18 **Tilak GS**, Hsu LY, Hoyt RF Jr, Arai AE, Aletras AH. In vivo T2-weighted magnetic resonance imaging can accurately determine the ischemic area at risk for 2-day-old nonreperfused myocardial infarction. *Invest Radiol* 2008; **43**: 7-15

19 **Janssens S**, Dubois C, Bogaert J, Theunissen K, Deroose C, Desmet W, Kalantzi M, Herbots L, Sinnaeve P, Dens J, Maertens J, Rademakers F, Dymarkowski S, Gheysens O, Van Cleemput J, Bormans G, Nuyts J, Belmans A, Mortelmans L, Boogaerts M, Van de Werf F. Autologous bone marrow-derived stem-cell transfer in patients with ST-segment elevation myocardial infarction: double-blind, randomised controlled trial. *Lancet* 2006; **367**: 113-121

20 **Miller TD**, Christian TF, Hopfenspirger MR, Hodge DO, Gersh BJ, Gibbons RJ. Infarct size after acute myocardial infarction measured by quantitative tomographic 99mTc sestamibi imaging predicts subsequent mortality. *Circulation* 1995; **92**: 334-341

21 **Santoro GM**, Bisi G, Sciagrà R, Leoncini M, Fazzini PF, Meldolesi U. Single photon emission computed tomography with technetium-99m hexakis 2-methoxyisobutyl isonitrile in acute myocardial infarction before and after thrombolytic treatment: assessment of salvaged myocardium and prediction of late functional recovery. *J Am Coll Cardiol* 1990; **15**: 301-314

22 **Wackers FJ**, Gibbons RJ, Verani MS, Kayden DS, Pellikka PA, Behrenbeck T, Mahmarian JJ, Zaret BL. Serial quantitative planar technetium-99m isonitrile imaging in acute myocardial infarction: efficacy for noninvasive assessment of thrombolytic therapy. *J Am Coll Cardiol* 1989; **14**: 861-873

23 **Shapiro MD**, Guarraia DL, Moloo J, Cury RC. Evaluation of acute coronary syndromes by cardiac magnetic resonance imaging. *Top Magn Reson Imaging* 2008; **19**: 25-32

24 **Bragadeesh T**, Jayaweera AR, Pascotto M, Micari A, Le DE, Kramer CM, Epstein FH, Kaul S. Post-ischaemic myocardial dysfunction (stunning) results from myofibrillar oedema. *Heart* 2008; **94**: 166-171

25 **Kwong RY**, Chan AK, Brown KA, Chan CW, Reynolds HG, Tsang S, Davis RB. Impact of unrecognized myocardial scar detected by cardiac magnetic resonance imaging on event-free survival in patients presenting with signs or symptoms of coronary artery disease. *Circulation* 2006; **113**: 2733-2743

26 **Ingkanisorn WP**, Kwong RY, Bohme NS, Geller NL, Rhoads KL, Dyke CK, Paterson DI, Syed MA, Aletras AH, Arai AE. Prognosis of negative adenosine stress magnetic resonance in patients presenting to an emergency department with chest pain. *J Am Coll Cardiol* 2006; **47**: 1427-1432

27 **Schwitter J**, Wacker CM, van Rossum AC, Lombardi M, Al-Saadi N, Ahlstrom H, Dill T, Larsson HB, Flamm SD, Marquardt M, Johansson L. MR-IMPACT: comparison of perfusion-cardiac magnetic resonance with single-photon emission computed tomography for the detection of coronary artery disease in a multicentre, multivendor, randomized trial. *Eur Heart J* 2008; **29**: 480-489

28 **Achenbach S**, Daniel WG. Current role of cardiac computed tomography. *Herz* 2007; **32**: 97-107

29 **Kopp AF**, Heuschmid M, Reimann A, Kuettner A, Beck T, Ohmer M, Burgstahler C, Brodoefel H, Claussen CD, Schroeder S. Evaluation of cardiac function and myocardial viability with 16- and 64-slice multidetector computed tomography. *Eur Radiol* 2005; **15** Suppl 4: D15-D20

30 **Mollet NR**, Cademartiri F, Nieman K, Saia F, Lemos PA, McFadden EP, Serruys PW, Krestin GP, de Feyter PJ. Noninvasive assessment of coronary plaque burden using multislice computed tomography. *Am J Cardiol* 2005; **95**: 1165-1169

31 **Schuleri KH**, Centola M, George RT, Amado LC, Evers KS, Kitagawa K, Vavere AL, Evers R, Hare JM, Cox C, McVeigh ER, Lima JA, Lardo AC. Characterization of peri-infarct zone heterogeneity by contrast-enhanced multidetector computed tomography: a comparison with magnetic resonance imaging. *J Am Coll Cardiol* 2009; **53**: 1699-1707

32 **Furtado AD**, Carlsson M, Wintermark M, Ordovas K, Saeed M. Identification of residual ischemia, infarction, and microvascular impairment in revascularized myocardial infarction using 64-slice MDCT. *Contrast Media Mol Imaging* 2008; **3**: 198-206

33 **Baks T**, Cademartiri F, Moelker AD, van der Giessen WJ, Krestin GP, Duncker DJ, de Feyter PJ. Assessment of acute reperfused myocardial infarction with delayed enhancement 64-MDCT. *AJR Am J Roentgenol* 2007; **188**: W135-W137

34 **Mahnken AH**, Bruners P, Mühlenbruch G, Emmerich M, Hohl C, Günther RW, Wildberger JE. Low tube voltage improves computed tomography imaging of delayed myocardial contrast enhancement in an experimental acute myocardial infarction model. *Invest Radiol* 2007; **42**: 123-129

35 **Kondo C**, Mori S, Endo M, Kusakabe K, Suzuki N, Hattori A, Kusakabe M. Real-time volumetric imaging of human heart without electrocardiographic gating by 256-detector row computed tomography: initial experience. *J Comput Assist Tomogr* 2005; **29**: 694-698

36 **Sanz J**, Weeks D, Nikolaou K, Sirol M, Rius T, Rajagopalan S, Dellegrottaglie S, Strobeck J, Fuster V, Poon M. Detection of healed myocardial infarction with multidetector-row

computed tomography and comparison with cardiac magnetic resonance delayed hyperenhancement. *Am J Cardiol* 2006; **98**: 149-155

37 **Amado LC**, Schuleri KH, Saliaris AP, Boyle AJ, Helm R, Oskouei B, Centola M, Eneboe V, Young R, Lima JA, Lardo AC, Heldman AW, Hare JM. Multimodality noninvasive imaging demonstrates in vivo cardiac regeneration after mesenchymal stem cell therapy. *J Am Coll Cardiol* 2006; **48**: 2116-2124

38 **Jacquier A**, Boussel L, Amabile N, Bartoli JM, Douek P, Moulin G, Paganelli F, Saeed M, Revel D, Croisille P. Multidetector computed tomography in reperfused acute myocardial infarction. Assessment of infarct size and no-reflow in comparison with cardiac magnetic resonance imaging. *Invest Radiol* 2008; **43**: 773-781

39 **Jacquier A**, Revel D, Saeed M. MDCT of the myocardium: a new contribution to ischemic heart disease. *Acad Radiol* 2008; **15**: 477-487

40 **Klein C**, Nekolla SG, Bengel FM, Momose M, Sammer A, Haas F, Schnackenburg B, Delius W, Mudra H, Wolfram D, Schwaiger M. Assessment of myocardial viability with contrast-enhanced magnetic resonance imaging: comparison with positron emission tomography. *Circulation* 2002; **105**: 162-167

41 **Zamorano J**, Delgado J, Almería C, Moreno R, Gómez Sánchez M, Rodrigo J, Fernández C, Ferreiros J, Rufilanchas J, Sánchez-Harguindey L. Reason for discrepancies in identifying myocardial viability by thallium-201 redistribution, magnetic resonance imaging, and dobutamine echocardiography. *Am J Cardiol* 2002; **90**: 455-459

42 **Kim RJ**, Hillenbrand HB, Judd RM. Evaluation of myocardial viability by MRI. *Herz* 2000; **25**: 417-430

43 **Weiss CR**, Aletras AH, London JF, Taylor JL, Epstein FH, Wassmuth R, Balaban RS, Arai AE. Stunned, infarcted, and normal myocardium in dogs: simultaneous differentiation by using gadolinium-enhanced cine MR imaging with magnetization transfer contrast. *Radiology* 2003; **226**: 723-730

44 **Connelly KA**, Detsky JS, Graham JJ, Paul G, Vijayaragavan R, Dick AJ, Wright GA. Multicontrast late gadolinium enhancement imaging enables viability and wall motion assessment in a single acquisition with reduced scan times. *J Magn Reson Imaging* 2009; **30**: 771-777

45 **Choi KM**, Kim RJ, Gubernikoff G, Vargas JD, Parker M, Judd RM. Transmural extent of acute myocardial infarction predicts long-term improvement in contractile function. *Circulation* 2001; **104**: 1101-1107

46 **Lund GK**, Stork A, Saeed M, Bansmann MP, Gerken JH, Müller V, Mester J, Higgins CB, Adam G, Meinertz T. Acute myocardial infarction: evaluation with first-pass enhancement and delayed enhancement MR imaging compared with 201Tl SPECT imaging. *Radiology* 2004; **232**: 49-57

47 **Sandstede JJ**, Lipke C, Beer M, Harre K, Pabst T, Kenn W, Neubauer S, Hahn D. Analysis of first-pass and delayed contrast-enhancement patterns of dysfunctional myocardium on MR imaging: use in the prediction of myocardial viability. *AJR Am J Roentgenol* 2000; **174**: 1737-1740

48 **Kwong RY**, Yucel EK. Cardiology patient pages. Computed tomography scan and magnetic resonance imaging. *Circulation* 2003; **108**: e104-e106

49 **Tarantini G**, Razzolini R, Cacciavillani L, Bilato C, Sarais C, Corbetti F, Marra MP, Napodano M, Ramondo A, Iliceto S. Influence of transmurality, infarct size, and severe microvascular obstruction on left ventricular remodeling and function after primary coronary angioplasty. *Am J Cardiol* 2006; **98**: 1033-1040

50 **Roes SD**, Kelle S, Kaandorp TA, Kokocinski T, Poldermans D, Lamb HJ, Boersma E, van der Wall EE, Fleck E, de Roos A, Nagel E, Bax JJ. Comparison of myocardial infarct size assessed with contrast-enhanced magnetic resonance imaging and left ventricular function and volumes to predict mortality in patients with healed myocardial infarction. *Am J Cardiol* 2007; **100**: 930-936

51 **Abdel-Aty H**, Zagrosek A, Schulz-Menger J, Taylor AJ, Messroghli D, Kumar A, Gross M, Dietz R, Friedrich MG. Delayed enhancement and T2-weighted cardiovascular magnetic resonance imaging differentiate acute from chronic myocardial infarction. *Circulation* 2004; **109**: 2411-2416

52 **Saeed M**, Weber O, Lee R, Do L, Martin A, Saloner D, Ursell P, Robert P, Corot C, Higgins CB. Discrimination of myocardial acute and chronic (scar) infarctions on delayed contrast enhanced magnetic resonance imaging with intravascular magnetic resonance contrast media. *J Am Coll Cardiol* 2006; **48**: 1961-1968

53 **Nieman K**, Shapiro MD, Ferencik M, Nomura CH, Abbara S, Hoffmann U, Gold HK, Jang IK, Brady TJ, Cury RC. Reperfused myocardial infarction: contrast-enhanced 64-Section CT in comparison to MR imaging. *Radiology* 2008; **247**: 49-56

54 **Nikolaou K**, Flohr T, Knez A, Rist C, Wintersperger B, Johnson T, Reiser MF, Becker CR. Advances in cardiac CT imaging: 64-slice scanner. *Int J Cardiovasc Imaging* 2004; **20**: 535-540

55 **Dick AJ**, Lederman RJ. MRI-guided myocardial cell therapy. *Int J Cardiovasc Intervent* 2005; **7**: 165-170

56 **Dicks D**, Saloner D, Martin A, Carlsson M, Saeed M. Percutaneous transendocardial VEGF gene therapy: MRI guided delivery and characterization of 3D myocardial strain. *Int J Cardiol* 2009; :

57 **Hill JM**, Dick AJ, Raman VK, Thompson RB, Yu ZX, Hinds KA, Pessanha BS, Guttman MA, Varney TR, Martin BJ, Dunbar CE, McVeigh ER, Lederman RJ. Serial cardiac magnetic resonance imaging of injected mesenchymal stem cells. *Circulation* 2003; **108**: 1009-1014

58 **Saeed M**, Martin A, Jacquier A, Bucknor M, Saloner D, Do L, Ursell P, Su H, Kan YW, Higgins CB. Permanent coronary artery occlusion: cardiovascular MR imaging is platform for percutaneous transendocardial delivery and assessment of gene therapy in canine model. *Radiology* 2008; **249**: 560-571

59 **Saeed M**, Martin A, Ursell P, Do L, Bucknor M, Higgins CB, Saloner D. MR assessment of myocardial perfusion, viability, and function after intramyocardial transfer of VM202, a new plasmid human hepatocyte growth factor in ischemic swine myocardium. *Radiology* 2008; **249**: 107-118

60 **Saeed M**, Saloner D, Martin A, Do L, Weber O, Ursell PC, Jacquier A, Lee R, Higgins CB. Adeno-associated viral vector-encoding vascular endothelial growth factor gene: effect on cardiovascular MR perfusion and infarct resorption measurements in swine. *Radiology* 2007; **243**: 451-460

61 **Carlsson M**, Wilson M, Martin AJ, Saeed M. Myocardial microinfarction after coronary microembolization in swine: MR imaging characterization. *Radiology* 2009; **250**: 703-713

62 **Jacquier A**, Higgins CB, Martin AJ, Do L, Saloner D, Saeed M. Injection of adeno-associated viral vector encoding vascular endothelial growth factor gene in infarcted swine myocardium: MR measurements of left ventricular function and strain. *Radiology* 2007; **245**: 196-205

63 **Saeed M**, Martin AJ, Lee RJ, Weber O, Revel D, Saloner D, Higgins CB. MR guidance of targeted injections into border and core of scarred myocardium in pigs. *Radiology* 2006; **240**: 419-426

64 **Weinreb JC**, Abu-Alfa AK. Gadolinium-based contrast agents and nephrogenic systemic fibrosis: why did it happen and what have we learned? *J Magn Reson Imaging* 2009; **30**: 1236-1239

65 **Keeley EC**, Boura JA, Grines CL. Primary angioplasty versus intravenous thrombolytic therapy for acute myocardial infarction: a quantitative review of 23 randomised trials. *Lancet* 2003; **361**: 13-20

66 **Kloner RA**, Rude RE, Carlson N, Maroko PR, DeBoer LW, Braunwald E. Ultrastructural evidence of microvascular damage and myocardial cell injury after coronary artery occlusion: which comes first? *Circulation* 1980; **62**: 945-952

67 **Gibson CM**, Cannon CP, Daley WL, Dodge JT Jr, Alexander B Jr, Marble SJ, McCabe CH, Raymond L, Fortin T, Poole WK, Braunwald E. TIMI frame count: a quantitative method of assessing coronary artery flow. *Circulation* 1996; **93**: 879-888

68 **Ito H**, Taniyama Y, Iwakura K, Nishikawa N, Masuyama T, Kuzuya T, Hori M, Higashino Y, Fujii K, Minamino T. Intravenous nicorandil can preserve microvascular integrity and myocardial viability in patients with reperfused anterior wall myocardial infarction. *J Am Coll Cardiol* 1999; **33**: 654-660

69 **Gibson CM**, Murphy SA, Rizzo MJ, Ryan KA, Marble SJ, McCabe CH, Cannon CP, Van de Werf F, Braunwald E. Relationship between TIMI frame count and clinical outcomes after thrombolytic administration. Thrombolysis In Myocardial Infarction (TIMI) Study Group. *Circulation* 1999; **99**: 1945-1950

70 **Iwakura K**, Ito H, Takiuchi S, Taniyama Y, Nakatsuchi Y, Negoro S, Higashino Y, Okamura A, Masuyama T, Hori M, Fujii K, Minamino T. Alternation in the coronary blood flow velocity pattern in patients with no reflow and reperfused acute myocardial infarction. *Circulation* 1996; **94**: 1269-1275

71 **Rochitte CE**, Lima JA, Bluemke DA, Reeder SB, McVeigh ER, Furuta T, Becker LC, Melin JA. Magnitude and time course of microvascular obstruction and tissue injury after acute myocardial infarction. *Circulation* 1998; **98**: 1006-1014

72 **Wu KC**, Zerhouni EA, Judd RM, Lugo-Olivieri CH, Barouch LA, Schulman SP, Blumenthal RS, Lima JA. Prognostic significance of microvascular obstruction by magnetic resonance imaging in patients with acute myocardial infarction. *Circulation* 1998; **97**: 765-772

73 **Hombach V**, Grebe O, Merkle N, Waldenmaier S, Höher M, Kochs M, Wöhrle J, Kestler HA. Sequelae of acute myocardial infarction regarding cardiac structure and function and their prognostic significance as assessed by magnetic resonance imaging. *Eur Heart J* 2005; **26**: 549-557

74 **Gerber BL**, Rochitte CE, Melin JA, McVeigh ER, Bluemke DA, Wu KC, Becker LC, Lima JA. Microvascular obstruction and left ventricular remodeling early after acute myocardial infarction. *Circulation* 2000; **101**: 2734-2741

75 **Ito H**, Maruyama A, Iwakura K, Takiuchi S, Masuyama T, Hori M, Higashino Y, Fujii K, Minamino T. Clinical implications of the 'no reflow' phenomenon. A predictor of complications and left ventricular remodeling in reperfused anterior wall myocardial infarction. *Circulation* 1996; **93**: 223-228

76 **Topol EJ**, Yadav JS. Recognition of the importance of embolization in atherosclerotic vascular disease. *Circulation* 2000; **101**: 570-580

77 **Ørn S**, Manhenke C, Greve OJ, Larsen AI, Bonarjee VV, Edvardsen T, Dickstein K. Microvascular obstruction is a major determinant of infarct healing and subsequent left ventricular remodelling following primary percutaneous coronary intervention. *Eur Heart J* 2009; **30**: 1978-1985

78 **Mewton N**, Bonnefoy E, Revel D, Ovize M, Kirkorian G, Croisille P. Presence and extent of cardiac magnetic resonance microvascular obstruction in reperfused non-ST-elevated myocardial infarction and correlation with infarct size and myocardial enzyme release. *Cardiology* 2009; **113**: 50-58

79 **Nijveldt R**, Hofman MB, Hirsch A, Beek AM, Umans VA, Algra PR, Piek JJ, van Rossum AC. Assessment of microvascular obstruction and prediction of short-term remodeling after acute myocardial infarction: cardiac MR imaging study. *Radiology* 2009; **250**: 363-370

80 **Saeed M**, Higgins CB, Geschwind JF, Wendland MF. T1-relaxation kinetics of extracellular, intracellular and intravascular MR contrast agents in normal and acutely reperfused infarcted myocardium using echo-planar MR imaging. *Eur Radiol* 2000; **10**: 310-318

81 **van den Bos EJ**, Baks T, Moelker AD, Kerver W, van Geuns RJ, van der Giessen WJ, Duncker DJ, Wielopolski PA. Magnetic resonance imaging of haemorrhage within reperfused myocardial infarcts: possible interference with iron oxide-labelled cell tracking? *Eur Heart J* 2006; **27**: 1620-1626

82 **O'Regan DP**, Ahmed R, Karunanithy N, Neuwirth C, Tan Y, Durighel G, Hajnal JV, Nadra I, Corbett SJ, Cook SA. Reperfusion hemorrhage following acute myocardial infarction: assessment with T2* mapping and effect on measuring the area at risk. *Radiology* 2009; **250**: 916-922

83 **Ganame J**, Messalli G, Dymarkowski S, Rademakers FE, Desmet W, Van de Werf F, Bogaert J. Impact of myocardial haemorrhage on left ventricular function and remodelling in patients with reperfused acute myocardial infarction. *Eur Heart J* 2009; **30**: 1440-1449

84 **Arheden H**, Saeed M, Higgins CB, Gao DW, Bremerich J, Wyttenbach R, Dae MW, Wendland MF. Measurement of the distribution volume of gadopentetate dimeglumine at echo-planar MR imaging to quantify myocardial infarction: comparison with 99mTc-DTPA autoradiography in rats. *Radiology* 1999; **211**: 698-708

85 **Saeed M**, Wendland MF, Masui T, Connolly AJ, Derugin N, Brasch RC, Higgins CB. Myocardial infarction: assessment with an intravascular MR contrast medium. Work in progress. *Radiology* 1991; **180**: 153-160

86 **Dymarkowski S**, Ni Y, Miao Y, Bogaert J, Rademakers F, Bosmans H, Marchal G. Value of t2-weighted magnetic resonance imaging early after myocardial infarction in dogs: comparison with bis-gadolinium-mesoporphyrin enhanced T1-weighted magnetic resonance imaging and functional data from cine magnetic resonance imaging. *Invest Radiol* 2002; **37**: 77-85

87 **Krombach GA**, Higgins CB, Chujo M, Saeed M. Blood pool contrast-enhanced MRI detects suppression of microvascular permeability in early postinfarction reperfusion after nicorandil therapy. *Magn Reson Med* 2002; **47**: 896-902

88 **Saeed M**, Lund G, Wendland MF, Bremerich J, Weinmann H, Higgins CB. Magnetic resonance characterization of the peri-infarction zone of reperfused myocardial infarction with necrosis-specific and extracellular nonspecific contrast media. *Circulation* 2001; **103**: 871-876

89 **Jackson BM**, Gorman JH 3rd, Salgo IS, Moainie SL, Plappert T, St John-Sutton M, Edmunds LH Jr, Gorman RC. Border zone geometry increases wall stress after myocardial infarction: contrast echocardiographic assessment. *Am J Physiol Heart Circ Physiol* 2003; **284**: H475-H479

90 **Van Leuven SL**, Waldman LK, McCulloch AD, Covell JW. Gradients of epicardial strain across the perfusion boundary during acute myocardial ischemia. *Am J Physiol* 1994; **267**: H2348-H2362

91 **Pennell D**. Myocardial salvage: retrospection, resolution, and radio waves. *Circulation* 2006; **113**: 1821-1823

92 **Schmidt A**, Azevedo CF, Cheng A, Gupta SN, Bluemke DA, Foo TK, Gerstenblith G, Weiss RG, Marbán E, Tomaselli GF, Lima JA, Wu KC. Infarct tissue heterogeneity by magnetic resonance imaging identifies enhanced cardiac arrhythmia susceptibility in patients with left ventricular dysfunction. *Circulation* 2007; **115**: 2006-2014

93 **Yan AT**, Shayne AJ, Brown KA, Gupta SN, Chan CW, Luu TM, Di Carli MF, Reynolds HG, Stevenson WG, Kwong RY. Characterization of the peri-infarct zone by contrast-enhanced cardiac magnetic resonance imaging is a powerful predictor of post-myocardial infarction mortality. *Circulation* 2006; **114**: 32-39

94 **Saeed M**, Bremerich J, Wendland MF, Wyttenbach R, Weinmann HJ, Higgins CB. Reperfused myocardial infarction as seen with use of necrosis-specific versus standard extracellular MR contrast media in rats. *Radiology* 1999; **213**: 247-257

95 **Rubenstein JC**, Ortiz JT, Wu E, Kadish A, Passman R, Bonow

RO, Goldberger JJ. The use of periinfarct contrast-enhanced cardiac magnetic resonance imaging for the prediction of late postmyocardial infarction ventricular dysfunction. *Am Heart J* 2008; **156**: 498-505

96 **Rodríguez-Sinovas A**, Abdallah Y, Piper HM, Garcia-Dorado D. Reperfusion injury as a therapeutic challenge in patients with acute myocardial infarction. *Heart Fail Rev* 2007; **12**: 207-216

97 **Dong Z**, Saikumar P, Weinberg JM, Venkatachalam MA. Calcium in cell injury and death. *Annu Rev Pathol* 2006; **1**: 405-434

98 **Saeed M**, Lee RJ, Weber O, Do L, Martin A, Ursell P, Saloner D, Higgins CB. Scarred myocardium imposes additional burden on remote viable myocardium despite a reduction in the extent of area with late contrast MR enhancement. *Eur Radiol* 2006; **16**: 827-836

99 **Hashimoto T**, Kambara H, Fudo T, Tamaki S, Nohara R, Takatsu Y, Hattori R, Tokunaga S, Kawai C. Early estimation of acute myocardial infarct size soon after coronary reperfusion using emission computed tomography with technetium-99m pyrophosphate. *Am J Cardiol* 1987; **60**: 952-957

100 **Wheelan K**, Wolfe C, Corbett J, Rude RE, Winniford M, Parkey RW, Buja LM, Willerson JT. Early positive technetium-99m stannous pyrophosphate images as a marker of reperfusion after thrombolytic therapy for acute myocardial infarction. *Am J Cardiol* 1985; **56**: 252-256

101 **Mahnken AH**, Koos R, Katoh M, Wildberger JE, Spuentrup E, Buecker A, Günther RW, Kühl HP. Assessment of myocardial viability in reperfused acute myocardial infarction using 16-slice computed tomography in comparison to magnetic resonance imaging. *J Am Coll Cardiol* 2005; **45**: 2042-2047

102 **Carlsson M**, Ursell PC, Saloner D, Saeed M. Multidetector computed tomography for characterization of calcium deposits in reperfused myocardial infarction. *Acta Radiol* 2009; **50**: 396-405

103 **Antoniucci D**, Valenti R, Migliorini A, Moschi G, Parodi G, Dovellini EV, Bolognese L, Santoro GM. Comparison of impact of emergency percutaneous revascularization on outcome of patients > or =75 to those < 75 years of age with acute myocardial infarction complicated by cardiogenic shock. *Am J Cardiol* 2003; **91**: 1458-1461, A6

104 **Bolognese L**, Carrabba N, Santoro GM, Valenti R, Buonamici P, Antoniucci D. Angiographic findings, time course of regional and global left ventricular function, and clinical outcome in diabetic patients with acute myocardial infarction treated with primary percutaneous transluminal coronary angioplasty. *Am J Cardiol* 2003; **91**: 544-549

105 **Hardoff R**, Shefer A, Gips S, Merdler A, Flugelman MY, Halon DA, Lewis BS. Predicting late restenosis after coronary angioplasty by very early (12 to 24 h) thallium-201 scintigraphy: implications with regard to mechanisms of late coronary restenosis. *J Am Coll Cardiol* 1990; **15**: 1486-1492

106 **Wijns W**, Serruys PW, Reiber JH, de Feyter PJ, van den Brand M, Simoons ML, Hugenholtz PG. Early detection of restenosis after successful percutaneous transluminal coronary angioplasty by exercise-redistribution thallium scintigraphy. *Am J Cardiol* 1985; **55**: 357-361

107 **Holmes DR Jr**. Very early prediction of restenosis after successful coronary angioplasty: how early is early and can we identify it? *J Am Coll Cardiol* 1990; **15**: 265-266

108 **Rodés-Cabau J**, Candell-Riera J, Domingo E, Castell-Conesa J, Anívarro I, Angel J, Aguadé-Bruix S, Padilla F, Soto A, Soler-Soler J. Frequency and clinical significance of myocardial ischemia detected early after coronary stent implantation. *J Nucl Med* 2001; **42**: 1768-1772

109 **Jaffe R**, Haim SB, Karkabi B, Front A, Gips S, Weisz G, Khader N, Merdler A, Flugelman MY, Halon DA, Lewis BS. Myocardial perfusion abnormalities early (12-24 h) after coronary stenting or balloon angioplasty: implications regarding pathophysiology and late clinical outcome. *Cardiology* 2002; **98**: 60-66

110 **Bahrmann P**, Werner GS, Heusch G, Ferrari M, Poerner TC, Voss A, Figulla HR. Detection of coronary microembolization by Doppler ultrasound in patients with stable angina pectoris undergoing elective percutaneous coronary interventions. *Circulation* 2007; **115**: 600-608

111 **Skyschally A**, Schulz R, Erbel R, Heusch G. Reduced coronary and inotropic reserves with coronary microembolization. *Am J Physiol Heart Circ Physiol* 2002; **282**: H611-H614

112 **Porto I**, Selvanayagam JB, Van Gaal WJ, Prati F, Cheng A, Channon K, Neubauer S, Banning AP. Plaque volume and occurrence and location of periprocedural myocardial necrosis after percutaneous coronary intervention: insights from delayed-enhancement magnetic resonance imaging, thrombolysis in myocardial infarction myocardial perfusion grade analysis, and intravascular ultrasound. *Circulation* 2006; **114**: 662-669

113 **Anderson JL**, Adams CD, Antman EM, Bridges CR, Califf RM, Casey DE Jr, Chavey WE 2nd, Fesmire FM, Hochman JS, Levin TN, Lincoff AM, Peterson ED, Theroux P, Wenger NK, Wright RS, Smith SC Jr, Jacobs AK, Adams CD, Anderson JL, Antman EM, Halperin JL, Hunt SA, Krumholz HM, Kushner FG, Lytle BW, Nishimura R, Ornato JP, Page RL, Riegel B. ACC/AHA 2007 guidelines for the management of patients with unstable angina/non-ST-Elevation myocardial infarction: a report of the American College of Cardiology/American Heart Association Task Force on Practice Guidelines (Writing Committee to Revise the 2002 Guidelines for the Management of Patients With Unstable Angina/Non-ST-Elevation Myocardial Infarction) developed in collaboration with the American College of Emergency Physicians, the Society for Cardiovascular Angiography and Interventions, and the Society of Thoracic Surgeons endorsed by the American Association of Cardiovascular and Pulmonary Rehabilitation and the Society for Academic Emergency Medicine. *J Am Coll Cardiol* 2007; **50**: e1-e157

114 **Carlsson M**, Martin AJ, Ursell PC, Saloner D, Saeed M. Magnetic resonance imaging quantification of left ventricular dysfunction following coronary microembolization. *Magn Reson Med* 2009; **61**: 595-602

115 **Nassenstein K**, Breuckmann F, Bucher C, Kaiser G, Konorza T, Schäfer L, Konietzka I, de Greiff A, Heusch G, Erbel R, Barkhausen J. How much myocardial damage is necessary to enable detection of focal late gadolinium enhancement at cardiac MR imaging? *Radiology* 2008; **249**: 829-835

116 **Breuckmann F**, Nassenstein K, Bucher C, Konietzka I, Kaiser G, Konorza T, Naber C, Skyschally A, Gres P, Heusch G, Erbel R, Barkhausen J. Systematic analysis of functional and structural changes after coronary microembolization: a cardiac magnetic resonance imaging study. *JACC Cardiovasc Imaging* 2009; **2**: 121-130

117 **Selvanayagam JB**, Cheng AS, Jerosch-Herold M, Rahimi K, Porto I, van Gaal W, Channon KM, Neubauer S, Banning AP. Effect of distal embolization on myocardial perfusion reserve after percutaneous coronary intervention: a quantitative magnetic resonance perfusion study. *Circulation* 2007; **116**: 1458-1464

118 **Ricciardi MJ**, Wu E, Davidson CJ, Choi KM, Klocke FJ, Bonow RO, Judd RM, Kim RJ. Visualization of discrete microinfarction after percutaneous coronary intervention associated with mild creatine kinase-MB elevation. *Circulation* 2001; **103**: 2780-2783

119 **Choi JW**, Gibson CM, Murphy SA, Davidson CJ, Kim RJ, Ricciardi MJ. Myonecrosis following stent placement: association between impaired TIMI myocardial perfusion grade and MRI visualization of microinfarction. *Catheter Cardiovasc Interv* 2004; **61**: 472-476

120 **Selvanayagam JB**, Porto I, Channon K, Petersen SE, Francis

JM, Neubauer S, Banning AP. Troponin elevation after percutaneous coronary intervention directly represents the extent of irreversible myocardial injury: insights from cardiovascular magnetic resonance imaging. *Circulation* 2005; **111**: 1027-1032

121 **Caraballo V**. Fatal myocardial infarction resulting from coronary artery septic embolism after abortion: unusual cause and complication of endocarditis. *Ann Emerg Med* 1997; **29**: 175-177

122 **Garg RK**, Jolly N. Acute myocardial infarction secondary to thromboembolism in a patient with atrial fibrillation. *Int J Cardiol* 2007; **123**: e18-e20

123 **Quinn EG**, Fergusson DJ. Coronary embolism following aortic and mitral valve replacement: successful management with abciximab and urokinase. *Cathet Cardiovasc Diagn* 1998; **43**: 457-459

124 **Takenaka T**, Horimoto M, Igarashi K, Yoshie H, Tsujino I, Morihira M. Multiple coronary thromboemboli complicating valvular heart disease and atrial fibrillation. *Am Heart J* 1996; **131**: 194-196

125 **Yutani C**, Imakita M, Ueda-Ishibashi H, Katsuragi M, Fujita H. Coronary artery embolism with special reference to invasive procedures as the source. *Mod Pathol* 1992; **5**: 244-249

126 **Erbel R**. Spontaneous and interventional coronary microembolisation. *Heart* 2003; **89**: 986-989

127 **Mandell BF**. Cardiovascular involvement in systemic lupus erythematosus. *Semin Arthritis Rheum* 1987; **17**: 126-141

128 **Westwood MA**, Shah F, Anderson LJ, Strange JW, Tanner MA, Maceira AM, Howard J, Porter JB, Walker JM, Wonke B, Pennell DJ. Myocardial tissue characterization and the role of chronic anemia in sickle cell cardiomyopathy. *J Magn Reson Imaging* 2007; **26**: 564-568

129 **Bello D**, Fieno DS, Kim RJ, Pereles FS, Passman R, Song G, Kadish AH, Goldberger JJ. Infarct morphology identifies patients with substrate for sustained ventricular tachycardia. *J Am Coll Cardiol* 2005; **45**: 1104-1108

130 **Carlsson M**, Saloner D, Martin A, Ursell P, Saeed M. Heterogeneous microinfarcts caused by coronary microemboli: Evaluation with multidetector CT and MR imaging in swine model. *Radiology* 2010; In press

S- Editor Wang JL **L- Editor** Webster JR **E- Editor** Zheng XM

World Journal of Radiology

Online Submissions: http://www.wjgnet.com/1949-8470office
wjr@wjgnet.com
doi:10.4329/wjr.v2.i1.15

World J Radiol 2010 January 28; 2(1): 15-31
ISSN 1949-8470 (online)

TOPIC HIGHLIGHT

Hui-Xiong Xu, MD, PhD, *Series Editor*

Contrast enhanced ultrasound of renal masses

Andre Ignee, Bernd Straub, Gudrun Schuessler, Christoph Frank Dietrich

Andre Ignee, Gudrun Schuessler, Christoph Frank Dietrich, 2nd Department of Internal Medicine, Caritas Krankenhaus, Uhlandstrasse 7, 97980 Bad Mergentheim, Germany
Bernd Straub, Department of Urology, Caritas Krankenhaus, 97980 Bad Mergentheim, Germany
Author contributions: All authors contributed to this article.
Correspondence to: Christoph Frank Dietrich, Professor, 2nd Department of Internal Medicine, Caritas Krankenhaus, Uhlandstrasse 7, 97980 Bad Mergentheim, Germany. christoph.dietrich@ckbm.de
Telephone: +49-7931-582201 Fax: +49-7931-582290
Received: December 19, 2009 Revised: January 20, 2010
Accepted: January 22, 2010
Published online: January 28, 2010

Abstract

Contrast enhanced ultrasound (CEUS) has gained clinical importance over the last years for the characterization of hepatic masses. Its role in extrahepatic indications has been investigated repeatedly but has been less comprehensively studied. Currently more than 50% of renal masses are incidentally diagnosed, mostly by B-mode ultrasound. The method of choice for characterization of renal lesions is contrast enhanced computed tomography (CECT). In the case of cystic lesions CECT refers to the Bosniak classification for cystic lesions to assess the risk of malignant behavior. The majority of masses are renal cell carcinoma, but the exact proportion is controversial. Disadvantages of CECT are a significant risk for patients with impaired renal function, allergic reactions and hyperthyroidism due to iodinated contrast agents. Several studies concerning CEUS for the characterization of both solid and cystic renal lesions have been published, but prospective multicenter studies are missing, the presented data being mainly descriptive. The aim of the this manuscript is to review the current literature for CEUS in renal masses, to summarize the available data and focus on possible concepts for studies in the future.

Key words: Contrast enhanced ultrasound; Renal cell carcinoma; Angiomyolipoma; Oncocytoma; Sonovue; Biopsy

Peer reviewers: Herwig R Cerwenka, Professor, MD, Department of Surgery, Medical University of Graz, Auenbruggerplatz 29, A-8036 Graz, Austria; Yasunori Minami, MD, PhD, Division of Gastroenterology and Hepatology, Department of Internal Medicine, 377-2 Ohno-higashi Osaka-sayama Osaka 589-8511, Japan

Ignee A, Straub B, Schuessler G, Dietrich CF. Contrast enhanced ultrasound of renal masses. *World J Radiol* 2010; 2(1): 15-31 Available from: URL: http://www.wjgnet.com/1949-8470/full/v2/i1/15.htm DOI: http://dx.doi.org/10.4329/wjr.v2.i1.15

INTRODUCTION

Ultrasound (US) is the most frequently used imaging method since it is inexpensive, has no side effects and is widely available. The majority of asymptomatically diagnosed renal tumors are detected by US. Nevertheless, to date the standard method for staging purposes is contrast enhanced computed tomography (CECT). Contrast enhanced US (CEUS) has been introduced for diagnostic imaging in the liver, heart, pancreas, trauma and several other organs. Contrast agents are used for CECT and magnetic resonance imaging (MRI) techniques, and increase the sensitivity and specificity of these techniques. US contrast agents have been introduced relatively recently. They consist of microbubbles with a size similar to an erythrocyte. They resonate in the US beam and change the backscattered wave resulting in both an enhancement and a change in the waveform. This enables a selective presentation of contrast information. Both agents are usually given in a single bolus followed by a rapid saline flush intravenously, but extravascular use

has been described[1]. Whereas SHU 508A (Levovist®), a first generation contrast agent has some affinity with the reticuloendothelial system, BR1 (Sonovue®), a second generation contrast agent is a strictly vascular contrast agent. In contrast to SHU 508A, BR1 allows real time imaging because of the higher stability of the microbubbles, which contain an inert gas. Studies using SHU 508A could be confirmed with BR1.

Detection and characterization of focal liver lesions are the single most important application of CEUS in the abdomen[2,3]. CEUS now equals CECT, and in some instances exceeds it, in accuracy. Its use for renal evaluation has been less comprehensively studied. Several studies indicate also a role for CEUS in the characterization of renal masses and renal cell carcinoma (RCC) but the results are controversial[4]. The aim of this study is to analyze the role of CEUS in renal masses referring to the literature and our own experience.

RENAL MASSES

Cancer of the kidney represents about 2% of human all cancers. In Africa and Asia the incidence is lower than in Northern America and Western Europe. The incidence and detection of asymptomatic renal masses has increased over the last 25 years - e.g. by 38% in the United States of America between 1974 and 1990. Apart from an increase in average body weight and other risk factors, this is the result of improved imaging technology as well as improved understanding of the clinical and pathological findings of RCC[5-9]. It can be shown that the survival rate has improved over the years as a result of earlier diagnosis[7,10-12]. To date, most (61%) renal masses are found incidentally[13]. From the diagnostic point of view, in the case of a focal renal lesion, the following entities must be taken into account (Figure 1): neoplastic lesions, non-neoplastic lesions or masses (e.g. inflammatory, traumatic, ischemic lesions, simple and complicated non neoplastic cysts), and pseudotumors/lesions.

Neoplastic lesions can be divided into primary lesions that originate from the renal parenchyma or from the urinary system in the renal pelvis, and secondary lesions such as metastases, lymphoma, plasmocytoma, leukemia, and lesions close to the renal parenchyma e.g. urothelial/transitional cell carcinoma, adrenal lesions, and retroperitoneal lesions which mimic true renal lesions. The World Health Organization (WHO) distinguishes primary tumors of the kidney into renal cell tumors, metanephric tumors, nephroblastic tumors, mesenchymal tumors, neural/neuroendocrine tumors, hemotologic lesions, germ cell tumors.

In the following section the most frequent renal lesions (renal cell carcinoma, angiomyolipoma (AML), oncocytoma, renal adenoma) are presented. Table 1 presents an overview of rare renal tumors according to the current WHO classification.

Malignant tumors

Renal cell carcinoma: Renal cell lesions can be separated into RCC with its several subtypes, papillary adenoma and oncocytoma. This strict pathological organization is not suitable for imaging purposes. The majority of masses seen in imaging methods consist of renal cell tumors (RCC, oncocytomas, cystic lesions), metanephric tumors (metanephric adenomas), mesenchymal tumors (AML), secondary lesions (e.g. metastases), and inflammatory lesions.

The typical triad of flank pain, hematuria and flank mass is uncommon (about 10%) and is a sign of an advanced stage of disease. Syndromes such as hypercalcemia, Stauffer syndrome, anemia, and cachexia are frequently caused by metastatic lesions or paraneoplastic syndromes[14].

In 4%-22% of autopsied corpses small renal lesions are found which are malignant or pre-malignant. Patients are a mean of 65 years old at the time of diagnosis of RCC, and the majority is older than 40 years[15]. In up to 20% of RCC > 3 cm, synchronous RCC are found in the same kidney. Even small tumors grow in size and metastasize and there is a benefit for the patients if they undergo surgery at an early stage[7,16-21].

RCC are reported to grow at a rate of about 0.4 cm per year[17,22], but this depends on the size of the lesion. In a retrospectively reviewed series of 63 consecutive patients with observational treatment for renal cancer (mean age 77 years) with a mean tumor size of 4.3 cm, there was a 5-year cancer-specific survival of 93% and an overall survival of 43%. The mean annual growth rate was < 1 cm in 85% of cases. In patients with tumors ≤ 4 cm only 4% had a growth rate of > 1 cm/year but this was significantly higher for lesions > 4 cm. The authors conclude that observational strategies for small RCC in older and comorbid patients can give acceptable results in a period of 5 years[23].

Radical nephrectomy has been the standard for treatment of RCC. The parenchyma-sparing therapy proved to have a survival rate comparable to that for nephrectomy and is now considered to be the method of choice for small lesions. Arguments against this therapeutic approach are that 7%-11% of tumors appear multifocally and the local tumor recurrence rate is 4%-10%[24]. The rate of multicentricity for tumors ≤ 3 cm has been shown to be less than 3%. Thus parenchyma-sparing surgery should be considered when a small tumor is confined to the renal parenchyma and is encapsulated[25].

RCC can be divided into 4 subtypes, each developing from a different origin cell: clear cell RCC, papillary RCC, chromophobic RCC and collecting duct RCC. Clear cell RCC is the most frequent subtype of RCC. Multilocular (cystic) RCC consist entirely of cysts and the number of clear cell carcinoma cells is small whereas cysts in ordinary RCC are frequent; it cannot be distinguished from cystic clear cell RCC and should, therefore, be resected. Papillary RCC comprise 10% of RCC. Bilaterality is more frequent than in other RCC. There is a hereditary type, where multiple microscopic tumors

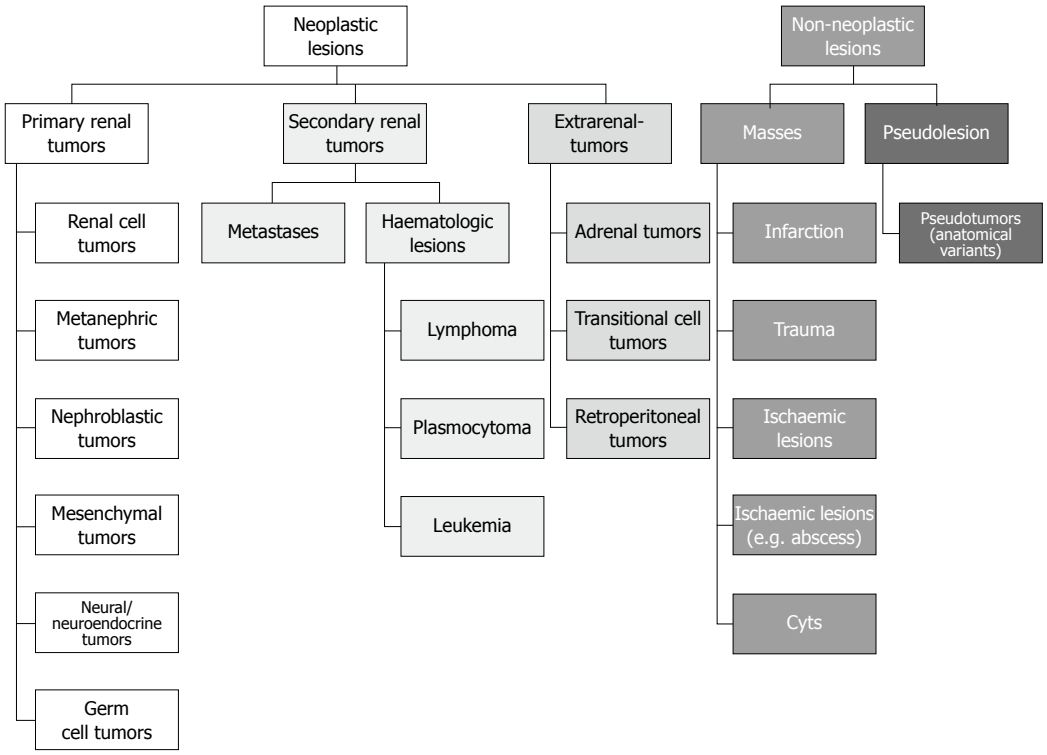

Figure 1 Differential diagnosis of renal masses.

are described. In angiographic studies, hypovascularity has been demonstrated which could be reproduced by CECT[26,27]. Chromophobe RCC comprises about 5% of RCC. A hereditary form exists also, and most of the tumors have a good prognosis. Typically, they are large and do not show necrosis or calcification. RCC of the collecting ducts of Bellini are a rare entity. Most patients show metastasis at the time of diagnosis. Renal medullary carcinoma is a rare entity as well. Those tumors are typically seen in young people with sickle cell disease; the prognosis is poor. Other rare entities are: (1) RCC associated with Xp11.2 translocations/TFE3 gene fusions; (2) RCC associated with neuroblastoma which appear in long term survivors of childhood neuroblastoma; (3) mucinous RCC; and (4) spindle cell RCC.

Unclassified RCC appear in 5% of patients in surgical series. This category contains tumors with varied appearances and sometimes a sarcomatoid change is found.

Bilateral RCC appear in about 5% of all patients with RCC. They are hereditary in about 10% (von-Hippel-Lindau-disease, hereditary papillary RCC, hereditary clear cell RCC). Bilateral oncocytomas are described also. The survival rate is similar to that of patients with singular RCC. Metachronous lesions can appear years later[28].

Metastases and lymphomas

Typically renal metastases are detected when a nonrenal malignancy progresses[29], and the median survival is low when renal metastases occur[30]. However, patients can present with a single renal metastasis without symptoms of tumor progression in follow-up investigations after a long period of stable disease[31,32]. Renal metastases from bronchogenic carcinoma, breast cancer, colon cancer, esophageal cancer, hepatocellular carcinoma, pancreatic adenocarcinoma, prostatic cancer, follicular and papillary thyroid carcinoma have been reported[32-39].

Secondary renal lymphomas are 30-fold more frequent than primary renal lymphoma without evidence of systemic involvement. They are mostly present in the advanced stages of the disease. Also, a plasmocytoma can occur as a manifestation of a disseminated multiple myeloma. In contrast to RCC metastases are suggestive if they show the following imaging features: (1) < 3 cm; (2) not totally spheric, sometimes wedge-shaped; (3) signs of "infiltrative" growth; (4) bilateral multiple; (5) no encapsulation; and (6) no calcification[40-42].

They often appear hypoenhanced in contrast enhanced studies[29]. The group around Lassau and Lamuraglia were able to monitor the response of advanced RCC to antiangiogenetic therapy with Sorafenib in a heterogeneous group including 2/30 patients (7%) with contralateral renal metastases. Nevertheless, there was no description of the enhancement pattern in CEUS before therapy. The group suggested quantitative CEUS for monitoring antiangiogenetic drug effectiveness which has been also proposed by our group[43]. In our experience, metastases in CEUS are typically hypovascular in more than 80% of cases. Since metastases typically do represent advanced tumor stages histologically proven elsewhere, we can only refer to one histologically proven metastasis in our patients which was hypoenhancing both in the arterial and late phase (unpublished data).

Table 1 Rare renal tumors according to the current WHO classification[76]

Entity	Dignity	Clinical meaning
Renal cell tumors		
RCC associated with neuroblastoma	Malignant	Long term survivors of childhood neuroblastoma
Nephroblastic tumors		
Nephroblastoma	Malignant	Malignant embryonal neoplasm; 1:8000 children, 98% < 10 yr; if treated excellent prognosis = Wilm's tumor
Nephrogenic rests and nephroblastomatosis	Malignant potential	Nephrogenic rests in 1% of infant autopsies; possible transformation into nephroblastoma
Mesenchymal tumors in children		
Ossifying renal tumor of infants	Benign	12 cases reported, mostly in children < 18 mo
Clear cell sarcoma	Malignant	Typically bone metastasis, metastases can develop late
Rhabdoid tumor	Malignant	Highly invasive; 80% ⩽ 2 yr; 2 yr survival rate < 20%
Congenital mesoblastic nephroma	Malignant	Excellent prognosis when completely excised; recurrence rate 5%; metastases in rare cases
Mesenchymal tumors in adults		
Leiomyoma	Benign	Arises typically from the renal capsule; incidental tumors < 10 mm, but sometimes large
Hemangioma	Benign	No mitosis and nuclear pleomorphism
Lymphangioma	Benign	Presenting as a peripelvic or renal sinus mass. Some cases may develop secondary to inflammatory lower urinary tract diseases; cystic
Juxtaglomerular cell tumor	Benign	Benign rennin-secreting tumor → hypertension; about 70 tumors described; typically < 3 cm
Renomedullary interstitial cell tumor	Benign	Common autopsy findings in adults; > 1 tumor in 50%; < 5 mm
Intrarenal Schwannoma	Benign	Common benign tumor of peripheral and auditory nerves
Cystic nephroma	Benign	Cystic; female >> male
Mixed epithelial and stromal tumor	Benign	Complex renal neoplasm; contains large cysts
Neuroblastoma	Benign	
Solitary fibrous tumor	Malignant potential	Frequent painless hematuria; confused with RCC
Paraganglioma/phaeochromocytoma	Malignant potential	
Leimyosarcoma (incl. renal vein)	Malignant	The most common renal sarcoma; 5-yr survival rate 35%; chemotherapy is ineffective
Osteosarcoma	Malignant	
Angiosarcoma	Malignant	Rare, aggressive; poor prognosis; strong male predominance, androgen factor possible; rapid metastases
Hemangiopericytoma	Malignant	
Malignant fibrous histiocytoma	Malignant	Pararenal and retroperitoneal extension
Synovial sarcoma	Malignant	Characterized by a specific translocation: *t* (X; 18)(p11.2; q11); recurrence is commonly seen
Renal carcinoid tumor	Malignant	Association with horseshoe kidney; carcinoid syndrome < 10%; cystic, calcification
Neuroendocrine carcinoma	Malignant	Poorly differentiated epithelial NPL with neuroendocrine differentiation; poor prognosis; necrotic mass
Primitive neuroectodermal tumor (Ewing sarcoma)	Malignant	Inhomogeneous, often replacing the entire kidney; hemorrhage, necrosis
Plasmocytoma, Lymphoma and Leukemia		
Lymphoma	Malignant	Typically secondary renal lymphomas; primary renal lymphoma very rare
Plasmocytoma	Malignant	Occurs as a manifestation of a disseminated multiple myeloma
Leukemia	Malignant	Interstitial infiltration of leukemic cells can be called extramedullary leukemia in the kidney
Germ cell tumors		
Teratoma	Benign	
Choriocarcinoma	Malignant	Difficult to differentiate from high grade urothelial carcinomas; mostly metastases from testicular germ cell tumors

RCC: Renal cell carcinoma; NPL: Neoplasia; >>: Much more frequent or predominantly seen in female.

Metastases in the kidney appear in advanced tumor stages and should be expected in the case of a hypoenhancing mass and/or evidence of a primary tumor. Biopsy can be discussed to rule out a secondary malignancy if this leads to therapeutic consequences. The evidence in the CEUS literature is rare.

Benign renal tumors

Angiomyolipoma (AML): The prevalence of AML (hamartomas) reported in the literature varies from 0.03%-0.07%[44]. They are composed of a variable proportion of adipose tissue, spindle and epithelioid smooth muscle cells and abnormal thick-walled blood vessels. AML can occur in patients with tuberous sclerosis. They belong to a family of lesions characterized by proliferation of perivascular epithelioid cells (PEC). Clonality could be shown. There is onset of AML after puberty as well as a progesterone receptor immunoreactivity in AML. Synchronous occurrence with oncocytomas or with RCC has been described. Vascular extension up to

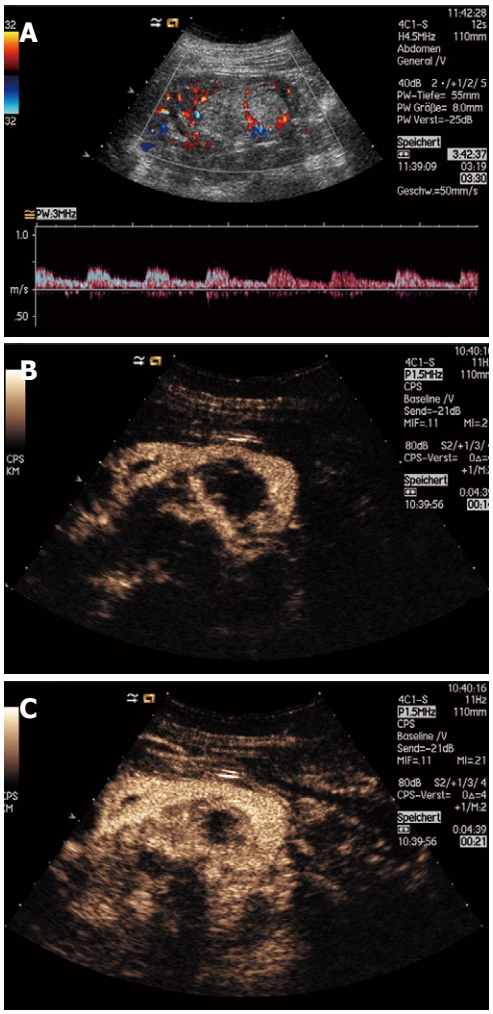

Figure 2 Histologically proven angiomyolipoma with typical central artery (which has been also described in some oncocytoma). Doppler US analysis reveals a relatively low resistance index (A); In CEUS the lesion shows a hypovascular enhancement (B, C).

the vena cava has also been reported, as well as 3 cases of sarcoma arising in AML[45-47]. Small precursor lesions consist of epithelioid smooth muscle cells whereas the proportion of adipocytes and spindle cells increase when they grow. Some rare cases are associated with spontaneous hemorrhage in lesions > 4 cm and in pregnant women. Epithelioid AML is a malignant variant. More than 50% of patients with epithelioid AML have tuberous sclerosis; the typical patient is 35-40 years old, and one-third suffer from metastatic disease at the time of diagnosis. Patients frequently present with pain. The tumors show typically a poor fat content, therefore, in imaging techniques they are rarely confused with classic AML.

AML are lesions which are frequently found in screening investigations. In patients investigated at our hospital the typical sonographic findings of AML were found in about 1% of 10 000 consecutive patients (unpublished data). Diagnosis using unenhanced CT is possible in most patients with respect to demonstration of fat equivalent density. AML represents a diagnostic challenge for every imaging method in case of hemorrhage, calcification, arteriovenous shunts ("highly vascular AML"), necrosis, and low fat content[48,49].

Up to 14% of all AML are wrongly diagnosed with CECT leading to unnecessary surgery. Papillary RCC can mimic AML with low fat appearance with homogeneous enhancement and slow washout[50]. Some authors suggest nephron-sparing surgery in the case of calcified lesions[51-53]. In US they show a typical snowball-like pronounced hyperechoic appearance. Up to 25% of small RCC are hyperechoic in comparison to the surrounding renal parenchyma (own unpublished data). Atypical only slightly hyperechoic AML are found in 30%, and iso- or hypoechoic variants in 6%.

Some reports focused on the fat content in renal cell carcinomas[54-57]. In particular, fat containing renal tumors can also be lipomas, liposarcomas, and oncocytomas[58]. Several reasons have been discussed, such as lipid producing necrosis, intra-tumoral bone metaplasia containing fatty marrow elements, and entrapment of perirenal or sinus fat[57-59].

In CEUS, AML appear typically as hypoenhancing with a progressive hypoenhancement in the late phase (Figure 2[60-62]). In other studies, AML showed a wide range of enhancement patterns without sharp discrimination in comparison to RCC[63].

The typical AML can be diagnosed with satisfying accuracy by unenhanced CT. Up to 14% of all AML are atypical and can lead to unnecessary surgery, especially when hemorrhage, calcification, arteriovenous shunts, necrosis or low fat content appears. RCC or oncocytoma can also contain fatty components. In CEUS, AML are typically less enhancing than RCC but there are overlaps in the CEUS appearance.

Renal adenoma: In the literature the concept of renal adenoma is controversial. The current WHO classification only describes papillary and metanephric adenomas, of which papillary adenomas are < 5 mm and, therefore, do not play a significant role in imaging of renal masses. All renal tumors of the clear cell type are considered malignant[64] since malignant transformation of renal adenomas have been described and genetic predictors of the transformation are unknown[5,27,65-68]. Papillary adenomas are tumors with low nuclear grade, show no mitotic figures and are ⩽ 5 mm. In autopsy studies they are found in 10% of patients < 40 years old and in 40% of patients > 70 years old. They are typically located below the renal capsule. They can be multiple and bilateral. Multiloculated adenomas are called renal adenomatosis. Metanephric adenoma, adenofibroma and stromal tumors are rare benign neoplasia with similar features occurring at different ages. Metanephric stromal tumors appear only in children, metanephric adenofibroma in children and young adults and metanephric adenomas in the young and old. One single case of a high grade sarcoma in association with metanephric adenoma has been reported[69]. An association of metanephric adenomas with Wilm's tumor or RCC has been described[70].

There are only a few reports on progression of these tumors[66,69]. Typically they have a size of 3-6 cm and are well circumscribed. Hemorrhage and necrosis are common. Twenty percent show calcification, as well as small cysts.

In studies using CEUS, metanephric adenomas appeared in only 2 patients of 2 different studies from the same group[60,61]. The contrast enhanced features revealed hyperenhancement in the arterial phase but progressive hypoenhancement in the late phase. Our own data revealed one metanephric adenoma which showed a rim enhancement with hypovascular appearance in the arterial and in the late phase.

Adenoma histology in renal tumors is rare. There is evidence for malignant transformation in some variants. Papillary adenoma is ⩽ 5 mm. Metanephric adenomas have no specific imaging features either in CECT or in CEUS.

Oncocytoma: Histologically, oncocytomas are composed of large cells with mitochondria-rich eosinophilic neoplasm, and originate from intercalated cells of the distal renal tubules. The entity was first described by Zippel in 1942. Oncocytosis or oncocytomatosis is a syndrome with oncocytic tumors, oncocytic changes in benign tubules, microcysts lined by oncocytic cells and clusters of oncocytes within the renal interstitium[64,71]. In the current WHO classification, oncocytomas are considered as benign lesions. Nevertheless there is an ongoing discussion on cases of oncocytomas developing metastases[72].

Oncocytomas are difficult to differentiate pathologically from an eosinophilic variant of chromophobe RCC which itself is considered to have low malignant potential. In a study by Breda *et al*[73] a chromophobe RCC was diagnosed via biopsy as an oncocytoma, and an oncocytoma was diagnosed via biopsy as an chromophobe RCC. In a case of oncocytosis, a hybrid oncocytoma/chromophobe RCC lesion was identified by Al-Saleem *et al*[74]. The literature concerning the rate of metastatic oncocytomas is weak, in some instances sometimes lacking histological confirmation of the oncocytoma origin of the metastases, and sometimes the oncocytoma diagnosis was questionable[72,75]. A review of non-urothelial renal tumors revealed 70/954 oncocytomas (7%)[76], of which 1/70 had an asymptomatic liver metastasis confirmed by needle biopsy.

In imaging, the diagnosis can also be difficult. Choudhary *et al*[77] investigated CECT imaging features in 21 patients with 28 histologically confirmed oncocytomas. The lesion size ranged from 1.2-12 cm, mean 4.9 cm. In all lesions contrast enhancement could be detected. In 64% the enhancement was isodense and in 36% the enhancement was hypodense in comparison to the renal cortex. In 5/28 lesions (18%) a central scar could be identified pathologically, but was detected by CECT only in 3/28 lesions (11%, lesion size 10-29 mm). The authors concluded that imaging features fail to demonstrate typical features in oncocytomas. The often discussed central scar is seen histologically in 18%-33% of tumors and correlates with the size of the lesion[64,77]. It can be confused with areas without enhancement in RCC (own data: 69% in 300 histologically proven RCC, 40% of 20 lesions published by Wink *et al*[78]). Correlation of this sign with tumor size has been published[79]. Therefore, the central scar sign lacks specificity as well as sensitivity. In the CEUS literature, the perfusion pattern in patients with oncocytomas is described by the group around Strobel[4]. They found a stellate scar in none of 3 oncocytoma, 2 of 3 (67%) were hypervascular in the arterial phase, 1 of 3 (33%) was hypovascular. In the late phase all were hypoenhancing compared to the surrounding renal parenchyma. Tamai *et al*[80] evaluated 29 patients with CEUS, 2/29 (7%) had an oncocytoma. In 50% of patients with an oncocytoma, a spoke-like enhancement pattern could be demonstrated with CEUS in contrast to CECT. Fan *et al*[62] reported that there were no characteristic patterns in one patient with oncocytoma.

Oncocytomas are benign lesions. Typical but rare signs for oncocytomas are a spoke-like enhancement and a central scar. Nevertheless neither in CECT nor in CEUS can both signs be displayed regularly, and positive and negative predictive values are low. We suggest discussing a biopsy in lesions with typical oncocytoma appearance. Histological diagnosis is also difficult.

Renal pseudotumors: Pseudotumors are mass-like anatomical variations without pathological significance. Besides fetal lobation, dromedary or splenic humps, a proportion of pseudotumors is caused by hypertrophied columns of Bertin. Those represent unresorbed polar parenchyma of one or both of 2 subkidneys that fuse to form a normal kidney and contain renal cortex, pyramids, and columns (septa) of Bertin. It can be referred to as junctional parenchyma[81,82]. In clinical practice, the ability of US and CECT to distinguish between anatomical variations and real neoplasia is frequently challenging. Typical US features are: (1) location between the overlapping portion of 2 renal sinus systems; (2) clear definition from the renal sinus; (3) a size < 3 cm; (4) comparable echogenicity to the renal parenchyma; (5) the structure is bordered by a junctional parenchymal line; and (6) the demonstration of regular/branch-like renal blood flow in the suspected lesion[83].

Ascenti *et al*[84] described their experience with contrast enhanced power Doppler with SHU 508A in 4 patients with renal pseudotumors. They could differentiate those changes from real neoplastic disease[84]. In more than 300 patients with renal masses investigated prospectively with US, color Doppler US (CDUS) and CEUS at our institution there were 4% histologically proven pseudotumors which could be reliably differentiated from real neoplasm. Neoplasia could not be ruled out with CECT. Nevertheless follow-up investigations must be performed in certain cases. Several other investigators have stressed this issue also[62,63,85-90].

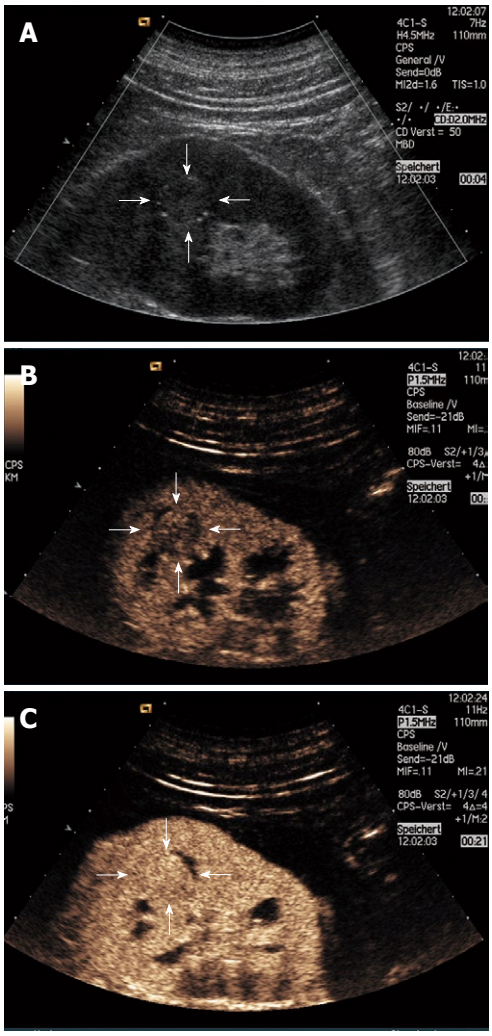

Figure 3 Small renal cell carcinoma (13 mm) not detectable by computed tomography (CT); B-mode reveals an isoechoic lesion without mass effect (A); contrast enhanced ultrasound (CEUS) in the arterial phase showed the lesion slightly hypoenhancing (B) and after 33 s isoenhancing (C); 2D Video shows the transcutaneous biopsy proving clear cell renal cell carcinoma; consecutively the patient underwent surgery.

In the diagnosis of pseudotumors with US there are different B-mode and CDUS criteria. If in CEUS a normal perfusion pattern can be distinguished, this represents a major criterion for the diagnosis of a pseudotumor. Published evidence is limited.

DETECTION OF RENAL MASSES

The accuracy of conventional B-mode alone, or in combination with CDUS in the detection and characterization of renal masses, is considered to be less reliable than other imaging techniques[91]. This is especially true if they are not contour deforming[16]. Jamis-Dow *et al*[6] reported detection rates for lesions < 30 mm, < 20 mm, and < 10 mm of 99%, 95% and 76%, respectively, for CECT. For US the rates were 95%, 70% and 20%, respectively. In more recent studies this is controversially discussed. Sixty patients with renal masses were investigated by Spahn and co-workers to assess the ability of CDUS for staging purposes in comparison to CECT and surgical findings which served as reference methods[92]. The sensitivity of CDUS for tumor detection and detection of lymph node metastases was 100%. CDUS was superior to CECT in the detection of renal vein involvement. In a study of Dong *et al*[93] the detection rate with conventional US in 42 patients with clear cell RCC (1.8-11.2 cm) was 30/42 (71%), which could be improved by CEUS to 100%. The size distribution of the lesions is not shown in the article whereas 33/42 lesions (78%) are referred to as "larger tumors". We must admit that the results were not in accordance with our own experiences. In 143 patients with renal masses submitted to our hospital with available histology and accessible CECT imaging there were 3/143 lesions (2%) with a < 15, 25 and 25 mm which were not detected in CECT but were detected in CEUS (unpublished data, Figure 3).

A major advantage of US in comparison to other imaging techniques is its ability in the characterization of cystic lesions. CECT sometimes fails to differentiate cysts containing blood or fluids with high protein content and, therefore, elevated density (in comparison to water). The detection of blood flow is a major issue in the detection of renal masses. Kitamura *et al*[94] evaluated the ability of CDUS in comparison to CECT in the staging of renal solid tumors. They investigated 110 patients with lesions < 7 cm. In 9/110 patients (8%), CECT showed enhancement in the cortical nephrographic phase whereas CDUS showed no flow. In 8/110 patients (7%), CDUS showed flow whereas CECT showed poor enhancement. Thus it can be concluded that CDUS has an accuracy for detection equal to CECT.

US (performed by a sophisticated investigator) has a detection rate comparable to that of CECT but the evidence is sparse. In the detection of blood flow in renal lesions CDUS, it has comparable sensitivity to CECT. CEUS is more sensitive than CDUS in the detection of blood and has been shown to be superior to CECT in a limited number of patients. Published data are limited.

The majority of renal masses are incidentally detected nowadays. The major issue for each imaging method is to characterize lesions when this leads to a therapeutic impact. For CEUS, this could be shown for liver lesions[95] or pancreatic lesions[96].

In contrast to liver or pancreas tumors, the characterization of renal tumors is more difficult. There is a small and heterogeneous proportion of benign lesions. Surgery is believed to be the method of choice for each solid renal lesion because of the high rate of malignancy. So most studies for characterization of renal masses with CEUS did not focus on the characterization but on the staging of renal masses with US. In the more recent literature this strategy is questioned. Particularly in small lesions (< 4 cm), the proportion of benign lesions has been reported to be higher than 13%[97-102] and histology obtained by transcutaneous biopsy is reliable and can be safely performed. An analysis of the literature for the proportion of benign lesions is given in Table 2.

Table 2 Frequency of benign lesions in consecutive patients

Author	*n*	Benign	Angiomyolipomas	Oncocytomas	Metanephric adenomas	Atypical cysts	Others	Population
[103]	396	5%			1%[7]		2%[8]	Surgery
[104]	30	17%	13%			3%		Ultrasound
[105]	70	26%	1%	4%		14%	7%[3]	Biopsy
[106]	40	23%	10%			13%		Ultrasound
[107]	35	17%	3%			10%	3%[1]	Surgery
[108]	173	14%	4%	8%		2%		Surgery
[109]	20	35%	5%	5%			25%[2]	Surgery
[110]	78	21%	3%	17%				Biopsy
[111]	26	21%	8%	12%				Biopsy
[60]	26	31%	27%		4%			Ultrasound
[80]	29	10%	3%	7%				Ultrasound
[61]	23	34%	30%		4%			Ultrasound
[112]	54	21%	4%	11%		6%		Biopsy
[113]	97	25%	25%					Ultrasound
[4]	30	10%		10%				Ultrasound
[114]	99	7%	1%	6%				Surgery/Biopsy
[115]	543	15%	5%	6%	0.2%		3%[4]	Surgery
[73]	31	13%		10%			3%[5]	Surgery
[59]	100	20%	3%	13%	2%		2%[6]	Biopsy
[64]	954	7%		7%				Surgery
[100]	2770	13%						Surgery
[78]	18	33%	11%			22%		Ultrasound
Own data (unpublished)	143	15%	3%	1%	1%	1%	8%[9]	Ultrasound

Data are given as percentage; N indicates the total number of included patients. [1]Leiomyoma; [2]1 abscess, 1 lesion associated with xanthogranulomatous pyelonephritis, 2 cysts, 1 arteriovenous fistula; [3]1 lesion associated with xanthogranulomatous pyelonephritis, 3 lesions associated with chronic pyelonephritis, 1 lesion associated with tuberculosis; [4]Leiomyoma 0.9%, papillary adenoma 0.6%, abscess 0.4%, haematoma 0.4%, giant cell fibroblastoma 0.2%, lipoma 0.2%, haemangioma 0.2%; [5]Benign lymphoid infiltrate; [6]Mixed epithelial and stromal tumor; [7]Adenoma, not further specified; [8]Haemangioma 1%, cystic nephroma 0.5%; [9]Abscess 2%, pseudotumour 4%,focal cystic dysplasia 1%, necrosis 1%.

Renal mass biopsy

Since there is a significant proportion of lesions with benign diagnosis especially in small lesions (Table 2), several studies reported on percutaneous renal mass biopsy guided either by CECT or US. In the analysis of the literature the rates for benign lesions were between 5% and 34% (Table 2). The question, which needle size to use was discussed by Breda *et al*[73]. They investigated intraoperatively 27/31 RCC (87%), 21/31 clear cell RCC (68%), 3/31 papillary RCC (10%), 3/31 chromophobe RCC (10%), 3/31 oncocytomas (10%), 1/31 benign lymphoid infiltrates (3%) with 14, 18 and 20 G core needle biopsies each after extirpation. They found a correlation of biopsy findings with final histology in 94%, 97% and 81%, respectively. They suggest 18 G to be a suitable size for renal biopsy. Wang *et al*[59] investigated the sufficiency and accuracy of percutaneous core biopsy in renal masses < 4 cm performed with CT or US guidance (60% *vs* 40%). A total of 110 biopsies were performed, of which 100/110 (91%) were sufficient. Histology revealed 35% benign lesions (Table 2). 8/110 complications (7%) were reported (1 hypotension, 2 hematomas without intervention, 4 patients with severe pain and 1 with wound infection). In 34 patients biopsy could be compared with final surgical histology, and the accuracy was 100%[59]. Shannon *et al*[116] investigated renal core biopsies of 222 lesions < 5 cm with respect to accuracy in comparison with surgical histology. The rate of diagnostic biopsies was 78%; 25% of the lesions were benign. The accuracy rate in comparison with final surgical histology was 100%. Significant complications appeared in 0.9% of patients. Kramer *et al*[117] report on their retrospective analysis of intraoperative biopsies before surgical cryoablation of renal tumors. There were 81/119 patients (68%) in which one core was taken, 38/119 patients (32%) had 3 cores taken. In the "one core group" 49/81 (60%) were malignant and 14/81 (17%) were not diagnostic. In the "3 core group" 27/38 (71%) were malignant ($P = 0.25$) and 2/38 (5%) were not diagnostic ($P = 0.03$). To increase the number of diagnostic biopsies it is reasonable to project this strategy to percutaneous biopsies, but there are no data concerning safety/complications.

As there is a significant proportion of benign lesions there is a need for preoperative histological analysis in selected cases. The reported rates for diagnostic biopsy range from 75% to 100%. It could be shown that at least 18 G core biopsies should be used from a histopathological standpoint but data concerning complications following multiple biopsies are not available. It could be also proven that 3 cores in one patient are more sufficient than one biopsy. This could not be shown for percutaneous biopsies for ethical reasons.

Differential diagnosis of solid renal tumors on US

Unenhanced US: Since B-mode US lacks specific characteristics to differentiate benign and malignant renal masses, CDUS characteristics were investigated in several settings. Habboub *et al*[118] could demonstrate renal

mass perfusion using CDUS in 42 of 44 patients (95%). In 60 patients with renal masses which were investigated by Spahn and co-workers, equal results were found with CECT and surgical findings[92]. Kitamura *et al*[94] evaluated the ability of CDUS in comparison to CECT in the staging of renal solid tumors. They investigated 110 patients with lesions < 7 cm. In 9/110 (8%) patients CECT showed enhancement in the cortical nephrographic phase whereas CDUS showed no flow. In 8/110 (7%) patients CDUS showed flow whereas CECT showed poor enhancement. The authors concluded that CDUS has a diagnostic accuracy equal to CECT. The detection of blood flow in renal solid tumors using CDUS and/or power Doppler US as a predictor for clear cell RCC histology was investigated by Raj *et al*[103]. Any flow that was detected with the methods mentioned above was defined as vascular flow. The authors did not give information about the CD settings. Two hundred and ninety nine patients were retrospectively analyzed and 97 patients were analyzed prospectively. The proportion of benign lesions for the retrospective and prospective groups were 4% and 7%, respectively, with a calculated rate of 5% for both groups. There was a strong association of vascular flow with clear cell RCC histology.

Unenhanced CDUS has a detection rate for blood flow comparable to CECT, whereas CEUS is superior to CECT. A characterization of benign and malignant lesions is not possible with satisfying accuracy using CDUS, CEUS or the traditional reference standard CECT.

Contrast enhanced ultrasound: Since the availability of US contrast agents, several studies have been performed for the characterization and staging of solid renal lesions (Figure 4). CEUS is always performed after conventional B-mode US and must, therefore, be regarded as a combination of both methods.

As early as 1994 Filippone *et al*[104] described contrast enhanced CD flow imaging with a high mechanical index and SHU 508A in 30 patients with 22/30 RCC (73%), 1/30 sarcoma (3%), 1/30 leiomyosarcoma (3%), 1/30 urothelial cell carcinoma (3%), 1/30 hemorrhagic cyst (3%) and 4 AML (13%). They found CD signals inside the lesion with conventional CDUS and CEUS in 13/30 (43%) and 26/30 (87%) patients, respectively.

Ascenti *et al*[84] demonstrated a sufficient diagnosis of renal pseudotumors with contrast-enhanced power Doppler US using SHU 508A in 4 patients. The same group performed contrast enhanced power Doppler with SHU 508A in 32 patients with 41 lesions (26 AML, 11 RCC, 3 pseudotumors, 1 metastasis) with hyperechoic lesions to evaluate its ability in the differential diagnosis of RCC *vs* AML. All malignant lesions were diagnosed histologically, all benign lesions with CECT or follow-up. In most cases, RCC showed peripheral and central enhancement, and AML showed a wide range of different patterns of vascularity. With CDUS a correct diagnosis could be found in 76%, which could not be improved by injection of SHU 508A[63].

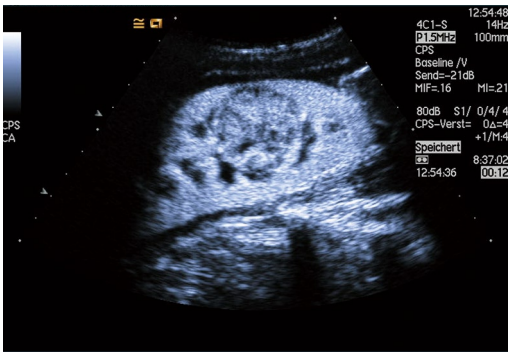

Figure 4 Renal cell carcinoma (T1), incidentally detected. CEUS investigation 12 s after injection of 2.4 mL BR1 (SonoVue®).

Quaia *et al*[60] investigated 23 lesions, including 15/23 RCC (65%), 1/23 metanephric adenoma (4%) and 7/23 AML (30%). With SHU 508A, heterogeneous behavior in the arterial phase was typical for RCC. The results in the late phase were not homogeneous. AML showed peripheral hypovascularity compared to renal tissue. Six of 7 AML were diagnosed by CT, all other tumors by histology.

In 2004, Tranquart *et al*[119] reported on their experience with the investigation of 18 patients with different focal and diffuse renal diseases using BR1 (Sonovue®) and contrast specific software. CECT or magnetic resonance imaging was used as the reference method. Compared to conventional B-mode US, they found a better tumor delineation, a better detection of venous extension and a better characterization of cystic masses.

The group around Siracusano and Quaia investigated 23 patients with renal masses using SHU 508A with contrast specific software[61]. CECT diagnosis or histology was used as the reference method. Results were solid RCC in 11/23 (48%), 7/23 AML (30%), 4/23 cystic RCC (17%), 1/23 metanephric adenoma (4%). Solid RCCs had a higher contrast enhancement than AML. The benign lesions showed a progressively decreasing enhancement in the delayed phase.

Kabakci *et al*[120] investigated 21 patients with RCC using conventional power Doppler and contrast enhanced power Doppler US with SHU 508A and correlated their findings with microvessel density. Microvessel density has been shown to be a significant prognostic factor in a subgroup of patients with low tumor stages. They found a significant correlation between color pixel ratio in conventional power Doppler and contrast enhanced power Doppler US and microvessel density.

Tamai *et al*[80] evaluated the usefulness of CEUS in the diagnosis of solid renal tumors. They included 29 patients who were investigated with conventional B-mode US and whose tumors were surgically resected. The histological diagnoses were RCC in 25/29 (86%), urothelial cell carcinoma in 1/29 (3%), oncocytomas in 2/29 (7%) and AML in 1/29 (3%) patients. CECT, here a multidetector scanner, failed to detect tumor blood flow in 5/29 patients (17%), while CEUS demonstrated flow in 29/29

(100%). In 1 of 2 patients with oncocytomas, a spoke-type enhancement pattern could be demonstrated with CEUS in contrast to CECT.

The group around Lassau and Lamuraglia reported on the experience with dynamic contrast enhanced Doppler US as a predictor of tumor response. They investigated a relatively heterogeneous group of 30 patients treated with Sorafenib for metastatic renal cell carcinomas [8/30 (27%) patients with lymph nodes involvement, 8/30 (27%) with liver metastases, 3/30 (10%) with recurrent renal lesions, 3/30 (10%) with adrenal metastases, 2/30 (7%) with contralateral renal metastases, 1/30 (3%) with pancreas metastases as well as more than one metastatic location in 5/30 (17%) patients]. They suggested quantitative CEUS for monitoring antiangiogenetic drug effectiveness in renal cancer[43].

Kawata *et al*[121] reported on 6 patients with recurrent RCC and demonstrated the utility of CEUS in this subgroup. In 5/6 patients (83%) the lesions were detected with conventional US, in 1 patient the diagnosis could only be made with CEUS.

Wink *et al*[78] examined 18 patients with renal masses using CEUS with BR1. Inhomogeneous enhancement was typical for RCC. In 4/10 patients (40%) with histological analysis, CEUS demonstrated areas without enhancement which correlated with necrosis pathologically. Fan *et al*[62] investigated 72 patients with renal lesions $\leqslant$ 5 cm with contrast specific software and BR1 (Sonovue®) [44 RCC (61%), 24 AML (32%), 2 hypertrophied columns of Bertin (3%), 1 oncocytoma (1%), and 1 abscess (1%)]. The rates of histological confirmation for RCC, AML, oncocytoma, hypertrophied columns of Bertin and abscesses were 100%, 17%, 100%, 0% and 0%, respectively[62]. They found hyperenhancement in the late phase to be predictive for RCC (sensitivity 77%, specificity 96%). Also heterogeneous enhancement was characteristic for RCC. AML were homogeneously enhancing with hypoenhancement in both the arterial and late phase.

Jiang *et al*[79] correlated CEUS features of 92 pathologically confirmed clear cell RCC in relation to tumor size. The degree of enhancement showed no correlation, but the homogenicity of enhancement correlated with tumor size. In tumors $\leqslant$ 3 cm, homogeneous enhancement was seen in 72% in contrast to tumors > 3 cm (9%). In patients with tumors $\leqslant$ 2 cm, a pseudocapsule appeared in 3/13 cases (23%), in tumors from > 2 to 5 cm in 38/58 cases (66%) and in tumors > 5 cm in 5/21 cases 24%. Inhomogeneous enhancement correlated with necrosis or cysts by histological analysis. A pseudocapsule was histologically diagnosed in 46/92 of the lesions (50%) and correlated with a rim of perilesional enhancement in 42/46 patients (91%).

Dong *et al*[93] characterized 42 patients with histologically proven clear cell RCC using time intensity curves received from video frames of second harmonic imaging with BR1. They could not differentiate a characteristic pattern. In time intensity curves, clear cell RCC had a time to peak enhancement shorter than that of normal renal parenchyma and the mean value of the descent slope rate was lower. Avascular areas or filling defects were predominantly seen in larger tumors (33/42 (78%).

Thirty patients with solid renal tumors were investigated by the group around Strobel and Bernatik[4]. RCC had a size of 65.4 ± 6.5 mm and were hypoechoic, isoechoic and hyperechoic in 52%, 36% and 12%, respectively. RCC showed a chaotic vascular pattern except for one lesion which was cystic and showed no enhancement at all. Hyperperfusion, isoperfusion and hypoperfusion was seen in the arterial phase in 12/25 (48%), 3/25 (12%) and 9/25 (36%), respectively. In the late phase hyperperfusion, isoperfusion and hypoperfusion was seen in 5/25 (20%), 9/25% (36%) and 10/25 (40%), respectively. The authors conclude that CEUS is not useful in the characterization of small renal masses.

Our group investigated more than 300 patients referred for surgical treatment of a renal mass. We performed conventional B-mode and color/power Doppler US as well as CEUS with BR1. In the majority of our patients histology was obtained by surgery (87%); in the other patients histology was obtained by biopsy (13%). Four percent of patients had lesions which finally proved to be of extrarenal origin, a proportion which is in accordance with the literature[105]. Overall there were 15% benign lesions, 22% of lesions < 40 mm had benign histology and 10% of lesions $\geqslant$ 40 mm had benign histology. In 77% of patients with histologically determined RCC, 9% were cystic. CEUS could predict malignancy with a sensitivity, specificity, positive predictive value, negative predictive value and accuracy of 97%, 45%, 91%, 75%, and 90%, respectively. CEUS (CECT) had a sensitivity, specificity, positive, negative predictive value and accuracy of 85% (38%), 97% (98%), 72% (63%), 98% (94%), and 96% (92%), respectively, for vein invasion. The correct staging was diagnosed by CEUS (CECT) in 83% (69%). The interpretation of the mentioned results favored CEUS in comparison to CECT for staging and characterization of RCC.

The majority of clear cell RCC are hypervascular. One third of papillary RCC are hypovascular, although this does not lead to immediate consequences. A significant proportion of RCC show unenhanced areas which correlate with necrosis in histology. A significant pattern for RCC which leads to sharp discrimination between RCC and benign lesions cannot be currently defined.

Staging of renal cell carcinoma with CEUS

Staging parameters in RCC are of prognostic importance. In early stage RCC, partial nephrectomy is recommended. The 5-year survival rate after radical nephrectomy is reported to be between 75%-95% for patients with organ confined disease and 0-5% for patients with metastatic disease at time of presentation[122]. In locally advanced RCC (T $\geqslant$ 3, N0 and M0) certain subgroups (especially T2 and T3a) differ significantly in survival rates[123]. In contrast to preoperative T3a staging, detection of

stages T3b and T3c is crucial since it influences the surgical approach. Renal vein invasion occurs in about 4%-10% of RCC[124,125]. Habboub *et al*[118] investigated the usefulness of CDUS in the assessment of venous invasion in RCC. The rate of venous invasion was 16/37 (43%), CDUS had a sensitivity, specificity, positive predictive value, negative predictive value and accuracy of 75%, 96%, 92%, 85%, and 87%, respectively, for renal venous involvement, in 2 false positive cases the intrarenal veins were involved. The detection rate for inferior vena cava involvement was 100% accurate. Bos and co-workers found that vein invasion was correctly staged in 93% with conventional B-mode US including CD and in 86% with CECT[126]. Sixty patients with renal masses were investigated by Spahn *et al*[92] to assess the ability of CDUS for staging purposes in comparison to CECT and surgical findings. The sensitivity for CDUS for tumor detection and detection of lymph node metastases was 100% (golden standard CECT). CDUS was superior to CECT in the detection of renal vein involvement. Gupta *et al*[127] compared CECT, MRI and CDUS for the detection of venous invasion in RCC. They investigated 59 patients with RCC and venous involvement, CDUS showed comparable results to CECT and MRI. Kitamura *et al*[94] evaluated the ability of CDUS in comparison to CECT in the staging of renal solid tumors. One hundred and ten patients with lesions < 7 cm were investigated. In 9/110 (8%) patients, CECT showed enhancement in the cortical nephrographic phase whereas CDUS showed no flow. In 8/110 (7%) patients, CDUS showed flow whereas CECT showed poor enhancement. The authors concluded that CDUS had a diagnostic accuracy equal to CECT.

In recent studies, the role of tumor pseudocapsule in the staging of RCC is discussed. RCC generally do not have a true histologic capsule. A pseudocapsule results from tumor growth producing ischemia and necrosis of adjacent normal parenchyma. It is composed of fibrous tissue and compressed renal parenchyma. This pseudocapsule is not described in the TNM classification[128] but is a pathologic feature frequently seen in early stage, low-grade RCC. It is a useful sign in the differential diagnosis of RCC and in the choice for a nephron sparing surgical approach. In MRI the pseudocapsule appears as a hypointense rim surrounding the tumor on T2-weighted images. In conventional B-mode US a pseudocapsule appears as a peritumoral hypoechoic halo. Ascenti *et al*[106] investigated the ability of second harmonic imaging using BR1 to detect a pseudocapsule in 32 patients with 40 renal masses [5/40 hemorrhagic cysts (13%), 4/40 AML (10%), 4/40 lymphoma (10%), 1/40 metastasis (3%), 26/40 RCC (65%)]. A pseudocapsule was correctly diagnosed in 12/14 histologically evaluated RCC (86%). In the other 12 renal cell carcinomas, a pseudocapsule was not found histologically. In all other lesions a pseudocapsule was not visible. The benign lesions were diagnosed with CT or MRI. The positive predictive value was 100% but the negative predictive value was below 50%[106]. Jiang *et al*[79] correlated CEUS features of 92 pathologically confirmed clear cell RCC in relation to tumor size. In patients with tumors ≤ 2 cm, a pseudocapsule appeared in 3/13 cases (23%), in 38/58 cases (66%) with tumors from > 2 to 5 cm and in 5/21 cases (24%) with tumors > 5 cm.

Staging for RCC can be performed with CEUS accurately with a diagnostic accuracy comparable to CECT. Even CDUS seems to have a high sensitivity, particularly if there is renal vein involvement. A pseudocapsule is a feature only seen in RCC; it indicates an early stage and can be seen in about 23%-66% of lesions. In CEUS a perilesional hypervascular rim can be seen with an accuracy of about 85%. The sign has a high positive predictive value, but the role of the pseudocapsule has not been defined in current TNM classifications.

Assessment of local ablation therapy for renal cell carcinomas

Local ablation therapy either with cryotherapy or radiofrequency ablation can be used for curative treatment of RCC. Wink *et al*[129] suggested CEUS for monitoring of cryotherapy as a curative treatment for patients with RCC < 4 cm. They presented a CEUS investigation which enabled easy identification of the lesion before and after treatment. They found the selective detection of contrast resulting in high accuracy for the diagnosis of flow *vs* no flow most helpful.

Since CEUS is the imaging method with the best separation of tissue and contrast signal and since US contrast agents stay strictly in the vascular bed it is mostly suitable for questions of vascularity and/or necrosis. There are preliminary data showing comparable results to reference imaging methods like CECT and MRI after radiofrequency ablation or cryotherapy of renal cell carcinomas.

Characterization of cystic lesions with CEUS

Cystic changes in RCC can be seen in 4%-15%. Only 5% of all lesions are mainly cystic. Those lesions are described by a (modified) Bosniak classification[130,131] for CECT and remain a challenge for all imaging methods. MRI often gives a hugher stage than CECT by depicting more septa and more wall thickening but is less sensitive for calcification[132]. In the literature the role of calcification in cystic lesions is controversial[133].

The original classification of Bosniak defines cysts as follows: Bosniak Ⅰ: hairline thin cyst wall, no calcifications, no solid components; no contrast enhancement; Bosniak Ⅱ: few hairline thin septae, fine calcification in the wall or in the septae; Bosniak ⅡF: multiple hairline thin septae, minimal smooth thickening of walls or septae, thick or nodular calcification of the wall or septae without contrast enhancement; Bosniak Ⅲ: thickened irregular or smooth walls or septae with measurable enhancement; Bosniak Ⅳ: enhanced soft tissue components independent of the wall or septae (Figure 5).

The classification is used to estimate the chance for

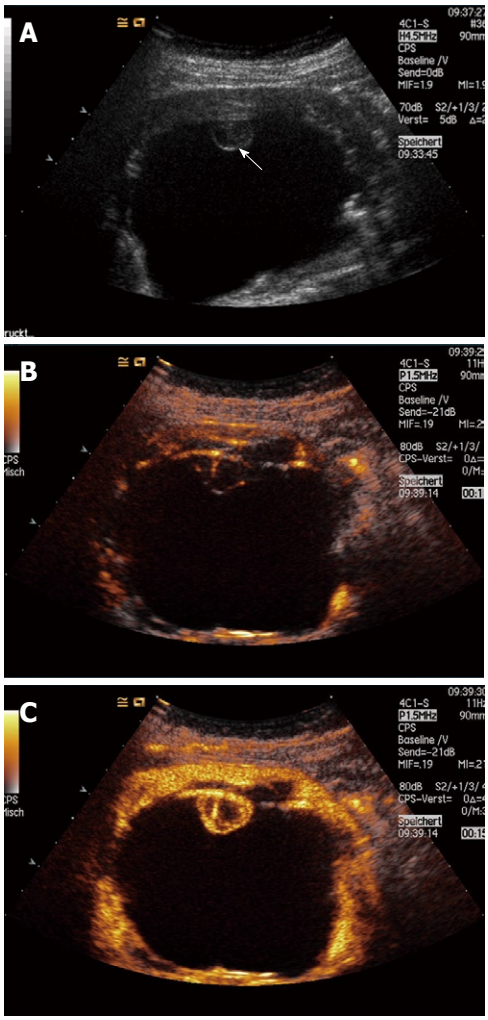

Figure 5 Cystic renal lesion with a small RCC (12 mm × 10 mm) not recognized by CT which has been histologically proven by surgery. B-mode US showed a nodularity inside the cyst (A); CEUS revealed contrast enhancement of the small lesion (B, C)[134].

malignancy in cystic lesions, but in the group of Bosniak Ⅲ and Ⅳ lesions there are several neoplastic and not necessarily malignant subtypes: cystic (typically clear cell) RCC, multilocular cystic RCC, cystic nephroma, mixed epithelial and stromal tumor. Bosniak Ⅰ and Ⅱ do not require further follow-up investigations. Category Bosniak ⅡF has been introduced for lesions which are difficult to define into Ⅱ or Ⅲ. Bosniak Ⅲ lesions are typically considered to require surgery since in the literature a rate of up to 60% malignant lesions is reported[135]. Bosniak Ⅳ lesions are reported to have a risk for malignancy between 67% and 100%[136,137]. Nevertheless, there is a significant interobserver variability for CECT investigations of cystic masses with complete agreement in only 59% of cases[138]. Hirai *et al*[139] investigated 10 patients with multilocular cystic lesions using conventional CDUS. Histological results were 3/10 (30%) cystic RCC, 3/10 (30%) hemorrhagic renal cysts, 1/10 (10%) benign multilocular cystic nephroma, 2/10 (20%) infected renal cysts and 1/10 (10%) multilocular cyst in a patient with von Hippel-Lindau disease. The authors report on demonstration of pulsatile high resistance flow in the patient with the cystic RCC. In the other lesions flow could only be detected in the peripheral margin where flow was comparable to the flow in the interlobar arteries[139]. Park *et al*[140] compared 31 pathologically confirmed cystic renal masses with SHU 508A and high MI contrast specific imaging and compared the findings with CECT. The diagnostic accuracy for CECT and CEUS for malignancy was 74% and 90%, respectively. There was an agreement in Bosniak's classification for both methods in 74%, in the remaining 26% there was always an upgrade with CEUS (Bosniak Ⅰ → Bosniak Ⅳ in 1/31 patients (3%), Bosniak Ⅱ → Bosniak Ⅳ in 2/31 patients (7%), Bosniak ⅡF → Bosniak Ⅲ in 2/31 patients (7%), Bosniak Ⅲ → Bosniak Ⅳ in 3/31 patients (10%). In conclusion, 10% of 31 lesions were categorized from Bosniak Ⅰ or Ⅱ to Ⅳ which leads to therapeutic consequences. Quaia *et al*[141] investigated a series of 40 patients with cystic renal masses with contrast specific software and BR1 and compared the findings with CECT. Three blinded readers in an offsite setting differentiated the lesions according to the Bosniak classification. There were 21/40 (53%) cystic RCC, 2/40 (5%) cystic nephroma (benign), 9/40 (23%) inflammatory or hemorrhagic cysts and 8/40 (20%) uncomplicated cysts. CEUS had a significantly higher diagnostic accuracy than CECT in the detection of malignancy in cystic renal lesions (80%-83% and 63%-75%, respectively)[141]. Clevert *et al*[142] investigated 32 consecutive patients with 37 complex cystic masses with CEUS with BR1 in comparison to multislice CT. In 14/32 (44%) lesions were surgically resected, the others were followed up for a period of 3 mo to 2 years. In addition, there was a blind reading of video clips of the CEUS investigation. Lesions were categorized as Bosniak Ⅱ with CECT and CEUS in 15/37 (41%) and in 8/37 (22%) cases, as Bosniak ⅡF in 7/37 (19%) and in 12/37 (32%) cases, as Bosniak Ⅲ in 8/37 (22%) and in 8/37 (22%) cases, and as Bosniak Ⅳ in 7/37 (19%) and in 9/37 (24) cases. CEUS proved to show more septa than CECT and upgraded wall thickness resulting in correction of Bosniak category Ⅱ to ⅡF. Two masses could not be classified with CECT, were categorized as Bosniak Ⅳ using CEUS and proved to be malignant. The authors conclude that CEUS is an additional examination to CECT and can give additional information[142].

CEUS is currently the best indication for cystic renal lesions in the kidney. There is evidence showing better results in the characterization of cystic renal lesions with therapeutic consequences in more than 10%.

CONCLUSION

CEUS represents the imaging method currently with the highest spatial contrast resolution as well as the highest differentiation between contrast and tissue signal (Figure 4). Its disadvantages are a high observer dependency and often a lack of representative image or video presentation during radiological demonstrations. US and

CEUS are widely used, and sophisticated techniques (hardware and software) improve the diagnostic impact. There is significant evidence for its strength in the detection and characterization of liver lesions, with lesser strength for solid pancreatic lesions. In other indications the evidence is less clear but promising, e.g. splenic and adrenal tumors[95,96,143,144]. Regarding CEUS for tumor evaluation of the kidneys, the number of published studies is impressive but the conclusive evidence is low.

The majority of tumors of the kidney are RCC. RCC are hypervascular in CEUS in most cases, especially in the case of clear cell histology. Here more than 90% are hypervascular in comparison to the surrounding renal parenchyma. Nevertheless it has to be taken into account that the bigger the lesion the higher the chance for large areas of necrosis or hemorrhage. In current studies with the development of sophisticated US techniques [e.g. cadence pulse sequencing (CPS)], avascular areas could be defined as necrosis by histological investigation[78,79] (own unpublished data). Avascular areas appear more frequent in large lesions. As those findings were formerly mixed with heterogeneous enhancement patterns the positive and negative predictive value of this sign has not been investigated so far. Papillary RCC in contrast to clear cell RCC was described as hypovascular in one third of cases[80] but, as papillary RCC are malignant tumors, this finding does not play an important role in clinical practice.

In the staging of malignant tumors of the kidney, the impact of CDUS and CEUS is high. Lymph node metastases, renal vein involvement as well as intraabdominal metastases elsewhere can be detected with results comparable to CECT, although multicenter studies with large patient numbers are not available so far. The detection of the pseudocapsule as a sign of early stage RCC is possible; nevertheless this feature has not been included in the current TNM classification.

The results for CEUS concerning the late phase are not satisfying. CEUS patterns for RCC as well as for benign lesions are heterogeneous for the same tumor entity as well as dissimilar in different studies[60,93]. Since in the kidney there is no dual blood supply the late phase in the renal parenchyma itself is less pronounced as compared to the liver. In this context, observations in the late phase are limited by certain bubble destruction leading to different results in hyper- and hypoenhancing lesions using different techniques. Nevertheless the late phase is of significant interest but should be investigated with objective measurements using time intensity curves and intermittent imaging to avoid bubble destruction.

Typical AML can be diagnosed with unenhanced CECT if they show a significant fat component. The frequency of atypical AML in CECT is controversial, and depends on necrosis, presence of shunts, low fat content and others. Nevertheless as well as in CECT, in CEUS the contrast agent enhancement patterns do not allow discrimination from RCC in all cases, and in case reports nearly all other tumor entities can present with fatty components as well. The typical AML in CEUS shows less contrast enhancement in the arterial phase in comparison to the typical clear cell RCC.

Oncocytoma represent a challenge for each imaging method. The typical central stellate scar can be histologically found in about 1/3 of oncocytoma, therefore, imaging methods cannot be sensitive and reliable. Furthermore this sign cannot be differentiated from small necrotic areas in RCC which are seen in a significant proportion of RCC (50%-80%, depending on the size).

Metanephric adenoma is a rare entity and its features in CEUS need to be investigated by a multicenter approach. Up to now there has been no possibility for sharp discrimination with other tumor entities. (1) In the currently available literature, CEUS showed comparable results to CECT in the staging of RCC; (2) The characterization of cystic lesions (this is to date the most promising issue); (3) The detection of blood flow in small masses (differential diagnosis to atypical cysts with elevated density due to protein/blood content on CT); and (4) After local ablative tumor therapy (radiofrequency ablation, cryotherapy).

Possible indications with potential for further investigations are: (1) Differentiation of abscess/infarction *vs* hypovascular tumors because of sharp discrimination of flow *vs* no flow; (2) Follow-up for palliative antiangiogenetic therapy in metastatic or recurrent RCC.

Issues to be investigated further for CEUS are as follows: (1) The potential of CEUS to discriminate features for preoperative biopsy, e.g. hypoenhancing lesions < 4 cm; (2) Time-intensity curves, e.g. for oncocytoma and AML; and (3) The rate of benign lesions in the subgroup of small (< 4 cm) hypoenhancing lesions.

REFERENCES

1 **Ignee A**, Baum U, Schuessler G, Dietrich CF. Contrast-enhanced ultrasound-guided percutaneous cholangiography and cholangiodrainage (CEUS-PTCD). *Endoscopy* 2009; **41**: 725-726

2 **Claudon M**, Cosgrove D, Albrecht T, Bolondi L, Bosio M, Calliada F, Correas JM, Darge K, Dietrich C, D'Onofrio M, Evans DH, Filice C, Greiner L, Jäger K, Jong N, Leen E, Lencioni R, Lindsell D, Martegani A, Meairs S, Nolsøe C, Piscaglia F, Ricci P, Seidel G, Skjoldbye B, Solbiati L, Thorelius L, Tranquart F, Weskott HP, Whittingham T. Guidelines and good clinical practice recommendations for contrast enhanced ultrasound (CEUS) - update 2008. *Ultraschall Med* 2008; **29**: 28-44

3 **Dietrich CF**. Comments and illustrations regarding the guidelines and good clinical practice recommendations for contrast-enhanced ultrasound (CEUS)--update 2008. *Ultraschall Med* 2008; **29** Suppl 4: S188-S202

4 **Haendl T**, Strobel D, Legal W, Frieser M, Hahn EG, Bernatik T. [Renal cell cancer does not show a typical perfusion pattern in contrast-enhanced ultrasound] *Ultraschall Med* 2009; **30**: 58-63

5 **Curry NS**. Small renal masses (lesions smaller than 3 cm): imaging evaluation and management. *AJR Am J Roentgenol* 1995; **164**: 355-362

6 **Jamis-Dow CA**, Choyke PL, Jennings SB, Linehan WM, Thakore KN, Walther MM. Small (< or = 3-cm) renal masses: detection with CT versus US and pathologic correlation.

Radiology 1996; **198**: 785-788
7 **Smith SJ**, Bosniak MA, Megibow AJ, Hulnick DH, Horii SC, Raghavendra BN. Renal cell carcinoma: earlier discovery and increased detection. *Radiology* 1989; **170**: 699-703
8 **Amendola MA**, Bree RL, Pollack HM, Francis IR, Glazer GM, Jafri SZ, Tomaszewski JE. Small renal cell carcinomas: resolving a diagnostic dilemma. *Radiology* 1988; **166**: 637-641
9 **Warshauer DM**, McCarthy SM, Street L, Bookbinder MJ, Glickman MG, Richter J, Hammers L, Taylor C, Rosenfield AT. Detection of renal masses: sensitivities and specificities of excretory urography/linear tomography, US, and CT. *Radiology* 1988; **169**: 363-365
10 **Robbin ML**, Lockhart ME, Barr RG. Renal imaging with ultrasound contrast: current status. *Radiol Clin North Am* 2003; **41**: 963-978
11 **Provet J**, Tessler A, Brown J, Golimbu M, Bosniak M, Morales P. Partial nephrectomy for renal cell carcinoma: indications, results and implications. *J Urol* 1991; **145**: 472-476
12 **Eggener SE**, Rubenstein JN, Smith ND, Nadler RB, Kontak J, Flanigan RC, Waters WB, Picken M, Campbell SC. Renal tumors in young adults. *J Urol* 2004; **171**: 106-110
13 **Jayson M**, Sanders H. Increased incidence of serendipitously discovered renal cell carcinoma. *Urology* 1998; **51**: 203-205
14 **Curti BD**. Renal cell carcinoma. *JAMA* 2004; **292**: 97-100
15 **Scialpi M**, Di Maggio A, Midiri M, Loperfido A, Angelelli G, Rotondo A. Small renal masses: assessment of lesion characterization and vascularity on dynamic contrast-enhanced MR imaging with fat suppression. *AJR Am J Roentgenol* 2000; **175**: 751-757
16 **Bosniak MA**. The small (less than or equal to 3.0 cm) renal parenchymal tumor: detection, diagnosis, and controversies. *Radiology* 1991; **179**: 307-317
17 **Birnbaum BA**, Bosniak MA, Megibow AJ, Lubat E, Gordon RB. Observations on the growth of renal neoplasms. *Radiology* 1990; **176**: 695-701
18 **Talamo TS**, Shonnard JW. Small renal adenocarcinoma with metastases. *J Urol* 1980; **124**: 132-134
19 **Hajdu SI**, Thomas AG. Renal cell carcinoma at autopsy. *J Urol* 1967; **97**: 978-982
20 **Aizawa S**, Suzuki M, Kikuchi Y, Nikaido T, Matsumoto K. Clinicopathological study on small renal cell carcinomas with metastases. *Acta Pathol Jpn* 1987; **37**: 947-954
21 **Ellis WJ**, Bauer KD, Oyasu R, McVary KT. Flow cytometric analysis of small renal tumors. *J Urol* 1992; **148**: 1774-1777
22 **Beisland C**, Hjelle KM, Reisaeter LA, Bostad L. Observation should be considered as an alternative in management of renal masses in older and comorbid patients. *Eur Urol* 2009; **55**: 1419-1427
23 **O'Malley RL**, Godoy G, Phillips CK, Taneja SS. Is surveillance of small renal masses safe in the elderly? *BJU Int* 2009; Epub ahead of print
24 **Bosniak MA**, Birnbaum BA, Krinsky GA, Waisman J. Small renal parenchymal neoplasms: further observations on growth. *Radiology* 1995; **197**: 589-597
25 **Cheville JC**, Lohse CM, Zincke H, Weaver AL, Blute ML. Comparisons of outcome and prognostic features among histologic subtypes of renal cell carcinoma. *Am J Surg Pathol* 2003; **27**: 612-624
26 **Mydlo JH**, Bard RH. Analysis of papillary renal adenocarcinoma. *Urology* 1987; **30**: 529-534
27 **Van Poppel H**, Nilsson S, Algaba F, Bergerheim U, Dal Cin P, Fleming S, Hellsten S, Kirkali Z, Klotz L, Lindblad P, Ljungberg B, Mulders P, Roskams T, Ross RK, Walker C, Wersäll P. Precancerous lesions in the kidney. *Scand J Urol Nephrol Suppl* 2000; 136-165
28 **Grimaldi G**, Reuter V, Russo P. Bilateral non-familial renal cell carcinoma. *Ann Surg Oncol* 1998; **5**: 548-552
29 **Sánchez-Ortiz RF**, Madsen LT, Bermejo CE, Wen S, Shen Y, Swanson DA, Wood CG. A renal mass in the setting of a nonrenal malignancy: When is a renal tumor biopsy appropriate? *Cancer* 2004; **101**: 2195-2201
30 **Chassagne P**, Perol MB, Doucet J, Elyachkouri L, Grise P, Métayer J, Bercoff E. [Renal metastases from cancer. Apropos of 9 cases and review of the literature] *Ann Med Interne* (Paris) 1994; **145**: 103-106
31 **Abe K**, Hasegawa T, Onodera S, Oishi Y, Suzuki M. Renal metastasis of thyroid carcinoma. *Int J Urol* 2002; **9**: 656-658
32 **Takehara K**, Koga S, Nishikido M, Kanetake H, Hayashi T, Hara S, Ayabe H, Saito Y. Breast cancer metastatic to the kidney. *Anticancer Res* 1999; **19**: 5571-5573
33 **Aron M**, Nair M, Hemal AK. Renal metastasis from primary hepatocellular carcinoma. A case report and review of the literature. *Urol Int* 2004; **73**: 89-91
34 **Trompette A**, Clavel M, Paraf F, Sabatini M, Melloni B, Bonnaud F. [Symptomatic renal metastases of bronchial carcinoma] *Rev Mal Respir* 1999; **16**: 833-835
35 **Denti F**, Wisard M, Guillou L, Francke ML, Leisinger HJ. Renal metastasis from prostatic adenocarcinoma: a potential diagnostic pitfall. *Urol Int* 1999; **62**: 171-173
36 **Martino L**, Martino F, Coluccio A, Mangiarini MG, Chioda C. Renal metastasis from pancreatic adenocarcinoma. *Arch Ital Urol Androl* 2004; **76**: 37-39
37 **Sanz Mayayo E**, Mayayo Dehesa T, Gómez García I, Sáenz Medina J, Rodríguez-Patrón Rodríguez R, Escudero Barrilero A. [Renal metastasis of hepatocellular carcinoma] *Actas Urol Esp* 2003; **27**: 387-390
38 **Müller HJ**, Weckesser M, Schober O. Bilateral renal metastasis in follicular thyroid carcinoma. *Nuklearmedizin* 2000; **39**: 45-47
39 **Fukushima M**, Isoyama E, Sakaridani N, Sanematsu H, Kadowaki H, Hirakawa S, Miyagawa I. [Renal metastasis originating from liver cancer] *Nippon Hinyokika Gakkai Zasshi* 1996; **87**: 710-713
40 **Le Normand S**, Soyer P, Klein I, Hervé JM, Scherrer A. [Can primary kidney clear cell adenocarcinoma be differentiated from kidney metastasis with computed tomography?] *Prog Urol* 1997; **7**: 403-407
41 **Päivänalo M**, Tikkakoski T, Merikanto J, Suramo I. [Radiologic findings in renal metastases] *Aktuelle Radiol* 1993; **3**: 360-365
42 **Honda H**, Coffman CE, Berbaum KS, Barloon TJ, Masuda K. CT analysis of metastatic neoplasms of the kidney. Comparison with primary renal cell carcinoma. *Acta Radiol* 1992; **33**: 39-44
43 **Lamuraglia M**, Escudier B, Chami L, Schwartz B, Leclère J, Roche A, Lassau N. To predict progression-free survival and overall survival in metastatic renal cancer treated with sorafenib: pilot study using dynamic contrast-enhanced Doppler ultrasound. *Eur J Cancer* 2006; **42**: 2472-2479
44 **Fröhlich T**, Brands A, Thon WF, Weskott HP, Ostertag H. Angiomyolipoma of the kidney and lymph nodes. *World J Urol* 1999; **17**: 123-125
45 **Tallarigo C**, Baldassarre R, Bianchi G, Comunale L, Olivo G, Pea M, Bonetti F, Martignoni G, Zamboni G, Mobilio G. Diagnostic and therapeutic problems in multicentric renal angiomyolipoma. *J Urol* 1992; **148**: 1880-1884
46 **Ferry JA**, Malt RA, Young RH. Renal angiomyolipoma with sarcomatous transformation and pulmonary metastases. *Am J Surg Pathol* 1991; **15**: 1083-1088
47 **Cibas ES**, Goss GA, Kulke MH, Demetri GD, Fletcher CD. Malignant epithelioid angiomyolipoma (‚sarcoma ex angiomyolipoma') of the kidney: a case report and review of the literature. *Am J Surg Pathol* 2001; **25**: 121-126
48 **Jinzaki M**, Tanimoto A, Narimatsu Y, Ohkuma K, Kurata T, Shinmoto H, Hiramatsu K, Mukai M, Murai M. Angiomyolipoma: imaging findings in lesions with minimal fat. *Radiology* 1997; **205**: 497-502
49 **Kim JK**, Park SY, Shon JH, Cho KS. Angiomyolipoma with minimal fat: differentiation from renal cell carcinoma at

biphasic helical CT. *Radiology* 2004; **230**: 677-684
50 **Bret PM**, Bretagnolle M, Gaillard D, Plauchu H, Labadie M, Lapray JF, Roullaud Y, Cooperberg P. Small, asymptomatic angiomyolipomas of the kidney. *Radiology* 1985; **154**: 7-10
51 **Hélénon O**, Chrétien Y, Paraf F, Melki P, Denys A, Moreau JF. Renal cell carcinoma containing fat: demonstration with CT. *Radiology* 1993; **188**: 429-430
52 **Strotzer M**, Lehner KB, Becker K. Detection of fat in a renal cell carcinoma mimicking angiomyolipoma. *Radiology* 1993; **188**: 427-428
53 **Davidson AJ**, Davis CJ Jr. Fat in renal adenocarcinoma: never say never. *Radiology* 1993; **188**: 316
54 **D'Angelo PC**, Gash JR, Horn AW, Klein FA. Fat in renal cell carcinoma that lacks associated calcifications. *AJR Am J Roentgenol* 2002; **178**: 931-932
55 **Lesavre A**, Correas JM, Merran S, Grenier N, Vieillefond A, Hélénon O. CT of papillary renal cell carcinomas with cholesterol necrosis mimicking angiomyolipomas. *AJR Am J Roentgenol* 2003; **181**: 143-145
56 **Roy C**, Tuchmann C, Lindner V, Guth S, Vasilescu C, Saussine C, Jacqmin D. Renal cell carcinoma with a fatty component mimicking angiomyolipoma on CT. *Br J Radiol* 1998; **71**: 977-979
57 **Schuster TG**, Ferguson MR, Baker DE, Schaldenbrand JD, Solomon MH. Papillary renal cell carcinoma containing fat without calcification mimicking angiomyolipoma on CT. *AJR Am J Roentgenol* 2004; **183**: 1402-1404
58 **Hélénon O**, Merran S, Paraf F, Melki P, Correas JM, Chrétien Y, Moreau JF. Unusual fat-containing tumors of the kidney: a diagnostic dilemma. *Radiographics* 1997; **17**: 129-144
59 **Wang R**, Wolf JS Jr, Wood DP Jr, Higgins EJ, Hafez KS. Accuracy of percutaneous core biopsy in management of small renal masses. *Urology* 2009; **73**: 586-590; discussion 590-591
60 **Quaia E**, Siracusano S, Bertolotto M, Monduzzi M, Mucelli RP. Characterization of renal tumours with pulse inversion harmonic imaging by intermittent high mechanical index technique: initial results. *Eur Radiol* 2003; **13**: 1402-1412
61 **Siracusano S**, Quaia E, Bertolotto M, Ciciliato S, Tiberio A, Belgrano E. The application of ultrasound contrast agents in the characterization of renal tumors. *World J Urol* 2004; **22**: 316-322
62 **Fan L**, Lianfang D, Jinfang X, Yijin S, Ying W. Diagnostic efficacy of contrast-enhanced ultrasonography in solid renal parenchymal lesions with maximum diameters of 5 cm. *J Ultrasound Med* 2008; **27**: 875-885
63 **Ascenti G**, Zimbaro G, Mazziotti S, Gaeta M, Settineri N, Scribano E. Usefulness of power Doppler and contrast-enhanced sonography in the differentiation of hyperechoic renal masses. *Abdom Imaging* 2001; **26**: 654-660
64 **Eble JN**, Sauter G, Epstein JI, Sesterhenn IAE. World Health Organization Classification of Tumours. Pathology and Genetics of Tumours of the Urinary System and Male Genital Organs, 2004
65 **Bennington JL**. Proceedings: Cancer of the kidney--etiology, epidemiology, and pathology. *Cancer* 1973; **32**: 1017-1029
66 **Delahunt B**, Velickovic M, Grebe SK. Evolving classification of renal cell neoplasia. *Expert Rev Anticancer Ther* 2001; **1**: 576-584
67 **Störkel S**. [Epithelial tumors of the kidney. Pathological subtyping and cytogenetic correlation] *Urologe A* 1999; **38**: 425-432
68 **Kiyoshima K**, Oda Y, Nakamura T, Migita T, Okumura K, Naito S, Tsuneyoshi M. Multicentric papillary renal cell carcinoma associated with renal adenomatosis. *Pathol Int* 2004; **54**: 266-272
69 **Picken MM**, Curry JL, Lindgren V, Clark JI, Eble JN. Metanephric adenosarcoma in a young adult: morphologic, immunophenotypic, ultrastructural, and fluorescence in situ hybridization analyses: a case report and review of the literature. *Am J Surg Pathol* 2001; **25**: 1451-1457
70 **Arroyo MR**, Green DM, Perlman EJ, Beckwith JB, Argani P. The spectrum of metanephric adenofibroma and related lesions: clinicopathologic study of 25 cases from the National Wilms Tumor Study Group Pathology Center. *Am J Surg Pathol* 2001; **25**: 433-444
71 **Tickoo SK**, Reuter VE, Amin MB, Srigley JR, Epstein JI, Min KW, Rubin MA, Ro JY. Renal oncocytosis: a morphologic study of fourteen cases. *Am J Surg Pathol* 1999; **23**: 1094-1101
72 **Van der Kwast T**, Perez-Ordoñez B. Renal oncocytoma, yet another tumour that does not fit in the dualistic benign/malignant paradigm? *J Clin Pathol* 2007; **60**: 585-586
73 **Breda A**, Treat EG, Haft-Candell L, Leppert JT, Harper JD, Said J, Raman S, Smith RB, Belldegrun AS, Schulam PG. Comparison of accuracy of 14-, 18- and 20-G needles in ex-vivo renal mass biopsy: a prospective, blinded study. *BJU Int* 2009; Epub ahead of print
74 **Al-Saleem T**, Cairns P, Dulaimi EA, Feder M, Testa JR, Uzzo RG. The genetics of renal oncocytosis: a possible model for neoplastic progression. *Cancer Genet Cytogenet* 2004; **152**: 23-28
75 **Amin R**, Anthony P. Metastatic renal oncocytoma: A case report and review of the literature. *Clin Oncol* (R Coll Radiol) 1999; **11**: 277-279
76 **Perez-Ordonez B**, Hamed G, Campbell S, Erlandson RA, Russo P, Gaudin PB, Reuter VE. Renal oncocytoma: a clinicopathologic study of 70 cases. *Am J Surg Pathol* 1997; **21**: 871-883
77 **Choudhary S**, Rajesh A, Mayer NJ, Mulcahy KA, Haroon A. Renal oncocytoma: CT features cannot reliably distinguish oncocytoma from other renal neoplasms. *Clin Radiol* 2009; **64**: 517-522
78 **Wink MH**, de la Rosette JJ, Laguna P, Lagerveld BW, Wijkstra H. Ultrasonography of renal masses using contrast pulse sequence imaging: a pilot study. *J Endourol* 2007; **21**: 466-472
79 **Jiang J**, Chen Y, Zhou Y, Zhang H. Clear cell renal cell carcinoma: Contrast-enhanced ultrasound features relation to tumor size. *Eur J Radiol* 2008; Epub ahead of print
80 **Tamai H**, Takiguchi Y, Oka M, Shingaki N, Enomoto S, Shiraki T, Furuta M, Inoue I, Iguchi M, Yanaoka K, Arii K, Shimizu Y, Nakata H, Shinka T, Sanke T, Ichinose M. Contrast-enhanced ultrasonography in the diagnosis of solid renal tumors. *J Ultrasound Med* 2005; **24**: 1635-1640
81 **Yeh HC**, Halton KP, Shapiro RS, Rabinowitz JG, Mitty HA. Junctional parenchyma: revised definition of hypertrophic column of Bertin. *Radiology* 1992; **185**: 725-732
82 **Patriquin H**, Lefaivre JF, Lafortune M, Russo P, Boisvert J. Fetal lobation. An anatomo-ultrasonographic correlation. *J Ultrasound Med* 1990; **9**: 191-197
83 **Leekam RN**, Matzinger MA, Brunelle M, Gray RR, Grosman H. The sonography of renal columnar hypertrophy. *J Clin Ultrasound* 1983; **11**: 491-494
84 **Ascenti G**, Zimbaro G, Mazziotti S, Gaeta M, Lamberto S, Scribano E. Contrast-enhanced power Doppler US in the diagnosis of renal pseudotumors. *Eur Radiol* 2001; **11**: 2496-2499
85 **Ascenti G**, Zimbaro G, Mazziotti S, Visalli C, Racchiusa S, Vinci S, Scribano E. [Doppler power with contrast media in the characterization of renal masses] *Radiol Med* 2000; **100**: 168-174
86 **Bono AV**, Lovisolo JA. Renal cell carcinoma--diagnosis and treatment: state of the art. *Eur Urol* 1997; **31** Suppl 1: 47-55
87 **Clevert DA**, Stock K, Klein B, Slotta-Huspenina J, Prantl L, Heemann U, Reiser M. Evaluation of Acoustic Radiation Force Impulse (ARFI) imaging and contrast-enhanced ultrasound in renal tumors of unknown etiology in comparison to histological findings. *Clin Hemorheol Microcirc* 2009; **43**: 95-107
88 **Jinzaki M**, Ohkuma K, Tanimoto A, Mukai M, Hiramatsu

K, Murai M, Hata J. Small solid renal lesions: usefulness of power Doppler US. *Radiology* 1998; **209**: 543-550
89 **Setola SV**, Catalano O, Sandomenico F, Siani A. Contrast-enhanced sonography of the kidney. *Abdom Imaging* 2007; **32**: 21-28
90 **Yang DM**, Yoon MH, Kim HS, Kim HS, Shin DB. Intrarenal pseudoaneurysms complicating renal choriocarcinoma metastases: treatment with coil embolization. *Clin Imaging* 2000; **24**: 217-220
91 **Maresca G**, Summaria V, De Gaetano AM, Danza FM, Valentini AL, Marano P. [Color Doppler echography in the tissue characterization of renal masses] *Radiol Med* 1995; **89**: 470-480
92 **Spahn M**, Portillo FJ, Michel MS, Siegsmund M, Gaa J, Alken P, Jünemann KP. Color Duplex sonography vs. computed tomography: accuracy in the preoperative evaluation of renal cell carcinoma. *Eur Urol* 2001; **40**: 337-342
93 **Dong XQ**, Shen Y, Xu LW, Xu CM, Bi W, Wang XM. Contrast-enhanced ultrasound for detection and diagnosis of renal clear cell carcinoma. *Chin Med J* (Engl) 2009; **122**: 1179-1183
94 **Kitamura H**, Fujimoto H, Tobisu K, Mizuguchi Y, Maeda T, Matsuoka N, Komiyama M, Nakagawa T, Kakizoe T. Dynamic computed tomography and color Doppler ultrasound of renal parenchymal neoplasms: correlations with histopathological findings. *Jpn J Clin Oncol* 2004; **34**: 78-81
95 **Dietrich CF**, Ignee A, Trojan J, Fellbaum C, Schuessler G. Improved characterisation of histologically proven liver tumours by contrast enhanced ultrasonography during the portal venous and specific late phase of SHU 508A. *Gut* 2004; **53**: 401-405
96 **Dietrich CF**, Braden B, Hocke M, Ott M, Ignee A. Improved characterisation of solitary solid pancreatic tumours using contrast enhanced transabdominal ultrasound. *J Cancer Res Clin Oncol* 2008; **134**: 635-643
97 **Mindrup SR**, Pierre JS, Dahmoush L, Konety BR. The prevalence of renal cell carcinoma diagnosed at autopsy. *BJU Int* 2005; **95**: 31-33
98 **Xipell JM**. The incidence of benign renal nodules (a clinicopathologic study). *J Urol* 1971; **106**: 503-506
99 **Reis M**, Faria V, Lindoro J, Adolfo A. The small cystic and noncystic noninflammatory renal nodules: a postmortem study. *J Urol* 1988; **140**: 721-724
100 **Frank I**, Blute ML, Cheville JC, Lohse CM, Weaver AL, Zincke H. Solid renal tumors: an analysis of pathological features related to tumor size. *J Urol* 2003; **170**: 2217-2220
101 **Silver DA**, Morash C, Brenner P, Campbell S, Russo P. Pathologic findings at the time of nephrectomy for renal mass. *Ann Surg Oncol* 1997; **4**: 570-574
102 **Tuncali K**, vanSonnenberg E, Shankar S, Mortele KJ, Cibas ES, Silverman SG. Evaluation of patients referred for percutaneous ablation of renal tumors: importance of a preprocedural diagnosis. *AJR Am J Roentgenol* 2004; **183**: 575-582
103 **Raj GV**, Bach AM, Iasonos A, Korets R, Blitstein J, Hann L, Russo P. Predicting the histology of renal masses using preoperative Doppler ultrasonography. *J Urol* 2007; **177**: 53-58
104 **Filippone A**, Muzi M, Basilico R, Di Giandomenico V, Trapani AR, Bonomo L. Color Doppler flow imaging of renal disease. Value of a new intravenous contrast agent: SH U 508 A (Levovist). *Radiol Med* 1994; **87**: 50-58
105 **Somani BK**, Nabi G, Thorpe P, N'Dow J, Swami S, McClinton S. Image-guided biopsy-diagnosed renal cell carcinoma: critical appraisal of technique and long-term follow-up. *Eur Urol* 2007; **51**: 1289-1295; discussion 1296-1297
106 **Ascenti G**, Gaeta M, Magno C, Mazziotti S, Blandino A, Melloni D, Zimbaro G. Contrast-enhanced second-harmonic sonography in the detection of pseudocapsule in renal cell carcinoma. *AJR Am J Roentgenol* 2004; **182**: 1525-1530
107 **Silverman SG**, Lee BY, Seltzer SE, Bloom DA, Corless CL, Adams DF. Small (< or = 3 cm) renal masses: correlation of spiral CT features and pathologic findings. *AJR Am J Roentgenol* 1994; **163**: 597-605
108 **Duchene DA**, Lotan Y, Cadeddu JA, Sagalowsky AI, Koeneman KS. Histopathology of surgically managed renal tumors: analysis of a contemporary series. *Urology* 2003; **62**: 827-830
109 **Toprak U**, Erdoğan A, Gülbay M, Karademir MA, Paşaoğlu E, Akar OE. Preoperative evaluation of renal anatomy and renal masses with helical CT, 3D-CT and 3D-CT angiography. *Diagn Interv Radiol* 2005; **11**: 35-40
110 **Schmidbauer J**, Remzi M, Memarsadeghi M, Haitel A, Klingler HC, Katzenbeisser D, Wiener H, Marberger M. Diagnostic accuracy of computed tomography-guided percutaneous biopsy of renal masses. *Eur Urol* 2008; **53**: 1003-1011
111 **Caoili EM**, Bude RO, Higgins EJ, Hoff DL, Nghiem HV. Evaluation of sonographically guided percutaneous core biopsy of renal masses. *AJR Am J Roentgenol* 2002; **179**: 373-378
112 **Jaff A**, Molinié V, Mellot F, Guth A, Lebret T, Scherrer A. Evaluation of imaging-guided fine-needle percutaneous biopsy of renal masses. *Eur Radiol* 2005; **15**: 1721-1726
113 **Tsuboi N**, Horiuchi K, Kimura G, Kondoh Y, Yoshida K, Nishimura T, Akimoto M, Miyashita T, Subosawa T. Renal masses detected by general health checkup. *Int J Urol* 2000; **7**: 404-408
114 **Campbell SC**, Fichtner J, Novick AC, Steinbach F, Stöckle M, Klein EA, Filipas D, Levin HS, Störkel S, Schweden F, Obuchowski NA, Hale J. Intraoperative evaluation of renal cell carcinoma: a prospective study of the role of ultrasonography and histopathological frozen sections. *J Urol* 1996; **155**: 1191-1195
115 **Remzi M**, Katzenbeisser D, Waldert M, Klingler HC, Susani M, Memarsadeghi M, Heinz-Peer G, Haitel A, Herwig R, Marberger M. Renal tumour size measured radiologically before surgery is an unreliable variable for predicting histopathological features: benign tumours are not necessarily small. *BJU Int* 2007; **99**: 1002-1006
116 **Shannon BA**, Cohen RJ, de Bruto H, Davies RJ. The value of preoperative needle core biopsy for diagnosing benign lesions among small, incidentally detected renal masses. *J Urol* 2008; **180**: 1257-1261; discussion 1261
117 **Kramer BA**, Whelan CM, Vestal JC, Schwartz BF. Increasing the number of biopsy cores before renal cryoablation increases the diagnostic yield. *J Endourol* 2009; **23**: 283-286
118 **Habboub HK**, Abu-Yousef MM, Williams RD, See WA, Schweiger GD. Accuracy of color Doppler sonography in assessing venous thrombus extension in renal cell carcinoma. *AJR Am J Roentgenol* 1997; **168**: 267-271
119 **Tranquart F**, Correas JM, Martegani A, Greppi B, Bokor D. [Feasability of real time contrast enhanced ultrasound in renal disease] *J Radiol* 2004; **85**: 31-36
120 **Kabakci N**, Igci E, Secil M, Yorukoglu K, Mungan U, Celebi I, Kirkali Z. Echo contrast-enhanced power Doppler ultrasonography for assessment of angiogenesis in renal cell carcinoma. *J Ultrasound Med* 2005; **24**: 747-753
121 **Kawata N**, Igarashi T, Ichinose T, Hirakata H, Hachiya T, Takimoto Y, Ogawa M. Usefulness of contrast-enhanced ultrasound for the diagnosis of recurrent renal cell carcinoma in contralateral kidney. *Int J Urol* 2006; **13**: 325-328
122 **Lam JS**, Belldegrun AS, Pantuck AJ. Long-term outcomes of the surgical management of renal cell carcinoma. *World J Urol* 2006; **24**: 255-266
123 **Margulis V**, Tamboli P, Matin SF, Meisner M, Swanson DA, Wood CG. Redefining pT3 renal cell carcinoma in the modern era: a proposal for a revision of the current TNM primary tumor classification system. *Cancer* 2007; **109**: 2439-2444
124 **Kim HL**, Zisman A, Han KR, Figlin RA, Belldegrun AS. Prognostic significance of venous thrombus in renal cell carcinoma. Are renal vein and inferior vena cava involvement

different? *J Urol* 2004; **171**: 588-591
125 **Moinzadeh A**, Libertino JA. Prognostic significance of tumor thrombus level in patients with renal cell carcinoma and venous tumor thrombus extension. Is all T3b the same? *J Urol* 2004; **171**: 598-601
126 **Bos SD**, Mensink HJ. Can duplex Doppler ultrasound replace computerized tomography in staging patients with renal cell carcinoma? *Scand J Urol Nephrol* 1998; **32**: 87-91
127 **Gupta NP**, Ansari MS, Khaitan A, Sivaramakrishna MS, Hemal AK, Dogra PN, Seth A. Impact of imaging and thrombus level in management of renal cell carcinoma extending to veins. *Urol Int* 2004; **72**: 129-134
128 **Roy C**, Tuchmann C, Morel M, Saussine C, Jacqmin D, Tongio J. Is there still a place for angiography in the management of renal mass lesions? *Eur Radiol* 1999; **9**: 329-335
129 **Wink MH**, Lagerveld BW, Laguna MP, de la Rosette JJ, Wijkstra H. Cryotherapy for renal-cell cancer: diagnosis, treatment, and contrast-enhanced ultrasonography for follow-up. *J Endourol* 2006; **20**: 456-458; discussion 458-459
130 **Bosniak MA**. Diagnosis and management of patients with complicated cystic lesions of the kidney. *AJR Am J Roentgenol* 1997; **169**: 819-821
131 **Bosniak MA**. Cystic renal masses: a reevaluation of the usefullness of the Bosniak Classification System. *Acad Radiol* 1996; **3**: 981-984
132 **Israel GM**, Hindman N, Bosniak MA. Evaluation of cystic renal masses: comparison of CT and MR imaging by using the Bosniak classification system. *Radiology* 2004; **231**: 365-371
133 **Israel GM**, Bosniak MA. Calcification in cystic renal masses: is it important in diagnosis? *Radiology* 2003; **226**: 47-52
134 **Dietrich CF**, Tuma J. Echokontrastmittel in der Sonographie des Urogenitalsystems. In: Tuma J, Trinkler FB, editors. Sonographische Differenzialdiagnose (Krankheiten des Urogenitalsystems). Köln: Deutscher Ärzteverlag, 2009: 519-533
135 **Harisinghani MG**, Maher MM, Gervais DA, McGovern F, Hahn P, Jhaveri K, Varghese J, Mueller PR. Incidence of malignancy in complex cystic renal masses (Bosniak category III): should imaging-guided biopsy precede surgery? *AJR Am J Roentgenol* 2003; **180**: 755-758
136 **Curry NS**, Cochran ST, Bissada NK. Cystic renal masses: accurate Bosniak classification requires adequate renal CT. *AJR Am J Roentgenol* 2000; **175**: 339-342
137 **Aronson S**, Frazier HA, Baluch JD, Hartman DS, Christenson PJ. Cystic renal masses: usefulness of the Bosniak classification. *Urol Radiol* 1991; **13**: 83-90
138 **Siegel CL**, McFarland EG, Brink JA, Fisher AJ, Humphrey P, Heiken JP. CT of cystic renal masses: analysis of diagnostic performance and interobserver variation. *AJR Am J Roentgenol* 1997; **169**: 813-818
139 **Hirai T**, Ohishi H, Yamada R, Imai Y, Hirohashi S, Hirohashi R, Honda N, Uchida H. Usefulness of color Doppler flow imaging in differential diagnosis of multilocular cystic lesions of the kidney. *J Ultrasound Med* 1995; **14**: 771-776
140 **Park BK**, Kim B, Kim SH, Ko K, Lee HM, Choi HY. Assessment of cystic renal masses based on Bosniak classification: comparison of CT and contrast-enhanced US. *Eur J Radiol* 2007; **61**: 310-314
141 **Quaia E**, Bertolotto M, Cioffi V, Rossi A, Baratella E, Pizzolato R, Cov MA. Comparison of contrast-enhanced sonography with unenhanced sonography and contrast-enhanced CT in the diagnosis of malignancy in complex cystic renal masses. *AJR Am J Roentgenol* 2008; **191**: 1239-1249
142 **Clevert DA**, Minaifar N, Weckbach S, Jung EM, Stock K, Reiser M, Staehler M. Multislice computed tomography versus contrast-enhanced ultrasound in evaluation of complex cystic renal masses using the Bosniak classification system. *Clin Hemorheol Microcirc* 2008; **39**: 171-178
143 **Dietrich CF**, Ignee A, Barreiros AP, Schreiber-Dietrich D, Sienz M, Bojunga J, Braden B. Contrast-Enhanced Ultrasound for Imaging of Adrenal Masses. *Ultraschall Med* 2009; Epub ahead of print
144 **Dietrich CF**, Ignee A, Braden B, Barreiros AP, Ott M, Hocke M. Improved differentiation of pancreatic tumors using contrast-enhanced endoscopic ultrasound. *Clin Gastroenterol Hepatol* 2008; **6**: 590-597.e1

S- Editor Cheng JX **L- Editor** Cant MR **E- Editor** Ma WH

World Journal of Radiology

Online Submissions: http://www.wjgnet.com/1949-8470office
wjr@wjgnet.com
doi:10.4329/wjr.v2.i1.32

World J Radiol 2010 January 28; 2(1): 32-36
ISSN 1949-8470 (online)

TOPIC HIGHLIGHT

Hui-Xiong Xu, MD, PhD, *Series Editor*

Diagnosis of liver cirrhosis with contrast-enhanced ultrasound

Guang-Jian Liu, Ming-De Lu

Guang-Jian Liu, Department of Medical Ultrasonics, Institute of Diagnostic and Interventional Ultrasound, The First Affiliated Hospital of Sun Yat-Sen University, Guangzhou 510080, Guangdong Province, China
Ming-De Lu, Department of Hepatobiliary Surgery, Institute of Diagnostic and Interventional Ultrasound, The First Affiliated Hospital of Sun Yat-Sen University, Guangzhou 510080, Guangdong Province, China
Correspondence to: Ming-De Lu, MD, DMSc, Department of Hepatobiliary Surgery, The First Affiliated Hospital of Sun Yat-Sen University, No. 58 Zhongshan Road 2, Guangzhou 510080, Guangdong Province, China. lumd@21cn.com
Telephone: +86-20-87765183 Fax: +86-20-87765183
Received: December 2, 2009 Revised: December 30, 2009
Accepted: January 4, 2010
Published online: January 28, 2010

Abstract

The assessment of the extent of liver fibrosis is very important for the prognosis and clinical management of chronic liver diseases. Although liver biopsy is the gold standard for the assessment of liver fibrosis, new non-invasive diagnostic methods are urgently needed in clinical work due to certain limitations and complications of biopsy. Noninvasive imaging studies play an important role in the diagnosis of focal liver disease and diffuse liver diseases. Among them, ultrasonography is the first choice for study of the liver in clinical work. With the development of ultrasound contrast agents and contrast specific imaging techniques, contrast-enhanced ultrasound (CEUS) shows good performance and great potential in the evaluation of liver fibrosis. Researchers have tried different kinds of contrast agent and imaging method, such as arrival time of contrast agent in the hepatic vein, and quantitative analysis of the enhancement level of liver parenchyma, to evaluate the degree of liver fibrosis during the past 10 years. This review mainly summarizes the clinical studies concerning the assessment of liver fibrosis using CEUS.

Key words: Diagnosis; Liver cirrhosis; Contrast media; Ultrasound

Peer reviewer: Djordjije Saranovic, MD, PhD, Professor, Department of Digestive Radiology (First Surgical Clinic), Institute of Radiology, Clinical Center of Serbia, Koste Todorovica 6, 11000 Belgrade, Serbia

Liu GJ, Lu MD. Diagnosis of liver cirrhosis with contrast-enhanced ultrasound. *World J Radiol* 2010; 2(1): 32-36 Available from: URL: http://www.wjgnet.com/1949-8470/full/v2/i1/32.htm
DOI: http://dx.doi.org/10.4329/wjr.v2.i1.32

INTRODUCTION

Liver fibrosis is mainly caused by chronic liver diseases such as chronic hepatitis and alcoholic liver disease. Biopsy is considered as the gold standard for estimation of fibrosis. Owing to its limitations of sampling error, inter-observer disagreement, and the risks and complications of this invasive procedure, new, reliable noninvasive diagnostic methods are necessary to take the place of liver biopsy as the first line assessment of fibrosis during clinical work[1-7]. Biochemical tests and imaging techniques are the two most active research areas for the noninvasive assessment of liver fibrosis. The biochemical tests which are based on the evaluation of a large numbers of serological markers show good performance in predicting the degree of liver fibrosis. However, there are still some limits, especially in cases of Gilbert syndrome, hemolysis and acute inflammation. Therefore, biomarkers alone are not sufficient for making a definite decision in a given patient, and the clinical data must be taken into account[8]. As to the imaging methods, ultrasonography, computed tomography (CT) and magnetic resonance imaging (MRI) are the most traditional and popular, and transient elastography is a newly developed technique which can rapidly and noninvasively measure mean tissue stiffness.

Conventional grey scale ultrasound is the first-line imaging modality in screening of liver cirrhosis. Blunt

liver edge, liver parenchymal abnormalities, and liver morphological changes are the direct signs for diagnosis of liver cirrhosis on grey scale ultrasound. Color Doppler ultrasound can supply some valuable parameters for different blood vessels in diagnosis of liver cirrhosis, but the reliability and reproducibility of the technique limits its clinical usage in noninvasive diagnosis and assessment of severity of hepatic fibrosis[9-13]. Conventional CT and MRI scans can identify irregular or nodular liver surface, liver parenchymal abnormalities and portal hypertension which are very important signs for diagnosis of hepatic cirrhosis. The diagnostic accuracies for liver cirrhosis using these imaging modalities were reported in a recent study as 70.3% for MRI, 67.0% for CT and 64.0% for ultrasound, and the sensitivities and specificities were 86.7%, 84.3%, 52.4% and 53.9%, 52.9%, 73.5%, respectively[14]. With the development of super-paramagnetic iron oxide contrast agents for MRI, Kupffer-specific imaging may prove to be a new point of view with which to diagnose and evaluate the severity of the liver cirrhosis on MRI scan[15-17].

CONTRAST-ENHANCED ULTRASOUND

Newly developed ultrasound contrast agents (UCAs) and contrast-enhanced ultrasound (CEUS) techniques show great potential in the diagnosis of focal and diffuse liver disease[18,19]. Currently, the UCAs used in clinical CEUS examination are characterized by a microbubble structure consisting of gas bubbles stabilized by a shell. Globally, there are three kinds of UCA which can be used in liver imaging : Levovist (air with a galactose/palmitic acid surfactant; SH U 508A; Schering, Berlin, Germany), SonoVue (sulfur hexafluoride with a phospholipid shell; BR1; Bracco, Milan, Italy) and Sonazoid (perfluorobutane with a lipid shell; NC100100; Amersham Health, Oslo, Norway)[18,19]. SonoVue (sulfur hexafluoride) and Sonazoid (perfluorobutane) contain low solubility gases and show higher microbubble stability than Levovist which contains air. After intravenous injection of UCA, the microbubbles act as blood pool tracers, strongly increase the ultrasound backscatter and are therefore useful for enhancement of blood echogenicity and for the assessment of blood flow in the vasculature. In addition, Levovist and Sonazoid have been proved by both *in vivo* and *in vitro* studies to be phagocytosed by the reticuloendothelial system of the liver and spleen. The liver parenchyma specific imaging can be obtained 10 min after administration of the contrast agents[20-24].

The visualization of enhancement caused by microbubbles requires contrast specific imaging techniques, which are generally based on the cancellation and/or separation of linear US signals from tissue and utilization of the nonlinear response from microbubbles. A non-linear response from microbubbles could not only be induced by microbubble disruption at high acoustic pressure but also by oscillations at low acoustic pressure. When Levovist is used as contrast agent, high mechanical index (MI) intermittent imaging with low frame rates should be used, due to the lower resistance to acoustic pressure of the air filled microbubble. When SonoVue or Sonazoid is used as contrast agent, low MI imaging could be used, which enables minimal disruption of microbubbles, real time and effective investigations of the dynamic enhancement pattern, and effective tissue signal suppression[18,19].

CEUS IN DIAGNOSIS OF LIVER CIRRHOSIS

Contrast enhanced ultrasound has been used in the diagnosis and evaluation of liver cirrhosis during the past 10 years. Researchers mainly focused their studies on the hemodynamic changes and kupffer cell function changes followed by liver fibrosis, and tried to find and prove these changes using different kinds of CEUS techniques and UCAs[25-36].

Hepatic vein arrival time

The hemodynamic changes which accompany hepatic cirrhosis mainly include arterialization of the liver, intrahepatic shunts, pulmonary arteriovenous shunts, and a hyperdynamic circulatory state. All of these changes will make the hepatic first pass of contrast agent injected into a peripheral vein faster in a cirrhotic liver compared with normal liver.

Albrecht *et al*[25] studied the hepatic vein transit time using continuous spectral Doppler ultrasonography and Levovist. They found patients with cirrhosis showed a much earlier onset of enhancement (arrival time; mean 18.3 s) and peak enhancement (mean 55.5 s) than controls (49.8 s and 97.5 s) or patients with non-cirrhotic diffuse liver disease (35.8 s and 79.7 s). All patients with cirrhosis had an arrival time of the bolus of less than 24 s, whereas the arrival time was 24 s or more in 22 of the 23 other participants. Taking a hepatic vein arrival time of 24 s as the diagnostic criteria for liver cirrhosis, the sensitivity and specificity were 100% and 96%, respectively. They also found that peak enhancement was higher in patients with cirrhosis (mean 48.7 units) than in the other two groups (12.5 and 12.3 units, respectively). They concluded that analysis of liver transit time of a bolus of UCA provides useful information about haemodynamic changes in patients with cirrhosis, and measurement of the arrival time of the bolus allows discrimination of patients with cirrhosis from controls and from patients with non-cirrhotic diffuse liver disease, and has potential as a non-invasive test for cirrhosis. Bang *et al*[26] compared pulse inversion imaging with spectral Doppler quantification in assessment of the arrival of a contrast agent in the hepatic veins in six patients. They found the hepatic vein arrival times measured by two different methods were within 2 s apart in five patients and within 5 s apart in one patient. They believe pulse inversion imaging will be a simple and accurate method for evaluation of hepatic vein arrival time. Sugimoto *et al*[27] evaluated hepatic vein arrival time using Levovist and pulse inversion imaging in 15 patients. They found that the time-acoustic intensity curves for hepatic vein could be classified as a gradual-rising curve which was seen in

all controls and non-cirrhotic patients and a rapid-rising curve which was seen in all cirrhotic patients. They also showed that the hepatic vein arrival time was significantly earlier in cirrhotic patients compared with normal and hepatitis patients (18 s *vs* 31 s, 30 s), respectively. They believe CEUS and hepatic vein transit time is a useful noninvasive diagnosis method for liver cirrhosis with high sensitivity and specificity.

With the development of contrast specific techniques and the emergence of new generation contrast agent, real-time CEUS became a powerful tool for evaluation of liver cirrhosis. Ridolfi *et al*[28] tried to use low MI CEUS with SonoVue to evaluate the severity of chronic hepatitis C. They found the mean hepatic vein arrival time decreased progressively with increasing severity of liver disease, all patients with liver cirrhosis had a hepatic vein arrival time of 17 s or less, whereas values of 18 s or more were recorded for all controls and for almost all patients (20/22) with non-cirrhotic liver disease. But within the group of chronic hepatitis C, Metavir scores of fibrosis and necro-inflammatory changes had no significant effect on hepatic vein arrival times. They concluded that hepatic vein arrival time might be a simple and non-invasive method for reliably excluding cirrhosis with signs of portal hypertension, but not for assessing the severity of either chronic hepatitis C or cirrhosis. Lim *et al*[29] compared Levovist and SonoVue in evaluation of hepatic vein arrival time in 40 hepatitis C-related liver disease patients and 25 normal volunteers. They found that mean hepatic vein arrival times in control, mild hepatitis, moderate or severe hepatitis, and cirrhosis groups were 38.3, 47.5, 29.5 and 17.6 s, respectively, with Levovist; and 29.4, 27.4, 22.9 and 16.4 s, respectively, with SonoVue. The hepatic vein arrival time decreased as severity increased in imaging with both contrast agents. There was no significant difference in hepatic vein arrival time between mild and moderate hepatitis groups with SonoVue; however, there were significant differences in hepatic vein arrival time between all patient groups using Levovist. Hepatic vein arrival time of SonoVue was shorter than that of Levovist in all groups except the cirrhosis group where the hepatic vein arrival time of the two contrast agents was similar. Although hepatic vein arrival time seems to fulfill the task of diagnosis of liver cirrhosis, some researchers also found that the hepatic vein transit time was accelerated in the liver with metastatic liver tumors[37-39]. This is the main limitation of using hepatic vein transit time to diagnose liver cirrhosis since there may be many other situations which will also result in similar hemodynamic changes.

Some researchers also studied the micro-hemodynamic changes which follow liver cirrhosis using CEUS. Giuseppetti *et al*[33] used the destruction and replenishment CEUS technique to evaluate the changes in hepatic parenchymal blood flow in cirrhotic patients and normal patients. Pulse inversion harmonic imaging was obtained at progressively increasing pulse intervals of 2, 4, 7 and 10 s in the same scan plane during infusion of Levovist (300 mg/mL, 150 mL/h). Pulse intervals *vs* signal intensity (PI-SI) plots were made to illustrate the speed of blood in the liver parenchyma. They found the slope of the PI-SI plot of the Child A cirrhotic patients was significantly lower than the slope of the normal controls and of the Child C cirrhotic patients; conversely, no significant differences were found between the slope of the patients with Child C cirrhosis and of the normal controls. The slope of the patients with liver cirrhosis presented with a significantly higher variability than was observed in the normal controls. They explained their findings by suggesting the slope of the PI-SI plot obtained by placing the ROI in a region of parenchyma reflects the average speed of both the arterial and the venous components of the microcirculation. They thought that liver perfusion was provided mainly by the portal circulation in most patients with Child A cirrhosis, and because the velocity of the portal blood flow is reduced, an overall reduction of the average velocity of the parenchymal blood is observed. In patients with Child C cirrhosis and advanced disease, however, the portal component of the hepatic blood flow can be markedly reduced, with increased arterial perfusion and significant portosystemic venous and arteriovenous shunting. These hemodynamic changes can cause a prevalence of the arterial component of the microcirculation, with higher velocity flows, causing an overall increase of the average velocity of the parenchymal blood.

Enhancement level of liver parenchyma

Some researchers have tried to use enhancement level of liver parenchyma on CEUS to diagnose liver cirrhosis based on the theory of diminished or function damage of Kupffer cells accompanied with the hepatic cirrhosis. Fujita *et al*[34] used Levovist and stimulated acoustic emission imaging, and studied 114 patients with alcoholic liver disease and other chronic liver disease. They compared the enhancement level of the hepatic parenchyma and right kidney at 20 s, 90 s, and 5 min after injection of Levovist. The contrast patterns of the liver and kidney were divided into three patterns. In pattern A, only the kidney was strongly enhanced at 20 s, both liver and kidney were strongly enhanced at 90 s, and only the liver was enhanced at 5 min. In pattern B, both the liver and the kidney were strongly enhanced at 20 s and 90 s, but only the liver was strongly enhanced at 5 min. In pattern C, both the liver and the kidney were strongly enhanced at 20 s and 90 s, and both organs were weakly enhanced at 5 min. They found 83% of normal livers showed pattern A, whereas pattern B was found in 60%-86% of patients with chronic liver disease, and almost all of the patients with alcoholic liver cirrhosis had pattern C. They supposed that Kupffer cell dysfunction in liver cirrhosis resulted in slower clearance of contrast agent and thus weak enhancement of liver parenchyma in pattern C. Gasparini *et al*[35] studied 10 normal volunteers, 16 Child A and 16 Child C cirrhotic patients with CEUS using Levovist. They found the enhancement level of liver

parenchyma in late phase (7 min after administration of contrast agent) decreased significantly both in patients with Child A ($P < 0.05$) and Child C ($P < 0.001$) cirrhosis compared with normal liver, and a statistically significant signal intensity decrease was also observed from the patients with Child A to those with Child C cirrhosis ($P < 0.01$). Their explanation was that the decreased uptake of the Levovist microbubbles by the reticuloendothelial system in cirrhotic liver due to impaired functional capacity of the Kupffer cells secondary to increased portosystemic shunting of blood resulted in the observed difference between the groups. Kaneko *et al*[36] compared the parenchyma enhancement with the degree of liver dysfunction using pulse-inversion ultrasonography and Levovist. They found there was a significant inverse correlation between the gray scale of the liver parenchyma and the hepatic fibrosis index ($r = -0.809$, $P < 0.01$). The average signal intensity of the liver parenchyma was 144.5 in a normal liver, 133.6 in chronic hepatitis, and 102.6 in liver cirrhosis, demonstrating a significant difference between a normal and cirrhotic liver ($P < 0.01$). They concluded that the signal intensity of a microbubble disruption of the liver parenchyma in the late phase of enhancement with Levovist could reflect the degree of hepatic fibrosis.

CONCLUSION

In conclusion, hepatic vein arrival time and enhancement level of liver parenchyma in late phase may be valuable clues for the diagnosis of liver cirrhosis. Most researchers believe that the hemodynamic changes in cirrhotic liver mainly happen within the liver which results in faster hepatic vein transit time on CEUS compared with normal liver. Taking a hepatic vein arrival time of less than 21 s as the diagnostic criteria, the sensitivity, specificity, positive predictive value and negative predictive value of CEUS in diagnosis of liver cirrhosis was 100%, 80%, 74% and 100%, respectively. Many researchers also pointed out that the hepatic vein arrival time correlated with the severity of liver fibrosis. Different contrast agents result in different hepatic vein arrival time on CEUS. The second generation contrast agent SonoVue, has faster hepatic vein arrival time than Levovist in normal and hepatitis patients. Finally, hepatic metastasis will also result in a faster hepatic vein arrival time on CEUS, which is another limitation of hepatic vein arrival time in the diagnosis of liver cirrhosis. Enhancement level of liver parenchyma in late phase of CEUS shows a negative correlation with the severity of liver cirrhosis. Due to dysfunction of Kupffer cells in cirrhotic liver, the enhancement of liver parenchyma in late phase was much darker than normal liver. In conclusion, CEUS may be an easy and valuable non-invasive method for diagnosis and assessment of liver cirrhosis.

REFERENCES

1 **Bravo AA,** Sheth SG, Chopra S. Liver biopsy. *N Engl J Med* 2001; **344**: 495-500

2 **Regev A**, Berho M, Jeffers LJ, Milikowski C, Molina EG, Pyrsopoulos NT, Feng ZZ, Reddy KR, Schiff ER. Sampling error and intraobserver variation in liver biopsy in patients with chronic HCV infection. *Am J Gastroenterol* 2002; **97**: 2614-2618

3 **Colloredo G**, Guido M, Sonzogni A, Leandro G. Impact of liver biopsy size on histological evaluation of chronic viral hepatitis: the smaller the sample, the milder the disease. *J Hepatol* 2003; **39**: 239-244

4 **Bedossa P**, Dargère D, Paradis V. Sampling variability of liver fibrosis in chronic hepatitis C. *Hepatology* 2003; **38**: 1449-1457

5 **Ratziu V**, Charlotte F, Heurtier A, Gombert S, Giral P, Bruckert E, Grimaldi A, Capron F, Poynard T. Sampling variability of liver biopsy in nonalcoholic fatty liver disease. *Gastroenterology* 2005; **128**: 1898-1906

6 **Bedossa P**, Poynard T, Naveau S, Martin ED, Agostini H, Chaput JC. Observer variation in assessment of liver biopsies of alcoholic patients. *Alcohol Clin Exp Res* 1988; **12**: 173-178

7 **Poynard T**, Ratziu V, Bedossa P. Appropriateness of liver biopsy. *Can J Gastroenterol* 2000; **14**: 543-548

8 **Poynard T**, Morra R, Ingiliz P, Imbert-Bismut F, Thabut D, Messous D, Munteanu M, Massard J, Benhamou Y, Ratziu V. Assessment of liver fibrosis: noninvasive means. *Saudi J Gastroenterol* 2008; **14**: 163-173

9 **Lim AK**, Patel N, Eckersley RJ, Kuo YT, Goldin RD, Thomas HC, Cosgrove DO, Taylor-Robinson SD, Blomley MJ. Can Doppler sonography grade the severity of hepatitis C-related liver disease? *AJR Am J Roentgenol* 2005; **184**: 1848-1853

10 **Zoli M**, Magalotti D, Bianchi G, Ghigi G, Orlandini C, Grimaldi M, Marchesini G, Pisi E. Functional hepatic flow and Doppler-assessed total hepatic flow in control subjects and in patients with cirrhosis. *J Hepatol* 1995; **23**: 129-134

11 **Colli A**, Cocciolo M, Riva C, Martinez E, Prisco A, Pirola M, Bratina G. Abnormalities of Doppler waveform of the hepatic veins in patients with chronic liver disease: correlation with histologic findings. *AJR Am J Roentgenol* 1994; **162**: 833-837

12 **Iwao T**, Toyonaga A, Shigemori H, Oho K, Sakai T, Tayama C, Masumoto H, Sato M, Tanikawa K. Hepatic artery hemodynamic responsiveness to altered portal blood flow in normal and cirrhotic livers. *Radiology* 1996; **200**: 793-798

13 **Piscaglia F**, Gaiani S, Zironi G, Gramantieri L, Casali A, Siringo S, Serra C, Bolondi L. Intra- and extrahepatic arterial resistances in chronic hepatitis and liver cirrhosis. *Ultrasound Med Biol* 1997; **23**: 675-682

14 **Kudo M**, Zheng RQ, Kim SR, Okabe Y, Osaki Y, Iijima H, Itani T, Kasugai H, Kanematsu M, Ito K, Usuki N, Shimamatsu K, Kage M, Kojiro M. Diagnostic accuracy of imaging for liver cirrhosis compared to histologically proven liver cirrhosis. A multicenter collaborative study. *Intervirology* 2008; **51** Suppl 1: 17-26

15 **Elizondo G**, Weissleder R, Stark DD, Guerra J, Garza J, Fretz CJ, Todd LE, Ferrucci JT. Hepatic cirrhosis and hepatitis: MR imaging enhanced with superparamagnetic iron oxide. *Radiology* 1990; **174**: 797-801

16 **Tanimoto A**, Yuasa Y, Shinmoto H, Jinzaki M, Imai Y, Okuda S, Kuribayashi S. Superparamagnetic iron oxide-mediated hepatic signal intensity change in patients with and without cirrhosis: pulse sequence effects and Kupffer cell function. *Radiology* 2002; **222**: 661-666

17 **Aguirre DA**, Behling CA, Alpert E, Hassanein TI, Sirlin CB. Liver fibrosis: noninvasive diagnosis with double contrast material-enhanced MR imaging. *Radiology* 2006; **239**: 425-437

18 **Albrecht T**, Blomley M, Bolondi L, Claudon M, Correas JM, Cosgrove D, Greiner L, Jäger K, Jong ND, Leen E, Lencioni R, Lindsell D, Martegani A, Solbiati L, Thorelius L, Tranquart F, Weskott HP, Whittingham T. Guidelines for the use of contrast agents in ultrasound. January 2004. *Ultraschall Med* 2004; **25**: 249-256

19 **Claudon M**, Cosgrove D, Albrecht T, Bolondi L, Bosio M, Calliada F, Correas JM, Darge K, Dietrich C, D'Onofrio M, Evans DH, Filice C, Greiner L, Jäger K, Jong N, Leen E, Lencioni R, Lindsell D, Martegani A, Meairs S, Nolsøe C, Piscaglia F, Ricci P, Seidel G, Skjoldbye B, Solbiati L, Thorelius L, Tranquart F, Weskott HP, Whittingham T. Guidelines and good clinical practice recommendations for contrast enhanced ultrasound (CEUS) - update 2008. *Ultraschall Med* 2008; **29**: 28-44

20 **Blomley MJ**, Albrecht T, Cosgrove DO, Eckersley RJ, Butler-Barnes J, Jayaram V, Patel N, Heckemann RA, Bauer A, Schlief R. Stimulated acoustic emission to image a late liver and spleen-specific phase of Levovist in normal volunteers and patients with and without liver disease. *Ultrasound Med Biol* 1999; **25**: 1341-1352

21 **Suzuki S**, Iijima H, Moriyasu F, Sasaki S, Yanagisawa K, Miyahara T, Oguma K, Yoshida M, Horibe T, Ito N, Kakizaki D, Abe K, Tsuchiya K. Differential diagnosis of hepatic nodules using delayed parenchymal phase imaging of levovist contrast ultrasound: comparative study with SPIO-MRI. *Hepatol Res* 2004; **29**: 122-126

22 **Watanabe R**, Matsumura M, Munemasa T, Fujimaki M, Suematsu M. Mechanism of hepatic parenchyma-specific contrast of microbubble-based contrast agent for ultrasonography: microscopic studies in rat liver. *Invest Radiol* 2007; **42**: 643-651

23 **Yanagisawa K**, Moriyasu F, Miyahara T, Yuki M, Iijima H. Phagocytosis of ultrasound contrast agent microbubbles by Kupffer cells. *Ultrasound Med Biol* 2007; **33**: 318-325

24 **Iijima H**, Moriyasu F, Miyahara T, Yanagisawa K. Ultrasound contrast agent, Levovist microbubbles are phagocytosed by Kupffer cells-In vitro and in vivo studies. *Hepatol Res* 2006; **35**: 235-237

25 **Albrecht T**, Blomley MJ, Cosgrove DO, Taylor-Robinson SD, Jayaram V, Eckersley R, Urbank A, Butler-Barnes J, Patel N. Non-invasive diagnosis of hepatic cirrhosis by transit-time analysis of an ultrasound contrast agent. *Lancet* 1999; **353**: 1579-1583

26 **Bang N**, Nielsen MB, Rasmussen AN, Osterhammel PA, Pedersen JF. Hepatic vein transit time of an ultrasound contrast agent: simplified procedure using pulse inversion imaging. *Br J Radiol* 2001; **74**: 752-755

27 **Sugimoto H**, Kaneko T, Hirota M, Tezel E, Nakao A. Earlier hepatic vein transit-time measured by contrast ultrasonography reflects intrahepatic hemodynamic changes accompanying cirrhosis. *J Hepatol* 2002; **37**: 578-583

28 **Ridolfi F**, Abbattista T, Marini F, Vedovelli A, Quagliarini P, Busilacchi P, Brunelli E. Contrast-enhanced ultrasound to evaluate the severity of chronic hepatitis C. *Dig Liver Dis* 2007; **39**: 929-935

29 **Lim AK**, Patel N, Eckersley RJ, Goldin RD, Thomas HC, Cosgrove DO, Taylor-Robinson SD, Blomley MJ. Hepatic vein transit time of SonoVue: a comparative study with Levovist. *Radiology* 2006; **240**: 130-135

30 **Lim AK**, Taylor-Robinson SD, Patel N, Eckersley RJ, Goldin RD, Hamilton G, Foster GR, Thomas HC, Cosgrove DO, Blomley MJ. Hepatic vein transit times using a microbubble agent can predict disease severity non-invasively in patients with hepatitis C. *Gut* 2005; **54**: 128-133

31 **Blomley MJ**, Lim AK, Harvey CJ, Patel N, Eckersley RJ, Basilico R, Heckemann R, Urbank A, Cosgrove DO, Taylor-Robinson SD. Liver microbubble transit time compared with histology and Child-Pugh score in diffuse liver disease: a cross sectional study. *Gut* 2003; **52**: 1188-1193

32 **Gaiani S**, Serra C, Piscaglia F, Celli N, Rasciti L, Miglioli M, Bolondi L. Effect of Levovist on splanchnic hemodynamics in cirrhotic patients. *Ultrasound Med Biol* 2003; **29**: 643-648

33 **Giuseppetti GM**, Argalia G, Abbattista T. Liver cirrhosis: evaluation of haemodynamic changes using an ultrasound contrast agent. *Eur J Radiol* 2004; **51**: 27-33

34 **Fujita Y**, Watanabe M, Sasao K, Wakui N, Shinohara M, Ishii K, Sumino Y. Investigation of liver parenchymal flow using contrast-enhanced ultrasound in patients with alcoholic liver disease. *Alcohol Clin Exp Res* 2004; **28**: 169S-173S

35 **Gasparini C**, Bertolotto M, Crocè SL, Perrone R, Quaia E, Tiribelli C. Evaluation of liver parenchymal blood flow with contrast-enhanced US: preliminary results in healthy and cirrhotic patients. *Acad Radiol* 2003; **10**: 869-876

36 **Kaneko T**, Teshigawara O, Sugimoto H, Hirota M, Inoue S, Takeda S, Nakao A. Signal intensity of the liver parenchyma in microbubble contrast agent in the late liver phase reflects advanced fibrosis of the liver. *Liver Int* 2005; **25**: 288-293

37 **Blomley MJ**, Albrecht T, Cosgrove DO, Jayaram V, Eckersley RJ, Patel N, Taylor-Robinson S, Bauer A, Schlief R. Liver vascular transit time analyzed with dynamic hepatic venography with bolus injections of an US contrast agent: early experience in seven patients with metastases. *Radiology* 1998; **209**: 862-866

38 **Zhou JH**, Li AH, Cao LH, Jiang HH, Liu LZ, Pei XQ, Han F. Haemodynamic parameters of the hepatic artery and vein can detect liver metastases: assessment using contrast-enhanced ultrasound. *Br J Radiol* 2008; **81**: 113-119

39 **Bernatik T**, Strobel D, Häusler J, Hahn EG, Becker D. [Hepatic transit time of an ultrasound echo enhancer indicating the presence of liver metastases - first clinical results] *Ultraschall Med* 2002; **23**: 91-95

S- Editor Cheng JX **L- Editor** Lalor PF **E- Editor** Zheng XM

World Journal of Radiology

Online Submissions: http://www.wjgnet.com/1949-8470office
wjr@wjgnet.com
doi:10.4329/wjr.v2.i1.37

World J Radiol 2010 January 28; 2(1): 37-40
ISSN 1949-8470 (online)

OBSERVATION

Ewald Moser, PhD, *Series Editor*

Ultra-high-field magnetic resonance: Why and when?

Ewald Moser

Ewald Moser, MR Center of Excellence, Center for Medical Physics and Biomedical Engineering, Medical University of Vienna, A-1180 Vienna, Austria
Author contributions: Moser E is the sole author of this editorial.
Supported by An unrestricted research grant between Siemens Medical Solutions and the Medical University of Vienna, Vienna, Austria
Correspondence to: Ewald Moser, PhD, MR Center of Excellence, Center for Medical Physics and Biomedical Engineering, Medical University of Vienna, A-1180 Vienna, Austria. ewald.moser@meduniwien.ac.at
Telephone: +43-1-404006459 Fax: +43-1-404006475
Received: December 11, 2009 Revised: January 10, 2010
Accepted: January 13, 2010
Published online: January 28, 2010

Abstract

This paper briefly summarizes the development of magnetic resonance imaging and spectroscopy in medicine. Aspects of magnetic resonancephysics and -technology relevant at ultra-high magnetic fields as well as current limitations are highlighted. Based on the first promising studies, potential clinical applications at 7 Tesla are suggested. Other aims are to stimulate awareness of the potential of ultra-high field magnetic resonance and to stimulate active participation in much needed basic or clinical research at 7 Tesla or higher.

Key words: Alzheimer's disease; Brain tumors; Cartilage; Functional magnetic resonance imaging; Magnetic resonance; Magnetic resonance spectroscopy; Multiple sclerosis; Ultra-high field magnetic resonance methods

Peer reviewer: Juebin Huang, MD, PhD, Assistant Professor, Department of Neurology, The University of Mississippi Medical Center, 2500 N. State Street, Jackson, MS 39216, United States

Moser E. Ultra-high-field magnetic resonance: Why and when? *World J Radiol* 2010; 2(1): 37-40 Available from: URL: http://www.wjgnet.com/1949-8470/full/v2/i1/37.htm DOI: http://dx.doi.org/10.4329/wjr.v2.i1.37

From the very beginning, optimum field strength was a topic of debate in clinical proton magnetic resonance imaging (MRI)[1]. Earlier on it was even suggested that whole-body MRI would not be possible above 10 MHz or 0.24 Tesla[2]. Furthermore, based on *ex vivo* studies it was expected that T_1-contrast between various tissues and pathologies in the human body would strongly diminish above 100 MHz, leading to reduced image contrast[3]. Diagnostic contrast based on relaxation times, in general, was shown to be strongest at very low fields. As we all know, however, the brilliance of high-field MRI ($\geqslant$ 1.5 T) won the race and also benefited magnetic resonance spectroscopy (MRS)[4]. After a decade of high-end clinical 1.5 T MRI, and based on initial experience at 4 T in a few laboratories, research at 3 T started and translated very well into clinical imaging[5,6]. Despite the fact that 3 T clinical MR-systems started selling spectacularly, physicists and engineers continued to work on 7 T and higher fields in human MR-research (following the leading chemical and biochemical NMR work as well as animal research, now operating at up to 20 T for small animals). Note, however, that the first 7 T/90 cm magnet was already installed in 1999 demonstrating increasing signal-to-noise ratio (SNR) and more artifacts as compared to 4 T[7].

Still, it seems to be appropriate to ask whether or not patients will ever actually benefit from higher magnetic field strengths in clinical MRI and MRS, or will this field stay an academic playground? This paper will briefly review some MR-physics and -technology at around 7 T, and touch on current and future applications in clinical diagnostics.

Basically, the application of MR is not simple but the technique is rather versatile[8] in stark contrast to computed tomography or positron-emission tomography (PET) where endogenous contrast manipulation is rather

limited [i.e. image contrast is often achieved *via* exogenous contrast agents (CAs) or tracers]. In MR, three different magnetic fields (i.e. static, circular polarized, (linear) orthogonal gradients) have to interact properly and several data acquisition parameters need to be adjusted in a sensible way in order to obtain reliable diagnostic information. Furthermore, it is not so much the field strength (and corresponding resonance frequency) but the wavelength within the human body, which dictates interaction and, thus, information content. The lower the field strength the longer the length of RF-waves in the tissue will be, changing from about 1 m for protons at 1.5 T to several centimeters at ≥ 7 T. It seems obvious that the much shorter wavelength in proton MRI - now in the range of body organ dimensions - will lead to changing interactions and artifacts. This leads to standing and traveling wave phenomena[9-11] depending on the dielectric properties of the sample causing, at least, B1-inhomogeneities and inhomogeneous sensitivity profiles (e.g. "center bright" in the brain). In addition, spin-lattice and spin-spin interactions, i.e. relaxation times, change with field strength and quite possibly, the various relaxation mechanisms for different nuclei may be weighted differently. Therefore, we cannot expect to simply copy-and-paste techniques developed at lower fields and just linearly adjust certain sequence parameters (e.g. flip angle, echo time, repetition time).

Proton imaging at ≤ 3 T, the workhorse in clinical MRI, is currently rather advanced yet endures sensitivity limits for several applications. On the other hand, specific absorption rate (SAR) represents a legal limit, which is independent of the magnetic field strength and, thus, is more often met at higher fields as SAR increases with the square of the magnetic field strength. Therefore, and due to the lack of efficient whole body coils at 7 T or higher, local SAR replaces global SAR (Note: local SAR limit is about 5 times higher). As a rule of thumb, every application or pulse sequence hitting the SAR limit at 3 T cannot be used the same way at 7 T. On the other hand, any application lacking SNR should definitely be carried over to 7 T as long as SAR is not prohibitive. Alternatively, one could always try to change excitation pulse length (may cause offsets, increasing chemical shift artifacts) or type (e.g. adiabatic pulses), and/or repetition time, to reduce SAR in a particular patient group.

Imaging techniques originally developed at 1.5 T and already applicable at 7 T include high-resolution anatomical MRI[12,13], BOLD-based functional MRI[13,14], functional MR-Angiography[13,15], and susceptibility weighted imaging (SWI)[16,17]. In addition to standard magnitude images, phase images reveal new and additional information at 7 T[13,17,18]. Basically, these techniques do not use 180°-pulses, which are critical in terms of SAR and B_1-homogeneity, and gain from increased image SNR or time series SNR. The latter, relevant for functional MRI (fMRI), is limited by physiological noise[19]. On the other hand, high spatial resolution is not only possible but a must at 7 T in order to fully exploit the advantages at high field strength[13,20-23]. As a consequence, 1 mm^3 isotropic resolution is not only achievable for anatomical but also for functional MRI and this information may be mapped onto each other easily[13]. This enables brain research and pre-clinical tumor diagnosis to be performed at a new level, greatly helping neurosurgeons. As of today, there are first results available[13,24] and several applications are already close to clinical use. Of course, they still require confirmation by larger, multi-center studies: musculo-skeletal applications, in particular cartilage[13,25-27], multiple sclerosis[12,28], and whole body imaging[13]. Based on these promising studies, I would expect preoperative brain tumor surgery planning, using high resolution fMRI, multiple sclerosis and Alzheimer's disease, using high resolution MRI and SWI, and early diagnosis of defects in cartilage and vertebral discs to represent the first useful clinical applications of 7 T proton MRI.

Imaging methods not gaining as much at 7 T include diffusion weighted imaging (DWI), which gains in SNR but not from the basic physical mechanism which is field independent, and contrast-enhanced MRI, when standard, gadolinium-based CAs are used. Of note, iron-based CAs like USPIO are now approved for human use and will do a much better job at 7 T. In addition to MRI, MRS is gaining substantially from the high field, which was known for a long time in *ex vivo* NMR and animal studies[4,13,29,30]. Non-proton techniques, employing, e.g. ^{23}Na and ^{31}P nuclei, gain even more as they are lacking sensitivity at lower fields due to the lower gyromagnetic ratio and resonance frequency. Sodium imaging, which was developed at 1.5 T many years ago[31,32], despite its general importance in many diseases like stroke or brain tumors, might become a useful clinical tool only at 7 T or higher[13,33]. This may improve clinical diagnosis in stroke patients and help to better differentiate brain tumors and surrounding edema. I believe that ^{31}P-MRS will gain the most from higher fields. Why? Because for many applications ^{31}P-MRS and MRSI need better SNR than available at 3 T today and will profit also from the increased spectral dispersion (line splitting), enabling improved quantification of metabolites like phosphocreatine, adenosine triphosphate, inorganic phosphate, phosphomonoesters and phosphodiesters, relevant for energy metabolism. Furthermore, there is no nuisance background to be suppressed, like water and fat in proton-MRS. Finally, in a recent study, we demonstrated that metabolites' T_1-relaxation times in human skeletal muscle actually decreased with field strength[34], as compared to 1.5 T and 3 T[35], enabling faster scanning without loss in SNR (or saturation). This will enable fast, dynamic and localized ^{31}P-MRS[36,37] to study energy metabolism in patients and also higher resolution ^{31}P-MRSI (i.e. spectroscopic imaging), thus increasing specificity. In my opinion, ^{31}P relaxation times are also decreasing in human brain tissue if interpreted correctly[38]. Potential clinical applications are all kinds of metabolic disturbances of skeletal muscles based on

genetic or functional defects like muscle dystrophies or diabetes.

What has been discussed so far, can be achieved on a "standard", first generation 7 T system, i.e. with single channel transmit and local multi-array-receive coils (i.e. in the brain, skeletal muscle, joints, cartilage, *etc.*). When attempting to scan the body trunk, e.g. heart, liver, kidneys, multi-channel transmit techniques are inevitable and they also may improve brain and joint imaging to name a few. However, this technology is still under development and problems with inhomogeneous and inefficient body excitation, causing not only degraded image quality but also SAR problems, have to be solved within the next few years[9-11,13]. Furthermore, multi-array receive coils are far from mature today. Together with improved coil designs, dedicated artifact reduction techniques have to be developed to achieve robust and reliable imaging quality within legal SAR limits[13]. At the end, it will be the best possible combination of organ size and location, tissue structure and composition, Tx/Rx coil, imaging protocol and contrast mechanism that will provide the best data quality available in a given time. Much improved MRI and MRS at UHF may also help foster multi-modal imaging, e.g. MR-PET[8,13]. This novel hybrid technique may help to gain more relevant information to better characterize the complexity of normal organ functions and, subsequently, characterize their breakdown, e.g. in brain tumors. This should pave the way towards novel and validated individualized therapies.

To summarize, novel contrast mechanisms, applicable through advanced technology and a sound understanding of MR-physics and -technology, pave the way to novel clinical applications. However, there are not only technical challenges, clinicians will also have to rethink and expand their current knowledge used to interpret diagnostic images at 1.5 T and 3 T. In some areas, such as standard contrast agent applications or DWI, nothing may change dramatically and one could argue to stay with the current 3 T systems. In other areas, however, only 7 T or even higher fields will enable scientists and clinicians to fully explore the potential of magnetic resonance techniques towards evidence based clinical diagnostics. Nevertheless, I would like to end this preliminary account on UHF-MR with a word of caution. We are only at the very beginning of UHF-MR applications and both hardware and measurement techniques are immature and need to be improved substantially before any sound conclusions on the clinical use of UHF-systems in general can be made. In particular, several safety issues have to be clarified, including the potential hazard of body implants, in order to minimize any risk to patients and operators.

ACKNOWLEDGMENTS

The author is grateful to all his colleagues working at 7 T for their support, interesting discussions and suggestions, and his coworkers in Vienna for their contributions.

REFERENCES

1 **Hoult DI**, Chen CN, Sank VJ. The field dependence of NMR imaging. II. Arguments concerning an optimal field strength. *Magn Reson Med* 1986; **3**: 730-746
2 **Hoult DI**, Lauterbur PC. The sensitivity of the zeugmatographic experiment involving human samples. *J Magn Reson* 1979; **34**: 425-433
3 **Koenig SH**, Brown RD 3rd, Adams D, Emerson D, Harrison CG. Magnetic field dependence of 1/T1 of protons in tissue. *Invest Radiol* 1984; **19**: 76-81
4 **Uğurbil K**, Garwood M, Ellermann J, Hendrich K, Hinke R, Hu X, Kim SG, Menon R, Merkle H, Ogawa S. Imaging at high magnetic fields: initial experiences at 4 T. *Magn Reson Q* 1993; **9**: 259-277
5 **Moser E**, Trattnig S. 3.0 Tesla MR systems. *Invest Radiol* 2003; **38**: 375-376
6 **Kramer H**, Michaely HJ, Matschl V, Schmitt P, Reiser MF, Schoenberg SO. High-resolution magnetic resonance angiography of the lower extremities with a dedicated 36-element matrix coil at 3 Tesla. *Invest Radiol* 2007; **42**: 477-483
7 **Vaughan JT**, Garwood M, Collins CM, Liu W, DelaBarre L, Adriany G, Andersen P, Merkle H, Goebel R, Smith MB, Ugurbil K. 7T vs. 4T: RF power, homogeneity, and signal-to-noise comparison in head images. *Magn Reson Med* 2001; **46**: 24-30
8 **Moser E**, Stadlbauer A, Windischberger C, Quick HH, Ladd ME. Magnetic resonance imaging methodology. *Eur J Nucl Med Mol Imaging* 2009; **36** Suppl 1: S30-S41
9 **Yang QX**, Wang J, Zhang X, Collins CM, Smith MB, Liu H, Zhu XH, Vaughan JT, Ugurbil K, Chen W. Analysis of wave behavior in lossy dielectric samples at high field. *Magn Reson Med* 2002; **47**: 982-989
10 **Van de Moortele PF**, Akgun C, Adriany G, Moeller S, Ritter J, Collins CM, Smith MB, Vaughan JT, Uğurbil K. B(1) destructive interferences and spatial phase patterns at 7 T with a head transceiver array coil. *Magn Reson Med* 2005; **54**: 1503-1518
11 **Brunner DO**, De Zanche N, Fröhlich J, Paska J, Pruessmann KP. Travelling-wave nuclear magnetic resonance. *Nature* 2009; **457**: 994-998
12 **Metcalf M**, Xu D, Okuda DT, Carvajal L, Srinivasan R, Kelley DA, Mukherjee P, Nelson SJ, Vigneron DB, Pelletier D. High-Resolution Phased-Array MRI of the Human Brain at 7 Tesla: Initial Experience in Multiple Sclerosis Patients. *J Neuroimaging* 2009; Epub ahead of print
13 Siemens UHF-meeting; 2009 Sep 12-14; Leipzig, Germany
14 **Poser BA**, Norris DG. Investigating the benefits of multi-echo EPI for fMRI at 7 T. *Neuroimage* 2009; **45**: 1162-1172
15 **Heverhagen JT**, Bourekas E, Sammet S, Knopp MV, Schmalbrock P. Time-of-flight magnetic resonance angiography at 7 Tesla. *Invest Radiol* 2008; **43**: 568-573
16 **Lupo JM**, Banerjee S, Kelley D, Xu D, Vigneron DB, Majumdar S, Nelson SJ. Partially-parallel, susceptibility-weighted MR imaging of brain vasculature at 7 Tesla using sensitivity encoding and an autocalibrating parallel technique. *Conf Proc IEEE Eng Med Biol Soc* 2006; **1**: 747-750
17 **Deistung A**, Rauscher A, Sedlacik J, Stadler J, Witoszynskyj S, Reichenbach JR. Susceptibility weighted imaging at ultra high magnetic field strengths: theoretical considerations and experimental results. *Magn Reson Med* 2008; **60**: 1155-1168
18 **Duyn JH**, van Gelderen P, Li TQ, de Zwart JA, Koretsky AP, Fukunaga M. High-field MRI of brain cortical substructure based on signal phase. *Proc Natl Acad Sci USA* 2007; **104**: 11796-11801
19 **Triantafyllou C**, Hoge RD, Krueger G, Wiggins CJ, Potthast A, Wiggins GC, Wald LL. Comparison of physiological noise at 1.5 T, 3 T and 7 T and optimization of fMRI acquisition parameters. *Neuroimage* 2005; **26**: 243-250
20 **Moser EV**, Derntl B, Gerstl F, Robinson SD, Karlsson KÆ,

Windischberger C. Functional MR-imaging of human emotions: towards single subject diagnosis. *IFMBE Proc* 2009; **25**: 19-22
21 **Windischberger C**, Cunnington R, Lamm C, Lanzenberger R, Langenberger H, Deecke L, Bauer H, Moser E. Time-resolved analysis of fMRI signal changes using Brain Activation Movies. *J Neurosci Methods* 2008; **169**: 222-230
22 **Windischberger C**, Gerstl F, Fischmeister FPS, Schöpf V, Kaseß C, Moser E. Brain Activity Movie functional MRI with ultra-high temporal resolution at 7 Tesla. *IFMBE Proc* 2009; **25**: 192-194
23 **Windischberger C**, Fischmeister FP, Schöpf V, Sladky R, Moser E. [Functional magnetic resonance imaging with ultra-high fields.] *Radiologe* 2009; Epub ahead of print
24 **Hennig J**. Ultra high field MR: useful instruments or toys for the boys? *Magn Reson Mater Phy* 2008; 21: 1-3
25 **Behr B**, Stadler J, Michaely HJ, Damert HG, Schneider W. MR imaging of the human hand and wrist at 7 T. *Skeletal Radiol* 2009; **38**: 911-917
26 **Krug R**, Stehling C, Kelley DA, Majumdar S, Link TM. Imaging of the musculoskeletal system in vivo using ultra-high field magnetic resonance at 7 T. *Invest Radiol* 2009; **44**: 613-618
27 **Welsch GH**, Mamisch TC, Hughes T, Zilkens C, Quirbach S, Scheffler K, Kraff O, Schweitzer ME, Szomolanyi P, Trattnig S. In vivo biochemical 7.0 Tesla magnetic resonance: preliminary results of dGEMRIC, zonal T2, and T2* mapping of articular cartilage. *Invest Radiol* 2008; **43**: 619-626
28 **Tallantyre EC**, Brookes MJ, Dixon JE, Morgan PS, Evangelou N, Morris PG. Demonstrating the perivascular distribution of MS lesions in vivo with 7-Tesla MRI. *Neurology* 2008; **70**: 2076-2078
29 **Otazo R**, Mueller B, Ugurbil K, Wald L, Posse S. Signal-to-noise ratio and spectral linewidth improvements between 1.5 and 7 Tesla in proton echo-planar spectroscopic imaging. *Magn Reson Med* 2006; **56**: 1200-1210
30 **Ratai E**, Kok T, Wiggins C, Wiggins G, Grant E, Gagoski B, O'Neill G, Adalsteinsson E, Eichler F. Seven-Tesla proton magnetic resonance spectroscopic imaging in adult X-linked adrenoleukodystrophy. *Arch Neurol* 2008; **65**: 1488-1494
31 **Hilal SK**, Maudsley AA, Ra JB, Simon HE, Roschmann P, Wittekoek S, Cho ZH, Mun SK. In vivo NMR imaging of sodium-23 in the human head. *J Comput Assist Tomogr* 1985; **9**: 1-7
32 **Winkler SS**. Sodium-23 magnetic resonance brain imaging. *Neuroradiology* 1990; **32**: 416-420
33 **Nagel AM**, Schmitter1 S, Bock M, Moser E, Semmler W, Schad LR. Parameter Optimization for 7T 23Na-MRI. *Proc Intl Soc Mag Reson Med* 2009; **17**: 2465
34 **Bogner W**, Chmelik M, Schmid AI, Moser E, Trattnig S, Gruber S. Assessment of (31)P relaxation times in the human calf muscle: a comparison between 3 T and 7 T in vivo. *Magn Reson Med* 2009; **62**: 574-582
35 **Meyerspeer M**, Krssák M, Moser E. Relaxation times of 31P-metabolites in human calf muscle at 3 T. *Magn Reson Med* 2003; **49**: 620-625
36 **Meyerspeer M**, Mandl T, Scheenen T, Moser E. Dynamic 31P MRS of exercising human muscle in a 7T whole body system, with STEAM and semi-LASER localisation. *Proc Intl Soc Mag Reson Med* 2009; **17**: 553
37 **Meyerspeer M**, Kemp GJ, Mlynárik V, Krssák M, Szendroedi J, Nowotny P, Roden M, Moser E. Direct noninvasive quantification of lactate and high energy phosphates simultaneously in exercising human skeletal muscle by localized magnetic resonance spectroscopy. *Magn Reson Med* 2007; **57**: 654-660
38 **Qiao H**, Zhang X, Zhu XH, Du F, Chen W. In vivo 31P MRS of human brain at high/ultrahigh fields: a quantitative comparison of NMR detection sensitivity and spectral resolution between 4 T and 7 T. *Magn Reson Imaging* 2006; **24**: 1281-1286

S- Editor Cheng JX **L- Editor** Webster JR **E- Editor** Zheng XM

World Journal of Radiology

Online Submissions: http://www.wjgnet.com/1949-8470office
wjr@wjgnet.com
doi:10.4329/wjr.v2.i1.41

World J Radiol 2010 January 28; 2(1): 41-43
ISSN 1949-8470 (online)

GUIDELINES FOR CLINICAL PRACTICE

High attenuation mucoid impaction in allergic bronchopulmonary aspergillosis

Ritesh Agarwal

Ritesh Agarwal, Department of Pulmonary Medicine, Postgraduate Institute of Medical Education and Research Sector-12, Chandigarh 160012, India
Author contributions: Agarwal R conceived the idea and drafted the manuscript.
Correspondence to: Ritesh Agarwal, MD, DM, Assistant Professor, Department of Pulmonary Medicine, Postgraduate Institute of Medical Education and Research Sector-12, Chandigarh 160012, India. riteshpgi@gmail.com
Telephone: +91-172-2756825 Fax: +91-172-2748215
Received: December 15, 2009 Revised: January 20, 2010
Accepted: January 22, 2010
Published online: January 28, 2010

Abstract

Allergic bronchopulmonary aspergillosis (ABPA) is a complex hypersensitivity syndrome triggered against antigens of *Aspergillus fumigatus*, a fungus that most commonly colonizes the airways of patients with bronchial asthma and cystic fibrosis. It presents clinically with refractory asthma, hemoptysis and systemic manifestations including fever, malaise and weight loss. Radiologically, it presents with central bronchiectasis and recurrent episodes of mucus plugging. The mucus plugs in ABPA are generally hypodense but in up to 20% of patients the mucus can be hyperdense on computed tomography. This paper reviews the literature on the clinical significance of hyperattenuated mucus in patients with ABPA.

Key words: Allergic bronchopulmonary aspergillosis; Mucoid impaction; Hyperdense mucus; High attenuation mucus; Aspergillus

Peer reviewers: Georgios A Plataniotis, MD, PhD, Clinical Oncologist, Department of Oncology, Aberdeen Royal Infirmary, Foresterhill, Aberdeen, AB25 2ZN, United Kingdom; Jai Soung Park, MD, PhD, Professor, Department of Radiology, Soonchunhyang University Buchen Hospital, 1174 jung-dong, Wonmi-gu, Bucheon, Gyeonggi-do 420-767, South Korea

Agarwal R. High attenuation mucoid impaction in allergic bronchopulmonary aspergillosis. *World J Radiol* 2010; 2(1): 41-43 Available from: URL: http://www.wjgnet.com/1949-8470/full/v2/i1/41.htm DOI: http://dx.doi.org/10.4329/wjr.v2.i1.41

Allergic bronchopulmonary aspergillosis (ABPA) is a complex immunologic syndrome complicating the course of various pulmonary disorders including bronchial asthma[1]. The disease was first described by Hinson *et al*[2] as an association of bronchial asthma with hypersensitivity to *Aspergillus fumigatus*. It manifests clinically with uncontrolled asthma, hemoptysis and systemic manifestations such as fever, weight loss, malaise and fatigue[1]. The interest in this entity stems from the fact that that the condition responds remarkably to glucocorticoid therapy, and early detection and treatment may eliminate the risk of progression to end-stage fibrotic lung disease[3]. Radiologically, it is characterized by central bronchiectasis (bronchiectasis limited to the medial half of the lung, at a point midway between the hilum and the chest wall) with distal tapering of bronchi and recurrent episodes of mucus plugging[4]. The bronchial mucus plugging in ABPA is generally hypodense; however, the mucus secretions can also have high attenuation computed tomography (CT) values[5]. High attenuation mucus is said to be present if the mucus plug is visually denser than the normal skeletal muscle (Figure 1).

The occurrence of high attenuation mucoid impaction in ABPA was first described by Goyal *et al*[6] in 1992, and it is likely that this radiological diagnosis was missed previously[7] and even after 1992[8,9]. Subsequently, Logan *et al*[10] described the occurrence of high density mucus plugs in 4 out of 14 (28%) patients with ABPA over a 4 years period. Following this, numerous reports have

Figure 1 High-resolution computed tomography (CT) of the chest showing high attenuation mucus in a patient with allergic bronchopulmonary aspergillosis (solid arrow). The mucus is denser than the paraspinal skeletal muscle (asterisk).

described the finding of high attenuation mucus in ABPA[11-15]. Currently, the presence of hyperdense mucus is considered a characteristic, if not a pathognomonic, finding in ABPA[16]. The constituents of hyperdense mucus are not entirely clear. The hyperattenuating mucus probably has a basis similar to that seen in patients with allergic fungal sinusitis[17,18]. An initial theory proposed the role of hemosiderin occurring within inspissated mucin as responsible for the areas of increased signal intensity. This was disputed by Zinreich *et al*[19] who were unable to identify increased hemosiderin within typical allergic fungal mucin. The hyperattenuating mucus plugging seen on CT scans is currently attributed to the presence of calcium salts and metals (the ions of iron and manganese)[20] or desiccated mucus[21].

The clinical significance of high-attenuation mucoid impaction in ABPA was hitherto unknown. However, in a recent study, we screened 755 patients with bronchial asthma for ABPA using the *Aspergillus* skin test. Two hundred and ninety one patients (38.5%) were found to be aspergillus skin test positive, and ABPA was diagnosed in 155 patients. In a multivariate analysis, both the severity of bronchiectasis and high-attenuation mucus predicted relapses of ABPA (OR: 1.23, 95% CI: 1.13-1.42 and OR: 3.61, 95% CI: 1.23-10.61, respectively). However, failure to achieve long-term remission was influenced only by the severity of bronchiectasis but not by hyperdense mucus (OR: 1.55, 95% CI: 1.29-1.85 and OR: 3.41, 95% CI: 0.89-13.1, respectively)[14]. The exact reason why hyperdense mucus is associated with recurrent relapses remains unclear but one reason may be that the mucus is more impacted, and the higher attenuation points to a more inspissated type of mucus. It is also probable that it defines a subgroup of patients with more severe inflammation. Recently, interleukin-10 promoter and surfactant protein polymorphisms have been associated with genetic susceptibility to ABPA[22,23]. It may well be hypothesized that patients with hyperdense mucus have specific genetic alterations that lead to formation of high attenuation mucus, and the genetic abnormalities dictate a disease with more severe inflammation and poorer outcomes. However, more research is needed to investigate the exact reason for this association.

High attenuation mucus also has an important connotation in patients with cystic fibrosis (CF). Unlike asthma, recognition of ABPA in CF is difficult as ABPA shares many clinical characteristics with poorly controlled CF lung disease without ABPA. Wheezing (due to intercurrent infections), transient pulmonary infiltrates, bronchiectasis and mucus plugging are common manifestations of CF-related pulmonary disease with or without ABPA[3]. The finding of hyperdense mucus with CT in patients with CF suggests that the lung disease is due to ABPA rather than CF *per se*[15].

REFERENCES

1 **Agarwal R**. Allergic bronchopulmonary aspergillosis. *Chest* 2009; **135**: 805-826
2 **Hinson KF**, Moon AJ, Plummer NS. Broncho-pulmonary aspergillosis; a review and a report of eight new cases. *Thorax* 1952; **7**: 317-333
3 **Agarwal R**. Controversies in allergic bronchopulmonary aspergillosis. *Int J Respir Care* 2010; In press
4 **Shah A**. Allergic bronchopulmonary and sinus aspergillosis: the roentgenologic spectrum. *Front Biosci* 2003; **8**: e138-e146
5 **Agarwal R**, Gupta D, Aggarwal AN, Behera D, Jindal SK. Allergic bronchopulmonary aspergillosis: lessons from 126 patients attending a chest clinic in north India. *Chest* 2006; **130**: 442-448
6 **Goyal R**, White CS, Templeton PA, Britt EJ, Rubin LJ. High attenuation mucous plugs in allergic bronchopulmonary aspergillosis: CT appearance. *J Comput Assist Tomogr* 1992; **16**: 649-650
7 **Fraser RG**, Pare JAP, Pare PD, Fraser RS, Genereux GP. Mycotic and Actinomycotic pleuropulmonary infections. In: Diagnosis of Diseases of the Chest. 3rd ed. Philadelphia: WB Saunders, 1989: 940-1022
8 **Sandhu M**, Mukhopadhyay S, Sharma SK. Allergic bronchopulmonary aspergillosis: a comparative evaluation of computed tomography with plain chest radiography. *Australas Radiol* 1994; **38**: 288-293
9 **Aquino SL**, Kee ST, Warnock ML, Gamsu G. Pulmonary aspergillosis: imaging findings with pathologic correlation. *AJR Am J Roentgenol* 1994; **163**: 811-815
10 **Logan PM**, Müller NL. High-attenuation mucous plugging in allergic bronchopulmonary aspergillosis. *Can Assoc Radiol J* 1996; **47**: 374-377
11 **Karunaratne N**, Baraket M, Lim S, Ridley L. Case quiz. Thoracic CT illustrating hyperdense bronchial mucous plugging: allergic bronchopulmonary aspergillosis. *Australas Radiol* 2003; **47**: 336-338
12 **Molinari M**, Ruiu A, Biondi M, Zompatori M. Hyperdense mucoid impaction in allergic bronchopulmonary aspergillosis: CT appearance. *Monaldi Arch Chest Dis* 2004; **61**: 62-64
13 **Agarwal R**, Aggarwal AN, Gupta D. High-attenuation mucus in allergic bronchopulmonary aspergillosis: another cause of diffuse high-attenuation pulmonary abnormality. *AJR Am J Roentgenol* 2006; **186**: 904
14 **Agarwal R**, Gupta D, Aggarwal AN, Saxena AK, Chakrabarti A, Jindal SK. Clinical significance of hyperattenuating mucoid impaction in allergic bronchopulmonary aspergillosis: an analysis of 155 patients. *Chest* 2007; **132**: 1183-1190
15 **Morozov A**, Applegate KE, Brown S, Howenstine M. High-attenuation mucus plugs on MDCT in a child with cystic fibrosis: potential cause and differential diagnosis. *Pediatr*

Radiol 2007; **37**: 592-595
16 **Webb WR**, Muller NL, Naidich DP. Airway diseases. In: Webb WR, editor. High-resolution CT of the lung. 4th ed. Philadelphia: LWW, 2009: 492-554
17 **Manning SC**, Merkel M, Kriesel K, Vuitch F, Marple B. Computed tomography and magnetic resonance diagnosis of allergic fungal sinusitis. *Laryngoscope* 1997; **107**: 170-176
18 **Mukherji SK**, Figueroa RE, Ginsberg LE, Zeifer BA, Marple BF, Alley JG, Cooper LL, Nemzek WR, Yousem DM, Jones KR, Kupferberg SB, Castillo M. Allergic fungal sinusitis: CT findings. *Radiology* 1998; **207**: 417-422
19 **Zinreich SJ**, Kennedy DW, Malat J, Curtin HD, Epstein JI, Huff LC, Kumar AJ, Johns ME, Rosenbaum AE. Fungal sinusitis: diagnosis with CT and MR imaging. *Radiology* 1988; **169**: 439-444
20 **Kopp W**, Fotter R, Steiner H, Beaufort F, Stammberger H. Aspergillosis of the paranasal sinuses. *Radiology* 1985; **156**: 715-716
21 **Dillon WP**, Som PM, Fullerton GD. Hypointense MR signal in chronically inspissated sinonasal secretions. *Radiology* 1990; **174**: 73-78
22 **Saxena S**, Madan T, Shah A, Muralidhar K, Sarma PU. Association of polymorphisms in the collagen region of SP-A2 with increased levels of total IgE antibodies and eosinophilia in patients with allergic bronchopulmonary aspergillosis. *J Allergy Clin Immunol* 2003; **111**: 1001-1007
23 **Brouard J**, Knauer N, Boelle PY, Corvol H, Henrion-Caude A, Flamant C, Bremont F, Delaisi B, Duhamel JF, Marguet C, Roussey M, Miesch MC, Chadelat K, Boule M, Fauroux B, Ratjen F, Grasemann H, Clement A. Influence of interleukin-10 on Aspergillus fumigatus infection in patients with cystic fibrosis. *J Infect Dis* 2005; **191**: 1988-1991

S- Editor Cheng JX **L- Editor** Lutze M **E- Editor** Zheng XM

World Journal of Radiology

Online Submissions: http://www.wjgnet.com/1949-8470office
wjr@wjgnet.com
doi:10.4329/wjr.v2.i1.44

World J Radiol 2010 January 28; 2(1): 44-54
ISSN 1949-8470 (online)

REVIEW

Non-invasive MRI assessment of the articular cartilage in clinical studies and experimental settings

Yi-Xiang J Wang, James F Griffith, Anil T Ahuja

Yi-Xiang J Wang, James F Griffith, Anil T Ahuja, Department of Diagnostic Radiology and Organ Imaging, The Chinese University of Hong Kong, Prince of Wales Hospital, Shatin, Hong Kong, China
Author contributions: Wang YXJ guaranteed the integrity of the paper; Wang YXJ, Griffith JF and Ahuja AT searched the literature, drafted and revised the manuscript for important intellectual content.
Correspondence to: Dr. Yi-Xiang J Wang, Department of Diagnostic Radiology and Organ Imaging, The Chinese University of Hong Kong, Prince of Wales Hospital, Shatin, Hong Kong, China. yixiang_wang@cuhk.edu.hk
Telephone: +852-26322289 Fax: +852-26360012
Received: December 7, 2009 Revised: January 12, 2010
Accepted: January 20, 2010
Published online: January 28, 2010

Abstract

Attrition and eventual loss of articular cartilage are important elements in the pathophysiology of osteoarthritis (OA). Preventing the breakdown of cartilage is believed to be critical to preserve the functional integrity of a joint. Chondral injuries are also common in the knee joint, and many patients benefit from cartilage repair. Magnetic resonance imaging (MRI) and advanced digital post-processing techniques have opened possibilities for *in vivo* analysis of cartilage morphology, structure, and function in healthy and diseased knee joints. Techniques of semi-quantitative scoring of human knee cartilage pathology and quantitative assessment of human cartilage have been developed. Cartilage thickness and volume have been quantified in humans as well as in small animals. MRI detected cartilage loss has been shown to be more sensitive than radiographs detecting joint space narrowing. It is possible to longitudinally study knee cartilage morphology with enough accuracy to follow the disease-caused changes and also evaluate the therapeutic effects of chondro-protective drugs. There are also several MRI methods that may allow evaluation of the glycosaminoglycan matrix or collagen network of articular cartilage, and may be more sensitive for the detection of early changes. The clinical relevance of these methods is being validated. With the development of new therapies for OA and cartilage injury, MR images will play an important role in the diagnosis, staging, and evaluation of the effectiveness of these therapies.

Key words: Animal model; Cartilage; Osteoarthritis; Joint space narrowing; Knee; Magnetic resonance imaging; Radiography

Peer reviewer: AAK Abdel Razek, MD, Professor, Diagnostic Radiology Department, 62 El Nokri St, Meet Hadr, Mansoura Faculty of Medicine, Mansoura, Egypt

Wang YXJ, Griffith JF, Ahuja AT. Non-invasive MRI assessment of the articular cartilage in clinical studies and experimental settings. *World J Radiol* 2010; 2(1): 44-54 Available from: URL: http://www.wjgnet.com/1949-8470/full/v2/i1/44.htm DOI: http://dx.doi.org/10.4329/wjr.v2.i1.44

INTRODUCTION

Osteoarthritis (OA) is viewed as the clinical and pathological outcome of a range of disorders that result in structural degradation and functional failure of synovial joints. OA occurs when the dynamic equilibrium between the breakdown and repair of joint tissues becomes unbalanced, often in a situation in which the mechanical loads applied exceed those that can be tolerated by the joint tissues. This progressive joint failure may cause pain and disability and is being ranked as the leading cause of disability in the elderly. Although articular cartilage lacks nerves, recent studies have shown that cartilage pathology is associated with clinical symptoms[1,2]. Currently, no well accepted medical treatment for OA with structure or disease modification efficacy exists. Attrition and eventual loss of articular cartilage are crucial elements

in the pathophysiology of OA. Because of the avascular nature and small chondrocyte population in adults, the capacity of injured or degenerated cartilage to synthesize and secrete its extracellular matrix is poor. The healing response to cartilage injury and degeneration also decreases with age. Preventing the breakdown of cartilage is believed to be critical to preserve the functional integrity of a joint. Chondral injuries are common in the knee joint, and many patients benefit from cartilage repair. A number of promising therapeutic agents and surgical procedures are currently under development in this regard. In addition to investigating the pathophysiology of cartilage generation, there is a significant need for a non-invasive method of monitoring OA to judge the success of potential chondroregenerative and surgical treatments. Magnetic resonance imaging (MRI) offers a unique opportunity to characterize various pathologies of articular cartilage *in vivo*.

MRI detected cartilage loss has been shown to be more sensitive than radiographs detecting joint space narrowing (JSN). Amin *et al*[3] reported that cartilage loss was significantly associated with semi-quantitatively graded JSN of weight-bearing radiographs in the femoral-tibia joint, however, there was a substantial proportion of knees in which cartilage loss was detected with MRI but no radiographic JSN was observed. Raynauld *et al*[4] described no significant change in the medial femoral-tibia compartment of weight-bearing semiflexed radiographs positioned with fluoroscopy in 32 patients with OA over 2 years, but reported a highly significant change in cartilage volume from MRI both in the medial and lateral femoral-tibia compartment. The knee is the largest weight-bearing joint in the body and therefore most commonly affected by OA. Chondral injury is a frequent cause of pain and knee-function limitation. Cartilage repair surgery is a highly dynamic research field, and there is a pressing need for reliable and objective monitoring in order to evaluate and compare various surgical treatment options. This review discusses *in vivo* MRI methodology of the morphological assessment of knee cartilage, both in clinical studies and experimental settings. Novel techniques with potential of assessing macromolecular matrix of cartilage are also briefly discussed.

MR IMAGE ACQUISITION TECHNIQUES FOR HUMAN KNEE

MR images capable of resolving various structures of the knee joint require a good signal-to-noise ratio, good spatial resolution, and good tissue contrast. Given that knee cartilage is only 1.3-2.5 mm thick in healthy human subjects, and because of its complex morphology, knee cartilage presents a challenge in MRI[5-8]. The challenges are even greater in OA patients, as a decrease in signal and thinning make delineation of the articular cartilage more difficult.

MRI assessment of cartilage repair requires cartilage-sensitive sequences such as fat-suppressed (FS) 3D T1-weighted gradient echo (GE) sequences and proton-density and T2- or intermediate weighted fast spin echo (FSE) techniques. The pattern of joint structures as seen on MR images can be modified in various ways by the choice of MR pulse sequences. The MR sequences that have been most commonly used for cartilage assessment are FS T1-weighted spoiled GE sequences. FS is important for increasing the dynamic range between cartilage and adjacent structures and to eliminate chemical shift artifacts at the cartilage-bone interface. FS enhances the contrast for the cartilage and it has been reported that it can lead to better reproducibility for volumetric measurements[9]. GE sequences allow very short time of echo (TE), and this improves signal sensitivity when small structures are imaged. FS GE sequences with short TEs and relatively large flip angles provide T1-weighted images where the intra-articular fluid is less intense than the cartilage and fat is suppressed therefore maximizing the contrast between cartilage, fluid and marrow, with cartilage showing a bright signal. Because of the relatively short T2 relaxation times in articular cartilage, especially in deep cartilage adjacent to the bone interface, MR sequences for quantitative volume measurements should be used with TE as short as possible, preferably below 10 ms. A longer TE leads to cartilage signal decay. Eckstein *et al*[10] reported a significant underestimation of tibial cartilage thickness compared to CT arthrography, when using a GE sequence with a TE of 11 ms. It is particularly important to avoid this confounding effect of T2 relaxation on volume measurement in longitudinal studies of OA progression.

In general, 3D-GE sequences with FS allow the exact depiction of the thickness and surface of cartilage, whereas dual FSE sequences outline the normal and abnormal internal structure of hyaline cartilage. Cartilage demonstrates intermediate signals in intermediate - and T2-weighted sequences, whereas synovial fluid is bright and the internal structure of the cartilage displays a more heterogeneous signal and 'internal' pathological changes may be more readily displayed (Figure 1).

Sagittal scan plane is commonly used for cartilage evaluation. Although there is no current consensus on the optimal resolution for imaging knees in OA, 1.5 mm section thickness and 0.3 mm in-plane resolution has been commonly used, as these allow total coverage of the knee with imaging times of 10-12 min. Rubenstein *et al*[11] demonstrated that a voxel size under 300 μm is required to reveal fraying of the articular surface of cartilage. In a systematic comparison of images with different in-plane resolutions, Hardya *et al*[12] reported significantly larger precision errors for cartilage volume measurements derived from the lower-resolution (0.55 mm × 0.55 mm) images than for those from the higher-resolution (0.28 mm × 0.28 mm) images in the femur and tibia. Wluka *et al*[13] and Cicuttini *et al*[14] measured the rate of progression in tibial cartilage using sagittal images and also using reformatted coronal images. They reported a higher rate of progression of tibial cartilage loss in the reformatted coronal *vs* original sagittal images. These findings indicate

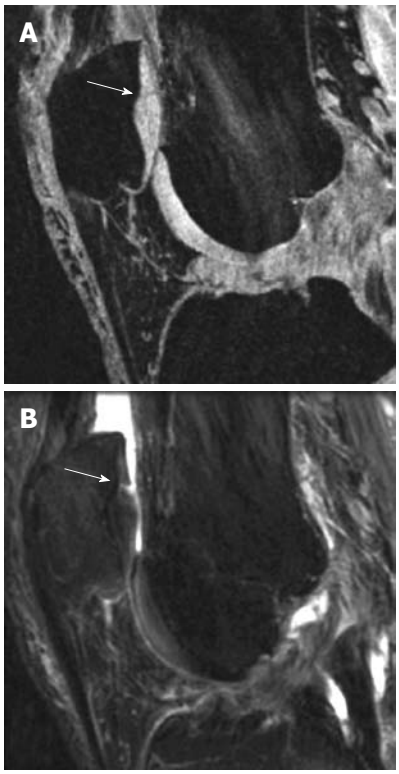

Figure 1 Comparison of gradient echo (GE) sequence and fat-suppressed (FS) sequence in depicting intra-cartilage lesion. A: Sagittal fat saturated spoiled GE image of the knee in a patient with early OA and a cartilage fissure (arrow); B: Sagittal FS intermediate weighted image of the same patient with the fissure (arrow). Note the difference in contrast with bright cartilage signal in (A) and intermediate cartilage signal in (B). Joint effusion in (B) with bright signal improves visualization of the cartilage fissure (Reproduced by permission of John Wiley & Sons, Ltd from Reference 8).

that changes may be more readily detected in coronal views of the knee. Which protocol (sagittal or a combination of axial and coronal scans) is preferable remains to be confirmed by future studies.

For human studies, MR images should be acquired within reasonable examination times (< 20 min per pulse sequence), in order to avoid movement artifacts, maintain patient comfort, and contain costs. Recently developed high-resolution 3D isotropic cartilage-sensitive sequences at 3 Tesla will further improve the assessment of quantitative morphologic aspects of volumetric cartilage[15]. New coil technologies with multi-element design allow the use of parallel imaging, which can additionally decrease the scan time. Higher magnetic field could potentially increase the quality of cartilage images, while scan times can be kept well below 10 min. At 3.0T, it was found that the signal to noise ratio and contrast to noise ratio efficiency for cartilage increased by a factor of 1.8 *vs* 1.5T for spoiled GE sequences. Cartilage volume and thickness measurements at 3.0T showed only small (non-significant) differences as compared with measurements at 1.5T[16,17]. Using a porcine model of artificial cartilage lesions, it was reported that the highest lesion detection rate was found with an intermediate-weighted FSE sequence at 3.0T (90% *vs* 62% at 1.5T), whereas the lesion grade was most accurately evaluated with spoiled GE sequences at 3.0T (83% *vs* 70% at 1.5T). Receiver operator characteristics analyses in the same model confirmed improved diagnostic performance in detecting cartilage lesions at 3.0T if high-resolution imaging protocols (slice thickness ⩽ 2 mm and in-plane resolution ⩽ 0.39 mm) were used[18,19]. Low-field systems should not be used for cartilage imaging as previous studies have shown that low-field MR scanners operating at field strengths of 0.18-0.20T have substantial limitations compared to high-field systems (1.5T) in visualizing cartilage pathology[20]. Further studies to improve both spatial and contrast resolution using novelly designed sequences are still ongoing[20,21].

Studies have shown that knee bends and squatting can cause a reduction of approx. Five percent in patellar cartilage volume and thickness and this effect can last for approx. 90 min[6]. To avoid differences in subject conditions due to differences in levels of physical activity prior to imaging, for cartilage volume and thickness measurements, study subjects need to rest for 1 h prior to image acquisition.

MR IMAGE ACQUISITION TECHNIQUES FOR ANIMAL KNEE

A number of animal models have been devised to investigate the pathogenesis of OA and cartilage trauma. It is a great advantage for research that the time course of OA in animal models is much more rapid than the development of OA pathology in humans. The knee is the mostly used joint for OA induction. MRI has already been applied to investigate a variety of OA animal models, including mouse, rat, guinea pig, rabbit, monkey, goat and dog[5]. The high resolution requirement for small animal knee MRI demands high performance of MR instruments. For imaging of large animals like dog and goat, clinical human scanners are commonly used, mostly together with a RF coil designed for human knees or wrists. For signal optimization, suitable RF coils for animal knee can be custom-made and interfaced to clinical human scanners.

High field research MR scanners, usually with a magnetic field of 4.7T or 7T, tend to be equipped with small bores which can hold up to the size of rabbits or rats. The RF coils are usually home-made, or made by some small specialist companies. The most commonly used is single-turn solenoid RF coils[8]. They are designed to open at the top. Animals can be placed on a Perspex platform with one hind leg extending through the RF coil, with the knee centered in it. While designed to completely cover the knee joint of the animal species imaged, the length and diameter of the coil are optimized to minimize the image field of view so as to obtain a good filling factor. To prevent motion, the animal's paw on the leg being scanned can be secured to a secondary lower platform. With clinical scanners, RF coils suitable for imaging human fingers can be used for imaging rat knee, although quantification of cartilage thickness or volume using this set-up remains challenging.

Similar MR sequences for human studies are used for animal studies. With high field MR scanners it is feasible to obtain 3D data sets of less than 100 micro meter resolution with scanning duration less than 1 h[22,23]. In the study by Tessier *et al*[24], MR image acquisition protocol for guinea pig knee cartilage evaluation was detailed. A 4.7T magnet and an FS 3D-GE sequence were used. The length and diameter of the solenoid RF coil used were optimized to minimize the image field of view (30 mm × 30 mm × 30 mm). A transverse image of the knee was used to select the orientation of the sagittal view of the 3D images such that they were parallel to the medial condyle. The image matrix was zero-filled to 512 × 256 × 128 after 3D Fourier transform and an apparent image resolution of 59 mm × 117 mm × 234 mm was achieved. The highest resolution (59 mm) was chosen across the cartilage thickness (approx 330 mm). For assessment of rat knee joint, Wang *et al*[22] used a 4.7T magnet; the RF coil was an in-house built double-balanced matched 3 cm diameter copper sheet solenoid, and was 1 cm in length. 3D data set at the sagittal plane was acquired using a spoiled multi-echo FS 3D-GE (TR = 75 ms, flip angle = 30°, 5 echoes TE1 = 2.8 ms, TE2 = 6.0 ms, TE3 = 9.2 ms, TE4 = 12.5 ms, TE5 = 15.7 ms). Echo summation provided a means of enhancing SNR and enabled acquisition of a high resolution 3D image of the rat knee in approximately 50 min. The images covered the entire knee joint with a resolution of 59 mm × 117 mm × 234 mm.

TECHNIQUES FOR ASSESSING CARTILAGE COMPOSITION

During the early stages of OA, articular cartilage constituents may degenerate before any substantial morphological changes occur. In recent years, a significant amount of research has been directed toward the development of techniques for assessing the loss of the macromolecular matrix of articular cartilage in the absence of macroscopic lesions. One of the main motivations behind this work has been the ongoing development of drugs designed to slow or reverse the development of OA at this early stage. During disease progression, changes in the tissue MR relaxation values [T1, T2, and T1 rho (or, T1 in the rotating frame)], diffusion-coefficient, magnetic transfer, sodium MRI and ultra-short TE imaging, and delayed gadolinium enhanced MRI of cartilage (dGEMRIC) may reflect early alterations in the tissue architecture and biochemical composition[5,25-27]. Among them, the most promising three techniques include (1) dGEMRIC; (2) T1 rho (spin-lock) imaging, and (3) T2 maps[20,21,25,28].

dGEMRIC works by allowing negatively charged gadolinium-diethylenetriamine pentaacetic acid $(DTPA)^{-2}$ to distribute in cartilage in inverse proportion to the negatively charged glycosaminoglycans. One of the most common MR contrast agents, gadopentetate dimeglumine ($Gd\text{-}DTPA^{-2}$; Magnevist®, Schering, Berlin, Germany), has a negative charge and will therefore show a lower concentration in cartilage areas of high glycosaminoglycan concentrations following penetration *via* diffusion. Double-dose $Gd\text{-}DTPA^{-2}$ is injected intravenously, and a delay of 90 min is used to allow the contrast material to diffuse into the cartilage. A map of the T1s in the cartilage can be computed, which reflects the underlying glycosaminoglycan content. Areas of glycosaminoglycan depletion can be seen in diseased cartilage. T1 rho (spin-lock) imaging employs a long, low-power, RF pulse at the resonant frequency that follows a 90° pulse and that is applied along the axis of the magnetization vector in the transverse plane. This pulse serves to "lock" the spins along the pulse, reducing the T2 decay that would normally cause the magnetization to dephase in the plane. Despite the reduction of T2 decay, there is still a loss of magnitude of the magnetization that is characterized by the time constant T1 rho (i.e. "T1 in the rotating frame"). This sequence is sensitive to the loss of proteoglycans, which is detected as an increase in T1 rho. The actual calculation of the spatial distribution of T1 rho values (maps) requires that the sequence be repeated several times while systematically varying the time length that the spin-lock pulse is applied. The T2 maps of articular cartilage are a function of the water content of the tissue. Measurement of the spatial distribution of the T2 may reveal areas of increased or decreased water content, which correlate with cartilage damage. Focal increases in T2 within cartilage have been associated with matrix damage, particularly loss of the collagen matrix.

Intuitively, compositional measures may have a significant role to play in examining changes that occur in early disease before gross defects are apparent, whereas morphologic measures - both semiquantitative and quantitative - may have a greater role in the later stages of disease. Overall, these cartilage composition imaging techniques require dedicated staff and careful attention to the MRI parameters and timings. The major drawback of the dGEMRIC technique is the long period of time, between the time of contrast agent injection and the commencement of imaging, needed to allow diffusion of the contrast into the cartilage. A lesser problem is the relatively long acquisition time needed to acquire sufficient data to create the T1 maps using a series of inversion-recovery sequences, during which the subject must remain motionless. The one limitation of T1 rho technique is that it is not commonly available on commercial MR systems. Custom software is also necessary to reconstruct and view the T1 rho maps. With T2 maps, correlation between T2 times and the changes in the macromolecular matrix is less certain. Further research is needed to show how clinically feasible these new biomarkers are as measures of early cartilage degeneration. Which of these techniques alone or perhaps in combination will prove most useful remains to be determined. Particularly for supposedly 'early' changes of OA, however, the natural course of these changes and the relationship with clinical outcome remain to be established. Additional research and validation is needed to guide interpretation of the results of these techniques.

MORPHOLOGICAL EVALUATION OF HUMAN KNEE CARTILAGE

Conventional radiography is the least expensive method for imaging joint structure. The progression of knee OA has been assessed by measuring changes in the width of the space between the medial femoral condyle and medial tibial plateau on plain radiographs, as the medial femorotibial compartment is the most common site of involvement in knee OA. A reduction in cartilage thickness is inferred from a reduction in this space. Observational studies show a weak relationship between radiographic structural change, pain, and function in OA[29]. Measurement errors related to the variability in knee positioning required considerable effort for the standardization of radiographic protocols, including the use of fluoroscopy. Progression in JSN also reflects OA changes in joint tissues other than articular cartilage, particularly extrusion and degenerative changes of the menisci. Data also suggest that knee pain itself can modify the appearance of joint space width in weight-bearing extended view radiographs[30].

Knee cartilage morphological evaluation with MRI includes qualitative assessment of articular cartilage pathology, semi-quantitative scoring of articular cartilage pathology, and quantitative assessment of articular cartilage volume and thickness. It has been reported that MRI based volume measurement of knee cartilage can demonstrate change undetectable with radiographs[4]. Using MRI assessment as the gold standard for cartilage loss, the specificity of radiography in detecting cartilage loss in the medial compartment was 91%; however, the sensitivity was only 23%[31]. MRI also has important applications in the study of cartilage repair. Specifically, MRI may (1) help to estimate the size, nature, and location of lesions preoperatively, in order to optimize surgical planning; (2) help to evaluate the quality and success of tissue repair processes after surgical treatment; and (3) allow one to monitor changes in the joint after cartilage repair. An excellent review on MRI monitoring of surgical repair of cartilage has been reported elsewhere[32].

Early degenerative disease may be seen on MRI as early alterations in cartilage contour morphology (fibrillation, surface irregularity); changes in cartilage thickness, including cartilage thinning or thickening, which may be an early feature predating cartilage volume loss; or intrachondral alterations in signal intensity potentially related to premorphologic intrasubstance collagen degeneration and increased free-water content. Advanced degenerative chondral lesions typically manifest on MRI as multiple areas of cartilage thinning of varying depth and size, usually seen on opposing surfaces of an articulation. Cartilage defects typically illustrate obtuse margins and may be associated with corresponding subchondral regions of increased T2-weighted signal reflective of subchondral edema or cysts or a low signal intensity reflective of subchondral fibrosis or trabecular sclerosis. Other associated MRI findings of degenerative cartilage disease include central and marginal articular osteophytes, joint effusion, and synovitis. Traumatic cartilage fragments may remain *in situ*, become partially detached, or become loose and displaced into the joint space.

Quantitative measurements of cartilage lesion depth, diameter, area, and volume have been validated in a porcine experimental model of OA[33]. Satisfactory specificity and sensitivity for detecting chondral lesions have been demonstrated in knee specimens and *in vivo* with arthroscopic verification. Bredella *et al*[34] reported a sensitivity of 93% and a specificity of 99% in detecting chondral lesions with MRI *vs* athroscopy when axial and coronal images were combined, and values of 94% and 99% when images in all three planes were used. In that study, accuracy was highest for severe cartilage lesions and lowest for smaller lesions, particularly for signal intensity alterations. In human knee cartilage, the mean difference between measured and actual artificial cartilage defect diameters was reported to be < 0.1 mm, whereas the lesion depth was underestimated in MRI by > 0.4 mm[35]. Graichen *et al*[36] reported an overestimation of the true size of artificial cartilage defects in the human knee, which decreased from 42% in 3 mm defects to 4% in 8 mm defects. It is expected as MRI field and gradient strength increase and RF coil techniques and sequences improve, the performance of lesion detection with MRI will further increase.

Semi-quantitative scoring of human knee cartilage pathology

A number of semi-quantitative scoring methods have been developed for evaluation of articular cartilage on MR images[37,38]. Most of these methods grade the severity of cartilage thinning from 0 to 3 or 4 based on subjective evaluations by one or more experienced readers. These systems commonly differentiate between cartilage lesions of < 50% depth, > 50% depth and full thickness cartilage lesions.

In an observer-dependent semi-quantitative manner, novel scoring approaches are used to assess a variety of features that are currently believed to be relevant to the functional integrity of the knee or potentially involved in the pathophysiology of OA. Peterfy *et al*[39] described a scoring system in which cartilage lesions are graded according to both depth and extent along the joint surface. This score is part of a more comprehensive scoring system, in which multiple features are graded within the knee, such as articular cartilage integrity, subarticular bone marrow abnormality, subarticular cysts, subarticular bone attrition and marginal osteophytes. The surface areas of the knee joint are subdivided into 15 different regional anatomical landmarks in the extended knee. Cartilage signal and morphology are scored in each of the articular-surface regions using FS T2-weighted FSE images and the FS 3D spoiled GE images. An eight-point scale for semi-quantitative scoring of articular cartilage signal and morphology was used[27]: 0 = normal thickness and signal; 1 = normal thickness but increased signal on T2-weighted MR images; 2.0 = partial-thickness focal defect < 1 cm in greatest width; 2.5 = full-thickness fo-

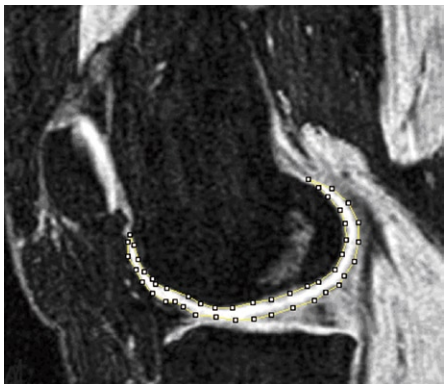

Figure 2 3D GE fat suppressed magnetic resonance imaging (MRI) at the sagittal plane. Bone cortex, bone marrow, and fat tissue appear to have a dark signal. Muscle appears to have a gray signal and cartilage a bright signal. The femur cartilage has been manually segmented at this slice.

cal defect < 1 cm in greatest width; 3 = multiple areas of partial-thickness (grade 2.0) defects intermixed with areas of normal thickness, or a grade 2.0 defect wider than 1 cm but < 75% of the region; 4 = diffuse (≥ 75% of the region) partial-thickness loss; 5 = multiple areas of full-thickness loss (grade 2.5) or a grade 2.5 lesion wider than 1 cm but < 75% of the region; 6 = diffuse (≥ 75% of the region) full-thickness loss. Peterfy *et al*[39] reported that despite the complexity of the system, the inter-observer agreement among two trained readers was high. However, Conaghan *et al*[40] reported some limitations when applying the WORMS grading system to knees of 336 subjects assessed by three readers. The authors commented that adding up individual scoring subscales, as recommended by WORMS, is problematic, and that several subscales (in particular those for cartilage signal and morphology and for osteophytes) may need to be redeveloped[40]. Other compartment-based knee OA scoring systems have also been published. Kornaat *et al*[41] reported a knee OA scoring system termed KOSS, with intraobserver reproducibility of 0.76-0.96 (intraclass correlation coefficient: ICC) and interobserver reproducibility amongst two independent observers of 0.63-0.91. In a recent report the reliability of a further novel MRI scoring system for evaluating OA of the knee was explored[42]. Nine intra-articular anatomical divisions and eight items were tested, including features of cartilage, bone-marrow lesions (BML), osteophytes, synovitis, effusions, and ligaments, and a scale of 0-3 was applied for each of these to yield the Boston-Leeds Osteoarthritis Knee Score (BLOKS). A series of iterative reliability exercises was performed to reduce the initial items. The interreader reliability for the final BLOKS items ranged from 0.51 for meniscal extrusion to 0.79 for meniscal tear, with that for cartilage morphology being 0.72. In another sample, both BLOKS and WORMS were used to score BML. Maximum BML size in BLOKS had a positive linear relationship with pain, whereas in WORMS it did not. Baseline BML was associated with cartilage loss on both the BLOKS and WORMS scale, but the association was stronger for BLOKS than for WORMS. These MRI semi-quantitative scoring approaches on OA have shown the ability to detect lesion progression over 1-2 years[43]. Although the sensitivity to change observed can sometimes be small[44], the ability to measure individual characteristics of OA is appealing in delineating structural risk factors for both pain and OA progression. The identification of early pathology in the course of disease may be enhanced by using these measures. For example, recent data suggest that full thickness defects may occur as part of early disease and that quantitative morphometry appears most useful (sensitive to change) in persons with late stage disease[45,46].

Quantitative assessment of human cartilage

Due to the relatively low contrast in some areas of the joint surface, fully automated segmentation of knee cartilage volume from MR images has not yet been achieved. Computer-generated measurements based on signal intensity or predefined shape is not always reliable. Editing of automatically generated segmentations, or complete manual segmentation by experienced readers, is frequently necessary, therefore cartilage segmentation remains time-consuming (Figure 2). After segmentation, computation of the cartilage volume is achieved by simply summing the voxels attributed to the segmented cartilage (Figure 3). Osteophytes are excluded from segmentation.

In the absence of OA, Hudelmaier *et al*[7,47] reported a 0.3%-0.5% reduction of cartilage thickness per annum due to cartilage thinning during normal aging. Other authors reported a faster rate of cartilage loss. Hanna *et al*[48] found a significant (-2.8% annual) reduction in total tibial cartilage volume over a 2 years period. With data summarized from studies on OA patients in the published literature, Eckstein *et al*[8] reported that the annual loss of cartilage volume was -136 μL (-4.1%) in the patella, -90 μL (-5.6%) in the medial tibia, and -107 μL (-6.0%) in the lateral tibia. The annual changes in cartilage volume/thickness exceeded the precision errors and appeared to be associated with clinical symptoms as well as with time to knee arthroplasty. However, results varied between published studies, the annual rate of change ranged from -0.3% to -7.4% in the medial tibia[8]. It has been reported that in early OA, cartilage may not be thin but rather thicker and swollen with water[49,50].

Because attrition in cartilage volume occurs at a very slow rate, measurement precision is of critical importance. Precision errors can be expressed as the standard deviation (SD) or coefficient of variation (CV%, SD divided by the mean value) of repeated measurements. Use of the CV% is most appropriate when SD is proportional to volume, for instance when comparing precision in different joint surfaces of the knee (i.e. medial tibia *vs* total femur). If the SD is independent of volume, it is more appropriate to compare SD values directly. It should be noted that when examining patients with severe OA, the CV% will be larger than that in healthy volunteers, even if the absolute error (SD) is similar. This is because patients with severe OA have less cartilage

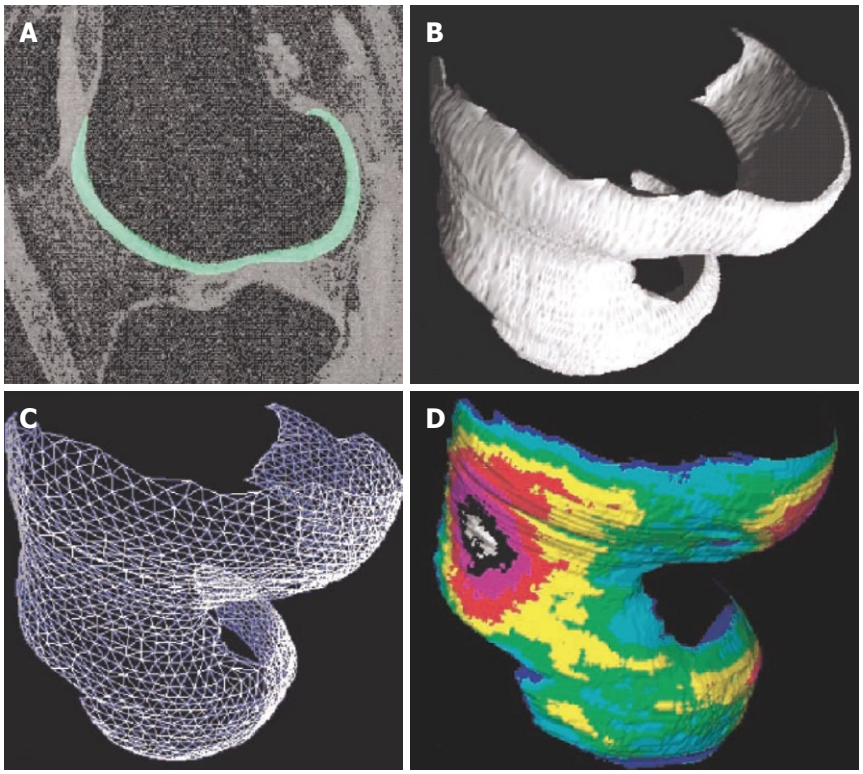

Figure 3 Quantitative 3D analysis of cartilage morphology from MRI. A: Sagittal MR image of human knee obtained with a fat-suppressed GE sequence, femoral cartilage is segmented; B: 3D volume reconstruction of the femoral cartilage; C: Analysis of joint surface area by a triangulation technique; D: Computation of 3D thickness distribution, independent of section orientation. (Reproduced from reference 6, with kind permission of Springer Science and Business Media).

volume. CV% of cartilage volume in the medial tibia in healthy volunteers has been reported to be in the range of 2%-3.5%. Precision errors for cartilage volume across studies at 1.5T for each cartilage component have been recently summarized[8]. Several studies examined the inter-observer and intra-observer precision of repeated analyses. It has been confirmed that segmenting all images in a subject's series by the same skilled reader is more accurate than segmenting by different readers. To alleviate reader bias, the results of several readers can be averaged. Re-segmentation of the same data sets over a period of 1 year by the same user involved larger errors than those involved by segmentation of different data sets immediately after each other[46]. Therefore, to ensure the smallest coefficient of variation, in longitudinal studies comparative analyses should be performed in one post-processing session. Blinding the user to the order of the exams is necessary in order to avoid bias.

Cartilage volume provides a first step in the analysis of cartilage morphology. More comprehensive information can be derived from separating the cartilage volume into its two factors, namely the cartilage thickness and the size of the joint surface area. Specific algorithms are required to differentiate between these factors. Other variables such as percent cartilaginous (or denuded) joint surface area, cartilage surface curvature, lesion size and depth can also be investigated. As overall volume and mean thickness for an entire cartilage plate may be relatively insensitive to regional/focal changes, several investigators developed techniques for displaying regional thickness patterns. Measuring cartilage volume in regions of the knee (e.g. medial tibia) and regional mean thickness as distinct from focal measures of change (region of interest analysis centered around focal defects) and measures of denuded cartilage may provide very different measurements about the important pathologic changes occurring in early disease. Distinguishing what measures are most discriminatory at each stage of the disease process is essential for utilizing these measures appropriately. Kshirsagar *et al*[51] suggested that analyzing subvolumes within the joint surface by such techniques can reduce precision errors relative to those from analyses of the entire cartilage plate and this was recently confirmed in a study by Koo *et al*[52] for the central weight-bearing regions of the femoral condyles. These types of 'local' approaches to measuring changes in cartilage morphology are technically challenging, but they can be important, because the overall cartilage volume can remain constant even if there are focal changes in cartilage thickness and denuded bone. In order to track local/regional thickness changes over time, the bone interfaces from two data sets are "matched", so that the thickness distribution can be compared on a point-by-point basis. Koo *et al*[52] suggested a 'trimmed' region defined to avoid errors arising at the edges of articulating surfaces, which are difficult to segment yet may be involved to only a minor degree in the disease process.

A substantial percentage of the variability in cartilage volume is determined by joint surface area[53]. Wang *et al*[54] demonstrated that the medial and lateral tibial plateau area increased over a 2-year period (2.2% and 1.5% per annum, respectively), with increases at the medial (but not lateral) tibia being stronger in male patients, in participants with high body mass index, and in patients with higher baseline grade of medial JSN. Metaphyseal enlargement with age and OA might create

problems for cartilage volume measurements that did not adjust for bone size[55], and either adjustment for subchondral bone area or the direct measurement of cartilage thickness has thus been recommended.

Quantitative MRI of cartilage is currently used in ongoing studies to monitor cartilage volume and will be used to assess structural effects of pharmacological therapies on cartilage in order to prove their effectiveness. However, until now the measurement of cartilage volume has not gained widespread usage in routine clinical practice partly due to its time-consuming nature. Although the volume measurements are typically semi-automated, they still require some degree of manual segmentation. Segmentation of cartilage will become easier with sequences that create improved contrast between cartilage and the surrounding bone and fluid, but will still likely require a high degree of user interaction for at least the near future.

MORPHOLOGICAL EVALUATION OF ANIMAL KNEE CARTILAGE

Cartilage thickness and volume have been quantified in animals as small as guinea pigs and rabbits. Cartilage of OA involves an initial swelling phase, and later attrition and loss, defect phases. These phases have been demonstrated in experimental animal models by sequential MRI[24,56]. Tessier *et al*[24] studied 19 male Dunkin-Hartley guinea pigs with MRI at 3, 6, 9, 10.5 and 12 mo of age. They found that at 6 mo, swollen cartilage was observed in all animals; at 9 mo, marked fragmentation of the medial tibial cartilage was seen in the areas not covered by the meniscus; at 12 mo, focal thinning of the cartilage was apparent with occasional full cartilage loss.

Tessier *et al*[24] detailed their segmentation methodology for guinea pig tibia cartilage. Segmentation of the cartilage of the medial plateau was performed on sagittal slices covering the medial side only. These slices were selected on the basis that they covered the 'flattest' region of the medial tibial surface. The slices covering the inner side where the cruciate ligament is attached were excluded because the images are subject to significant partial volume averaging. Slices at one time-point were matched as close as possible to those obtained at subsequent time-points based on anatomical references. Thus for any animal, the number of slices analyzed were equal for all time-points. However, the number of segmented slices was different between animals to account for the difference in the overall size of the tibial plateau. Their data showed that maximal cartilage loss (36%) occurs from the medial side of the tibial plateau from 9 to 12 mo of age.

In small animals like rats, due to the small size of their knee joint, assessment of cartilage thickness is challenging but has recently proved to be feasible. With a 7T MR scanner, Faure *et al*[23] reported that MRI could be used to detect arthritis and joint changes at a very early stage in living rats with rheumatoid arthritis. With a rat meniscus transection OA model 44 d post surgery, MRI was able to demonstrate qualitatively the decrease in cartilage thickness and loss of cartilage in some areas, as well as focal neo-cartilage proliferation at the joint margin (Figures 4 and 5)[22].

Recently, it was pointed out that to date MR tomographic knowledge of laboratory animal skeletal microanatomy remains limited. With MR images acquired in normal rats, many signs unfamiliar to radiologists can be noted, including notch-like bright signal areas in the epiphysis, gray signal areas in the epiphysis, and fuzzy joint surface of the epiphysis of the femur and tibia. Detailed inspection of the histology specimen showed more unfamiliar features of rat knee microanatomy, including curvy or dipped surface of the femur/tibia epiphysis, areas composed of a mixture of cartilage and bone components, normal notch structure, cyst-like structure, and a cavity between cortical lamellae under the joint cartilage (Figure 6)[57]. Further research is warranted to understand how these structures will affect articular cartilage assessment.

CLINICAL RELEVANCE OF CARTILAGE PATHOLOGIES DEMONSTRATED BY MRI

Satisfactory specificity and sensitivity for detecting chondral lesions by MRI have been demonstrated in cadaveric knees and *in vivo* with arthroscopic verification[38,58,59]. Knee cartilage defect severity, as measured from sagittal T1-weighted FS SPGR sequences, has been shown to be significantly associated with urinary levels of C-terminal cross-linking telopeptide of type Ⅱ collagen[60]. An association was also reported between cartilage defects and body mass index[61]. Link *et al*[1] showed that in patients with OA the degree of cartilage pathology seen in MR images is associated with clinical symptoms.

In a cross-sectional study, Hunter *et al*[62] observed a significant negative association between patellar cartilage volume and the WOMAC score in a population of 133 postmenopausal women. Wluka *et al*[63] reported a weak association between tibial cartilage volume and symptoms (WOMAC score) at baseline in a sample of 132 patients with symptomatic early knee OA, and worsening of symptoms over a 2 years period was associated with tibial cartilage loss. These data suggest that treatment targeted at reducing the rate of knee cartilage loss in subjects with symptomatic OA may relate to clinical outcomes and delay knee replacement.

MRI is very useful for cartilage repair surgical planning and follow-up. The combination of the clinical outcome after cartilage repair together with the morphological and composition description of the cartilage repair tissue as well as the surrounding cartilage may lead to a satisfactory follow-up evaluation. MRI can give a precise estimate of progressing degeneration and objective assessment of the long-term outcome of cartilage repair.

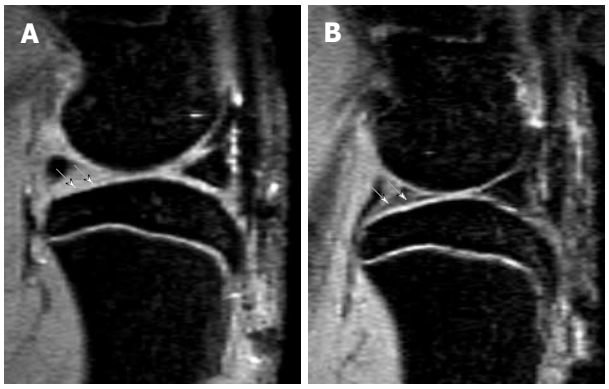

Figure 4 Sagittal view MRI at 4.7T of a rat knee with medial meniscal tear (A) and a rat with sham operation (B). A: Parts of the tibia cartilage become much thinner (white arrows). B: Normal tibia cartilage (white arrows). This animal model has been described in reference 22 (Wang *et al*[22] 2006).

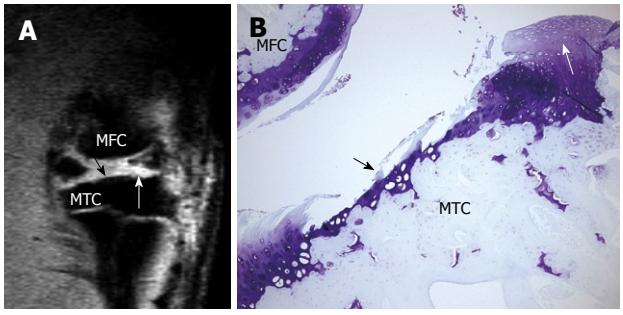

Figure 5 High resolution MRI demonstrates cartilage erosion and proliferation in rat knee joint. A: Sagittal view MRI of a rat knee with a medial meniscal tear. White arrow shows neo-cartilage proliferation and black arrow shows articular cartilage loss; B: Histology section of the medial tibial condyle stained with Toluidine blue (× 100), 28 d after meniscal tear. Cartilage erosion (black arrow) and neo-cartilage proliferation (white arrow) are seen in the tibia cartilage. MTC: Medial tibia condyle; MFC: Media femur condyle. This animal model has been described in reference 22 (Wang *et al*[22] 2006).

In animal based studies, MRI can be used to carry out *in vivo* longitudinal follow-up in the same animal and track the disease, monitor its progress and see how it responds to potential treatments[5]. In a recent study of a mono-iodoacetate induced arthritis model in rats[64], MRI demonstrated that intra-articular soft tissue inflammatory changes peaked at day 3 and then started to regress; bony damage appeared at day 14, peaked at day 21, with hallmarks of repair visible by day 35. A similar bi-phase pain response was observed clinically with the 1 mg mono-iodoacetate dose group, peaking at days 3 and 21. Therefore, MRI was able to characterize the pathological course of the arthritis model which enabled a link to be established between the structural changes and joint clinical discomfort. There are several "disease" or "structure" modifying OA drugs under clinical development. Although JSN on weight-bearing radiographs is still the accepted surrogate marker for demonstrating structural change by regulatory agencies, this is expected to change in the near future, given the limitations of radiography[3,4], and MRI will very likely

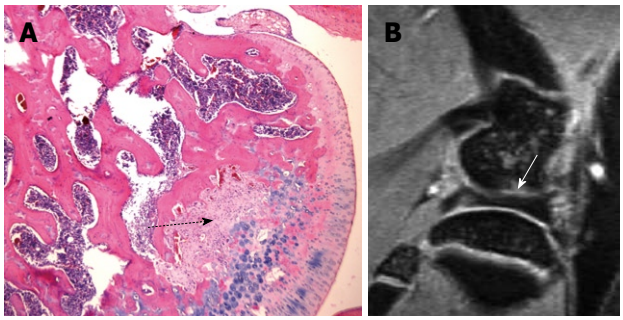

Figure 6 One example of the pitfalls in interpreting normal rat knee high resolution MR images. A: H&E-stained sections of a normal 3 mo rat knee, a mid-section through the femur. Dotted black arrow denotes the area of fibrous components together with their matrix, which are continuous with the cartilaginous component of the joint surface, and there is no bony component seen within this region. This region may appear as a notch or a cyst on MR images due to its higher signal; B: Sagittal MR image of a normal 3 mo old rat knee. White arrow in B denotes a gray area possibly composed of a mixture of cartilage and bone components.

replace radiography in this context. As the validation of MRI endpoints for OA trials in human studies is still incomplete, the design and interpretation of a clinical trial will be strengthened if the effect of the drug is shown by the same endpoint in a valid animal model. By measuring the volume of medial tibia cartilage in a spontaneous OA guinea pig model, MRI demonstrated that doxycycline treatment halved the cartilage loss as compared to the vehicle treatment[65].

CONCLUSION

MRI can semi-quantitatively assess cartilage morphology, and quantitatively evaluate regional cartilage volume and thickness. Other cartilage parameters including cartilage quality, cartilage surface smoothness, cartilage coverage, and distribution of change can also be evaluated. Progress made in MRI technology in the last few years allows longitudinal studies of human knee cartilage morphology with enough accuracy to follow the disease-caused changes and also evaluate the therapeutic effects of chondro-protective drugs[66]. For cartilage repair patients, future studies will be needed to determine whether MRI is prognostic of clinical outcome and can replace arthroscopic biopsy for monitoring repair-tissue histology. In animal experimental settings, high field MRI can non-invasively provide detailed images of joints and can be used to carry out *in vivo* longitudinal follow-up in the same animal and track the disease as well as see how it responds to potential treatments. There are also several MRI methods that may allow evaluation of the glycosaminoglycan matrix or collagen network of articular cartilage and may be the most sensitive method for the detection of early changes. These techniques are being further explored and validated. With the development of new therapies for OA and cartilage injury, MRI will play an important role in the diagnosis, staging, and evaluation of the effectiveness of these therapies.

REFERENCES

1 **Link TM**, Steinbach LS, Ghosh S, Ries M, Lu Y, Lane N, Majumdar S. Osteoarthritis: MR imaging findings in different stages of disease and correlation with clinical findings. *Radiology* 2003; **226**: 373-381

2 **Sowers MF**, Hayes C, Jamadar D, Capul D, Lachance L, Jannausch M, Welch G. Magnetic resonance-detected subchondral bone marrow and cartilage defect characteristics associated with pain and X-ray-defined knee osteoarthritis. *Osteoarthritis Cartilage* 2003; **11**: 387-393

3 **Amin S**, LaValley MP, Guermazi A, Grigoryan M, Hunter DJ, Clancy M, Niu J, Gale DR, Felson DT. The relationship between cartilage loss on magnetic resonance imaging and radiographic progression in men and women with knee osteoarthritis. *Arthritis Rheum* 2005; **52**: 3152-3159

4 **Raynauld JP**, Martel-Pelletier J, Berthiaume MJ, Labonté F, Beaudoin G, de Guise JA, Bloch DA, Choquette D, Haraoui B, Altman RD, Hochberg MC, Meyer JM, Cline GA, Pelletier JP. Quantitative magnetic resonance imaging evaluation of knee osteoarthritis progression over two years and correlation with clinical symptoms and radiologic changes. *Arthritis Rheum* 2004; **50**: 476-487

5 **Wang YX**. In vivo magnetic resonance imaging of animal models of knee osteoarthritis. *Lab Anim* 2008; **42**: 246-264

6 **Eckstein F**, Reiser M, Englmeier KH, Putz R. In vivo morphometry and functional analysis of human articular cartilage with quantitative magnetic resonance imaging--from image to data, from data to theory. *Anat Embryol* (Berl) 2001; **203**: 147-173

7 **Hudelmaier M**, Glaser C, Hohe J, Englmeier KH, Reiser M, Putz R, Eckstein F. Age-related changes in the morphology and deformational behavior of knee joint cartilage. *Arthritis Rheum* 2001; **44**: 2556-2561

8 **Eckstein F**, Burstein D, Link TM. Quantitative MRI of cartilage and bone: degenerative changes in osteoarthritis. *NMR Biomed* 2006; **19**: 822-854

9 **Sittek H**, Eckstein F, Gavazzeni A, Milz S, Kiefer B, Schulte E, Reiser M. Assessment of normal patellar cartilage volume and thickness using MRI: an analysis of currently available pulse sequences. *Skeletal Radiol* 1996; **25**: 55-62

10 **Eckstein F**, Stammberger T, Priebsch J, Englmeier KH, Reiser M. Effect of gradient and section orientation on quantitative analysis of knee joint cartilage. *J Magn Reson Imaging* 2000; **11**: 161-167

11 **Rubenstein JD**, Li JG, Majumdar S, Henkelman RM. Image resolution and signal-to-noise ratio requirements for MR imaging of degenerative cartilage. *AJR Am J Roentgenol* 1997; **169**: 1089-1096

12 **Hardya PA**, Newmark R, Liu YM, Meier D, Norris S, Piraino DW, Shah A. The influence of the resolution and contrast on measuring the articular cartilage volume in magnetic resonance images. *Magn Reson Imaging* 2000; **18**: 965-972

13 **Wluka AE**, Stuckey S, Snaddon J, Cicuttini FM. The determinants of change in tibial cartilage volume in osteoarthritic knees. *Arthritis Rheum* 2002; **46**: 2065-2072

14 **Cicuttini FM**, Wluka AE, Wang Y, Stuckey SL. Longitudinal study of changes in tibial and femoral cartilage in knee osteoarthritis. *Arthritis Rheum* 2004; **50**: 94-97

15 **Eckstein F**, Hudelmaier M, Wirth W, Kiefer B, Jackson R, Yu J, Eaton CB, Schneider E. Double echo steady state magnetic resonance imaging of knee articular cartilage at 3 Tesla: a pilot study for the Osteoarthritis Initiative. *Ann Rheum Dis* 2006; **65**: 433-441

16 **Kornaat PR**, Reeder SB, Koo S, Brittain JH, Yu H, Andriacchi TP, Gold GE. MR imaging of articular cartilage at 1.5T and 3.0T: comparison of SPGR and SSFP sequences. *Osteoarthritis Cartilage* 2005; **13**: 338-344

17 **Eckstein F**, Charles HC, Buck RJ, Kraus VB, Remmers AE, Hudelmaier M, Wirth W, Evelhoch JL. Accuracy and precision of quantitative assessment of cartilage morphology by magnetic resonance imaging at 3.0T. *Arthritis Rheum* 2005; **52**: 3132-3136

18 **Masi JN**, Sell CA, Phan C, Han E, Newitt D, Steinbach L, Majumdar S, Link TM. Cartilage MR imaging at 3.0 versus that at 1.5 T: preliminary results in a porcine model. *Radiology* 2005; **236**: 140-150

19 **Link TM**, Sell CA, Masi JN, Phan C, Newitt D, Lu Y, Steinbach L, Majumdar S. 3.0 vs 1.5 T MRI in the detection of focal cartilage pathology--ROC analysis in an experimental model. Osteoarthritis *Cartilage* 2006; **14**: 63-70

20 **Gold GE**, McCauley TR, Gray ML, Disler DG. What's new in cartilage? *Radiographics* 2003; **23**: 1227-1242

21 **Kneeland JB**, Reddy R. Frontiers in musculoskeletal MRI: articular cartilage. *J Magn Reson Imaging* 2007; **25**: 339-344

22 **Wang YX**, Westwood FR, Moores SM, Ball A, Heapy C, Pickford R, Tessier JJ, Bowyer J. In vivo high-resolution three-dimensional magnetic resonance imaging of a rat knee osteoarthritis model induced by meniscal transection. Proceedings of the International Society for Magnetic Resonance in Medicine, Seattle, 2006: No. 3633

23 **Faure P**, Doan BT, Beloeil JC. In-vivo high resolution three-dimensional MRI studies of rat joints at 7 T. *NMR Biomed* 2003; **16**: 484-493

24 **Tessier JJ**, Bowyer J, Brownrigg NJ, Peers IS, Westwood FR, Waterton JC, Maciewicz RA. Characterisation of the guinea pig model of osteoarthritis by in vivo three-dimensional magnetic resonance imaging. *Osteoarthritis Cartilage* 2003; **11**: 845-853

25 **Eckstein F**, Mosher T, Hunter D. Imaging of knee osteoarthritis: data beyond the beauty. *Curr Opin Rheumatol* 2007; **19**: 435-443

26 **Gray ML**, Burstein D. Molecular (and functional) imaging of articular cartilage. *J Musculoskelet Neuronal Interact* 2004; **4**: 365-368

27 **Roos EM**, Dahlberg L. Positive effects of moderate exercise on glycosaminoglycan content in knee cartilage: a four-month, randomized, controlled trial in patients at risk of osteoarthritis. *Arthritis Rheum* 2005; **52**: 3507-3514

28 **Link TM**, Stahl R, Woertler K. Cartilage imaging: motivation, techniques, current and future significance. *Eur Radiol* 2007; **17**: 1135-1146

29 **Creamer P**. Osteoarthritis pain and its treatment. *Curr Opin Rheumatol* 2000; **12**: 450-455

30 **Mazzuca SA**, Brandt KD, Lane KA, Katz BP. Knee pain reduces joint space width in conventional standing anteroposterior radiographs of osteoarthritic knees. *Arthritis Rheum* 2002; **46**: 1223-1227

31 **Amin S**, LaValley MP, Guermazi A, Grigoryan M, Hunter DJ, Clancy M, Niu J, Gale DR, Felson DT. The relationship between cartilage loss on magnetic resonance imaging and radiographic progression in men and women with knee osteoarthritis. *Arthritis Rheum* 2005; **52**: 3152-3159

32 **Recht MP**, Goodwin DW, Winalski CS, White LM. MRI of articular cartilage: revisiting current status and future directions. *AJR Am J Roentgenol* 2005; **185**: 899-914

33 **Lee KY**, Masi JN, Sell CA, Schier R, Link TM, Steinbach LS, Safran M, Ma B, Majumdar S. Computer-aided quantification of focal cartilage lesions using MRI: accuracy and initial arthroscopic comparison. *Osteoarthritis Cartilage* 2005; **13**: 728-737

34 **Bredella MA**, Tirman PF, Peterfy CG, Zarlingo M, Feller JF, Bost FW, Belzer JP, Wischer TK, Genant HK. Accuracy of T2-weighted fast spin-echo MR imaging with fat saturation in detecting cartilage defects in the knee: comparison with arthroscopy in 130 patients. *AJR Am J Roentgenol* 1999; **172**: 1073-1080

35 **McGibbon CA**, Trahan CA. Measurement accuracy of focal cartilage defects from MRI and correlation of MRI graded lesions with histology: a preliminary study. *Osteoarthritis Cartilage* 2003; **11**: 483-493

36 **Graichen H**, Al-Shamari D, Hinterwimmer S, von Eisenhart-Rothe R, Vogl T, Eckstein F. Accuracy of quantitative magnetic

resonance imaging in the detection of ex vivo focal cartilage defects. *Ann Rheum Dis* 2005; **64**: 1120-1125
37 **Drapé JL**, Pessis E, Auleley GR, Chevrot A, Dougados M, Ayral X. Quantitative MR imaging evaluation of chondropathy in osteoarthritic knees. *Radiology* 1998; **208**: 49-55
38 **Disler DG**, McCauley TR, Kelman CG, Fuchs MD, Ratner LM, Wirth CR, Hospodar PP. Fat-suppressed three-dimensional spoiled gradient-echo MR imaging of hyaline cartilage defects in the knee: comparison with standard MR imaging and arthroscopy. *AJR Am J Roentgenol* 1996; **167**: 127-132
39 **Peterfy CG**, Guermazi A, Zaim S, Tirman PF, Miaux Y, White D, Kothari M, Lu Y, Fye K, Zhao S, Genant HK. Whole-Organ Magnetic Resonance Imaging Score (WORMS) of the knee in osteoarthritis. *Osteoarthritis Cartilage* 2004; **12**: 177-190
40 **Conaghan PG**, Hunter D, Tennant A, Amin S, Clancy M, Guermazi A, Peterfy C, Genant H, Felson DT. Evaluation an MRI scoring system for osteoarthritis of the knee using modern psychometric approaches. *Osteoarthritis Cartilage* 2004; **12** (Suppl B): S119-S120
41 **Kornaat PR**, Ceulemans RY, Kroon HM, Riyazi N, Kloppenburg M, Carter WO, Woodworth TG, Bloem JL. MRI assessment of knee osteoarthritis: Knee Osteoarthritis Scoring System (KOSS)--inter-observer and intra-observer reproducibility of a compartment-based scoring system. *Skeletal Radiol* 2005; **34**: 95-102
42 **Hunter DJ**, Lo GH, Gale D, Grainger AJ, Guermazi A, Conaghan PG. The reliability of a new scoring system for knee osteoarthritis MRI and the validity of bone marrow lesion assessment: BLOKS (Boston Leeds Osteoarthritis Knee Score). *Ann Rheum Dis* 2008; **67**: 206-211
43 **Eckstein F**, Cicuttini F, Raynauld JP, Waterton JC, Peterfy C. Magnetic resonance imaging (MRI) of articular cartilage in knee osteoarthritis (OA): morphological assessment. *Osteoarthritis Cartilage* 2006; **14** Suppl A: A46-A75
44 **Hunter DJ**, Conaghan PG, Peterfy CG, Bloch D, Guermazi A, Woodworth T, Stevens R, Genant HK. Responsiveness, effect size, and smallest detectable difference of Magnetic Resonance Imaging in knee osteoarthritis. *Osteoarthritis Cartilage* 2006; **14** Suppl A: A112-A115
45 **Hunter DJ**, Niu JB, Zhang Y, LaValley M, McLennan CE, Hudelmaier M, Eckstein F, Felson DT. Premorbid knee osteoarthritis is not characterised by diffuse thinness: the Framingham Osteoarthritis Study. *Ann Rheum Dis* 2008; **67**: 1545-1549
46 **Eckstein F**, Heudorfer L, Faber SC, Burgkart R, Englmeier KH, Reiser M. Long-term and resegmentation precision of quantitative cartilage MR imaging (qMRI). Osteoarthritis *Cartilage* 2002; **10**: 922-928
47 **Hudelmaier M**, Glaser C, Englmeier KH, Reiser M, Putz R, Eckstein F. Correlation of knee-joint cartilage morphology with muscle cross-sectional areas vs. anthropometric variables. *Anat Rec A Discov Mol Cell Evol Biol* 2003; **270**: 175-184
48 **Hanna F**, Ebeling PR, Wang Y, O'Sullivan R, Davis S, Wluka AE, Cicuttini FM. Factors influencing longitudinal change in knee cartilage volume measured from magnetic resonance imaging in healthy men. Ann Rheum Dis 2005; **64**: 1038-1042
49 **Maroudas A**, Bullough P. Permeability of articular cartilage. *Nature* 1968; **219**: 1260-1261
50 **Mow V**, Setton L. Mechanical properties of normal and osteoarthritis articular cartilage. In: Brandt K, Doherty M, Lohmander LS, editors. Osteoarthritis. New York: Oxford Medical Publications, 1998: 108-122
51 **Kshirsagar AA**, Watson PJ, Tyler JA, Hall LD. Measurement of localized cartilage volume and thickness of human knee joints by computer analysis of three-dimensional magnetic resonance images. *Invest Radiol* 1998; **33**: 289-299
52 **Koo S**, Gold GE, Andriacchi TP. Considerations in measuring cartilage thickness using MRI: factors influencing reproducibility and accuracy. *Osteoarthritis Cartilage* 2005; **13**: 782-789
53 **Burgkart R**, Glaser C, Hinterwimmer S, Hudelmaier M, Englmeier KH, Reiser M, Eckstein F. Feasibility of T and Z scores from magnetic resonance imaging data for quantification of cartilage loss in osteoarthritis. *Arthritis Rheum* 2003; **48**: 2829-2835
54 **Wang Y**, Wluka AE, Cicuttini FM. The determinants of change in tibial plateau bone area in osteoarthritic knees: a cohort study. *Arthritis Res Ther* 2005; **7**: R687-R693
55 **Edinger DT**, Hayashi K, Hongyu Y, Markel MD, Manley PA. Histomorphometric analysis of the proximal portion of the femur in dogs with osteoarthritis. *Am J Vet Res* 2000; **61**: 1267-1272
56 **Calvo E**, Palacios I, Delgado E, Ruiz-Cabello J, Hernández P, Sánchez-Pernaute O, Egido J, Herrero-Beaumont G. High-resolution MRI detects cartilage swelling at the early stages of experimental osteoarthritis. *Osteoarthritis Cartilage* 2001; **9**: 463-472
57 **Wang HH**, Wang YX, Griffith JF, Sun YL, Zhang G, Chan CW, Qin L, Ahuja AT, Teng LS. Pitfalls in interpreting rat knee joint magnetic resonance images and their histological correlation. *Acta Radiol* 2009; **50**: 1042-1048
58 **Kawahara Y**, Uetani M, Nakahara N, Doiguchi Y, Nishiguchi M, Futagawa S, Kinoshita Y, Hayashi K. Fast spin-echo MR of the articular cartilage in the osteoarthrotic knee. Correlation of MR and arthroscopic findings. *Acta Radiol* 1998; **39**: 120-125
59 **Yoshioka H**, Stevens K, Hargreaves BA, Steines D, Genovese M, Dillingham MF, Winalski CS, Lang P. Magnetic resonance imaging of articular cartilage of the knee: comparison between fat-suppressed three-dimensional SPGR imaging, fat-suppressed FSE imaging, and fat-suppressed three-dimensional DEFT imaging, and correlation with arthroscopy. *J Magn Reson Imaging* 2004; **20**: 857-864
60 **Ding C**, Garnero P, Cicuttini F, Scott F, Cooley H, Jones G. Knee cartilage defects: association with early radiographic osteoarthritis, decreased cartilage volume, increased joint surface area and type II collagen breakdown. *Osteoarthritis Cartilage* 2005; **13**: 198-205
61 **Ding C**, Cicuttini F, Scott F, Cooley H, Jones G. Knee structural alteration and BMI: a cross-sectional study. *Obes Res* 2005; **13**: 350-361
62 **Hunter DJ**, March L, Sambrook PN. The association of cartilage volume with knee pain. *Osteoarthritis Cartilage* 2003; **11**: 725-729
63 **Wluka AE**, Wolfe R, Stuckey S, Cicuttini FM. How does tibial cartilage volume relate to symptoms in subjects with knee osteoarthritis? *Ann Rheum Dis* 2004; **63**: 264-268
64 **Wang YX**, Heapy C, Pickford R, Tessier JJ, Ball A, Holmes A, Read SJ. MRI structural changes and joint discomfort: an investigation in the mono-iodoacetate induced arthritis model in rats. Proceedings of the European Society for Magnetic Resonance in Medicine and Biology, Basle, 2005: No. 283
65 **Tessier J**, Bowyer J, Heapy C, Elliott J, Pickford R, Flannelly J, Maciewicz R. Doxycycline Slows MRI-Assessed Cartilage Volume Loss in the Guinea Pig Model of Osteoarthritis. Proceedings of the International Society for Magnetic Resonance in Medicine, Seattle, 2006: No. 61
66 **Berthiaume MJ**, Raynauld JP, Martel-Pelletier J, Labonté F, Beaudoin G, Bloch DA, Choquette D, Haraoui B, Altman RD, Hochberg M, Meyer JM, Cline GA, Pelletier JP. Meniscal tear and extrusion are strongly associated with progression of symptomatic knee osteoarthritis as assessed by quantitative magnetic resonance imaging. *Ann Rheum Dis* 2005; **64**: 556-563

S- Editor Cheng JX **L- Editor** Webster JR **E- Editor** Zheng XM

World Journal of Radiology

Online Submissions: http://www.wjgnet.com/1949-8470office
wjr@wjgnet.com
www.wjgnet.com

World J Radiol 2010 January 28; 2(1): I
ISSN 1949-8470 (online)

Acknowledgments to reviewers of *World Journal of Radiology*

Many reviewers have contributed their expertise and time to the peer review, a critical process to ensure the quality of *World Journal of Radiology*. The editors and authors of the articles submitted to the journal are grateful to the following reviewers for evaluating the articles (including those published in this issue and those rejected for this issue) during the last editing time period.

Herwig R Cerwenka, MD, Professor, Department of Surgery, Medical University of Graz, Auenbruggerplatz 29, A-8036 Graz, Austria

Patrick M Colletti, MD, Professor of Radiology and Medicine, Director Nuclear Medicine Fellowship, USC Keck School of Medicine, Professor of Biokinesiology, Professor of Pharmacology and Pharmaceutical Sciences, Chief of MRI, LAC+USC Imaging Science Center, University of Southern California, 1200 N State Street Room 3566, Los Angeles, CA 90033, United States

Juebin Huang, MD, PhD, Assistant Professor, Department of Neurology, The University of Mississippi Medical Center, 2500 N. State Street, Jackson, MS 39216, United States

Yasunori Minami, MD, PhD, Division of Gastroenterology and Hepatology, Department of Internal Medicine, 377-2 Ohno-higashi Osaka-sayama Osaka 589-8511, Japan

Yahya Paksoy, MD, Professor, Department of Radiology, Selcuk University Meram Chool of Medicine, 42085 Konya, Turkey

Jai Soung Park, MD, PhD, Professor, Department of Radiology, Soonchunhyang University Buchen Hospital, 1174 jung-dong, Wonmi-gu, Bucheon, Gyeonggi-do 420-767, South Korea

Georgios A Plataniotis, MD, PhD, Clinical Oncologist, Department of Oncology, Aberdeen Royal Infirmary, Foresterhill, Aberdeen, AB25 2ZN, United Kingdom

AAK Abdel Razek, MD, Professor, Diagnostic Radiology Department, 62 El Nokri St, Meet Hadr, Mansoura Faculty of Medicine, Mansoura, Egypt

Djordjije Saranovic, MD, PhD, Professor, Department of Digestive Radiology (First Surgical Clinic), Institute of Radiology, Clinical Center of Serbia, Koste Todorovica 6, 11000 Belgrade, Serbia

Lars Victor Baron von Engelhardt, MD, Department of Orthopedic and Trauma Surgery, St. Josef Hospital - Ruhr-University Bochum, Gudrunstrasse 56, 44791 Bochum, Germany

Hui-Xiong Xu, MD, PhD, Professor, Department of Medical Ultrasonics, Institute of Diagnostic and Interventional Ultrasound, Sun Yat-Sen University, 58 Zhongshan Road 2, Guangzhou 510080, Guangdong Province, China

World Journal of Radiology

Online Submissions: http://www.wjgnet.com/1949-8470office
wjr@wjgnet.com
www.wjgnet.com

World J Radiol 2010 January 28; 2(1): I
ISSN 1949-8470 (online)

Meetings

Events Calendar 2010

January 4-8
Beaver Creek, Colorado, United States
18th Annual Winter Diagnostic Imaging Update

January 7-9
Leuven, Belgium
4th Leuven Course on Ear Imaging

January 16-17
Hollywood, Florida, United States
The Symposium on Clinical Interventional Oncology

January 17-21
Hollywood, Florida, United States
The International Symposium on Endovascular Therapy

January 21-22
Cairo, Egypt
BGICC Breast Gyne International Cancer Conference

January 21-24
Phoenix, AZ, United States
13th Society for Cardiovascular Magnetic Resonance (SCMR) Annual Scientific Sessions

January 23-23
Atlanta, GA, United States
Emory Winship Cancer Institute: Breast Cancer 2010: Advances in Science, Emerging Data, and Novel Therapeutics

January 25-29
Maui, HI, United States
Musculoskeletal & Neuroradiology MR Imaging Update in Maui

January 27-February 2
Albuquerque, NM, United States
2010 SNM Conjoint Mid-Winter Meetings

January 29-30
Barcelona, Spain
7th European Congress: Perspectives in Gynecologic Oncology

February 7-12
Vail, CO, United States
15th Annual Vail 2010: Multislice CT in Clinical Practice

February 11-13
Las Vegas, NV, United States
5th Annual Symposium on PET/CT and Molecular Imaging

February 16-19
Park City, UT, United States
6th Interventional/ Neurointerventional Conference

February 18-19
London, United Kingdom
Diagnostic and Interventional Radiology

February 18-21
Las Vegas, NV, United States
American Society of Spine Radiology Annual Symposium

February 20-20
Jacksonville, Florida, United States
Mayo Clinic Molecular Markers and Management of Breast Cancer

February 20-21
Bethesda, Maryland, United States
25th Anniversary Washington Neuroradiology Review

February 21-26
Orlando, FL, United States
The Abdominal Radiology Course

February 21-27
Snowmass, CO, United States
16th Annual Snowmass 2010: Clinical Ultrasound

February 22-26
Bethesda, MD, United States
48th Annual Dr. Kenneth M. Earle Memorial Neuropathology Review

February 24-27
Lake Buena Vista, FL, United States
ACRO 2010 American College of Radiation Oncology Symposium: Clinical Radiation Oncology Challenges

February 25-27
Chandler, AZ, United States
Multidisciplinary Head and Neck Cancer Symposium

February 26-27
Brussels, Belgium
10èmes Mises au Point en Imagerie Ostéo-Articulaire

February 27-March 1
Cairo, Egypt
7th Gastroenterology Hepatology & Endoscopy Symposium

February 28-March 4
Scottsdale, AZ, United States
International Congress XXIII on Endovascular Interventions

February 28-March 5
Breckenridge, CO, United States
5th Annual Breckenridge 2010: Musculoskeletal MRI

March 3-6
Las Vegas, Nevada, United States
11th Annual Advances in Breast Imaging and Interventions

March 4-8
Vienna, Austria
European Congress of Radiology (ECR 2010) Annual Meeting

March 5-7
Mt Tremblant, QC, Canada
Neuroimaging and Head & Neck Radiology Update in Mt Tremblant

March 7-11
San Diego, CA, United States
SCBT-MR Masters in Body Imaging: "What's New, What's Hot, What You May Not Have Known"

March 10-13
San Antonio, Texas, United States
Clinical Osteoporosis 2010: An ISCD-NOF Symposium

March 11-13
Barcelona, Spain
EORTC Group Meeting: EORTC Radiation Oncology Group

March 11-13
Hannover, Germany
40. Kongress der Deutschen Gesellschaft für Endoskopie und Bildgebende Verfahren e.V.

March 13-18
Tampa, FL, United states
Society of interventional radiology 35th Annual Scientific Meeting

March 14-17
Park City, UT, United States
14th Annual Park City 2010: MRI in Clinical Practice

March 22-26
Beaver Creek, CO, United States
NYU Radiology Spring Skiing Symposium in Beaver Creek

March 22-26
Maui, HI, United States
18th Annual Spring Diagnostic Imaging Update

March 24-27
San Diego, California, United States
2010 American institute of ultrasound in Medicine Annual Convention Preliminary Program

March 24-27
Barcelona, Spain
7th European Breast Cancer Conference

April 8-12
Shanghai, China
The 26th International Congress of Radiology

September 8-12
Guangzhou, China
Chinese Society of Interventional Radiology, 2010 CSIR

November 28-December 03
Chicago, United States
Radiological Society of North America: 2010 Annual Meeting

World Journal of Radiology

Online Submissions: http://www.wjgnet.com/1949-8470office
wjr@wjgnet.com
www.wjgnet.com

World J Radiol 2010 January 28; 2(1): I-V
ISSN 1949-8470 (online)

Instructions to authors

GENERAL INFORMATION

World Journal of Radiology (*World J Radiol*, *WJR*, online ISSN 1949-8470, DOI: 10.4329), is a monthly, open-access (OA), peer-reviewed journal supported by an editorial board of 304 experts in Radiology from 38 countries.

The biggest advantage of the OA model is that it provides free, full-text articles in PDF and other formats for experts and the public without registration, which eliminates the obstacle that traditional journals possess and usually delays the speed of the propagation and communication of scientific research results. The open access model has been proven to be a true approach that may achieve the ultimate goal of the journals, i.e. the maximization of the value to the readers, authors and society.

The role of academic journals is to exhibit the scientific levels of a country, a university, a center, a department, and even a scientist, and build an important bridge for communication between scientists and the public. As we all know, the significance of the publication of scientific articles lies not only in disseminating and communicating innovative scientific achievements and academic views, as well as promoting the application of scientific achievements, but also in formally recognizing the "priority" and "copyright" of innovative achievements published, as well as evaluating research performance and academic levels. So, to realize these desired attributes of *WJR* and create a well-recognized journal, the following four types of personal benefits should be maximized. The maximization of personal benefits refers to the pursuit of the maximum personal benefits in a well-considered optimal manner without violation of the laws, ethical rules and the benefits of others. (1) Maximization of the benefits of editorial board members: The primary task of editorial board members is to give a peer review of an unpublished scientific article *via* online office system to evaluate its innovativeness, scientific and practical values and determine whether it should be published or not. During peer review, editorial board members can also obtain cutting-edge information in that field at first hand. As leaders in their field, they have priority to be invited to write articles and publish commentary articles. We will put peer reviewers' names and affiliations along with the article they reviewed in the journal to acknowledge their contribution; (2) Maximization of the benefits of authors: Since *WJR* is an open-access journal, readers around the world can immediately download and read, free of charge, high-quality, peer-reviewed articles from *WJR* official website, thereby realizing the goals and significance of the communication between authors and peers as well as public reading; (3) Maximization of the benefits of readers: Readers can read or use, free of charge, high-quality peer-reviewed articles without any limits, and cite the arguments, viewpoints, concepts, theories, methods, results, conclusion or facts and data of pertinent literature so as to validate the innovativeness, scientific and practical values of their own research achievements, thus ensuring that their articles have novel arguments or viewpoints, solid evidence and correct conclusion; and (4) Maximization of the benefits of employees: It is an iron law that a first-class journal is unable to exist without first-class editors, and only first-class editors can create a first-class academic journal. We insist on strengthening our team cultivation and construction so that every employee, in an open, fair and transparent environment, could contribute their wisdom to edit and publish high-quality articles, thereby realizing the maximization of the personal benefits of editorial board members, authors and readers, and yielding the greatest social and economic benefits.

The major task of *WJR* is to rapidly report the most recent improvement in the research of medical imaging and radiation therapy by the radiologists. *WJR* accepts papers on the following aspects related to radiology: Abdominal radiology, women health radiology, cardiovascular radiology, chest radiology, genitourinary radiology, neuroradiology, head and neck radiology, interventional radiology, musculoskeletal radiology, molecular imaging, pediatric radiology, experimental radiology, radiological technology, nuclear medicine, PACS and radiology informatics, and ultrasound. We also encourage papers that cover all other areas of radiology as well as basic research.

The columns in the issues of *WJR* will include: (1) Editorial: To introduce and comment on the substantial advance and its importance in the fast-developing areas; (2) Frontier: To review the most representative achievements and comment on the current research status in the important fields, and propose directions for the future research; (3) Topic Highlight: This column consists of three formats, including (A) 10 invited review articles on a hot topic, (B) a commentary on common issues of this hot topic, and (C) a commentary on the 10 individual articles; (4) Observation: To update the development of old and new questions, highlight unsolved problems, and provide strategies on how to solve the questions; (5) Guidelines for Basic Research: To provide Guidelines for basic research; (6) Guidelines for Clinical Practice: To provide guidelines for clinical diagnosis and treatment; (7) Review: To systemically review the most representative progress and unsolved problems in the major scientific disciplines, comment on the current research status, and make suggestions on the future work; (8) Original Articles: To originally report the innovative and valuable findings in radiology; (9) Brief Articles: To briefly report the novel and innovative findings in radiology; (10) Case Report: To report a rare or typical case; (11) Letters to the Editor: To discuss and make reply to the contributions published in *WJR*, or to introduce and comment on a controversial issue of general interest; (12) Book Reviews: To introduce and comment on quality monographs of radiology; and (13) Guidelines: To introduce Consensuses and Guidelines reached by international and national academic authorities worldwide on the research in radiology.

CSSN
ISSN 1949-8470 (online)

Published by
Beijing Baishideng BioMed Scientific Co., Ltd.

SUBMISSION OF MANUSCRIPTS

Manuscripts should be typed in 1.5 line spacing and 12 pt. Book Antiqua with ample margins. Number all pages consecutively, and start each of the following sections on a new page: Title Page, Abstract, Introduction, Materials and Methods, Results, Discussion, Acknowledgements, References, Tables, Figures, and Figure Legends. Neither the editors nor the publisher are responsible for the opinions expressed by contributors. Manuscripts formally accepted for publication become the permanent property of Beijing Baishideng BioMed Scientifc Co., Ltd., and may not be reproduced by any means, in whole or in part, without the written permission of both the authors and the publisher. We reserve the right to copy-edit and put onto our website accepted manuscripts. Authors should follow the relevant guidelines for the care and use of laboratory animals of their institution or national animal welfare committee. For the sake of transparency in regard to the performance and reporting of clinical trials, we endorse the policy of the International Committee of Medical Journal Editors to refuse to publish papers on clinical trial results if the trial was not recorded in a publicly-accessible registry at its outset. The only register now available, to our knowledge, is http://www. clinicaltrials.gov sponsored by the United States National Library of Medicine and we encourage all potential contributors to register with it. However, in the case that other registers become available you will be duly notified. A letter of recommendation from each author's organization should be provided with the contributed article to ensure the privacy and secrecy of research is protected.

Authors should retain one copy of the text, tables, photographs and illustrations because rejected manuscripts will not be returned to the author(s) and the editors will not be responsible for loss or damage to photographs and illustrations sustained during mailing.

Online submissions

Manuscripts should be submitted through the Online Submission System at: http://www.wjgnet.com/1949-8470office. Authors are highly recommended to consult the ONLINE INSTRUCTIONS TO AUTHORS (http://www.wjgnet.com/1949-8470/index.htm) before attempting to submit online. For assistance, authors encountering problems with the Online Submission System may send an email describing the problem to wjr@wjgnet.com, or by telephone: +86-10-59080036. If you submit your manuscript online, do not make a postal contribution. Repeated online submission for the same manuscript is strictly prohibited.

MANUSCRIPT PREPARATION

All contributions should be written in English. All articles must be submitted using word-processing software. All submissions must be typed in 1.5 line spacing and 12 pt. Book Antiqua with ample margins. Style should conform to our house format. Required information for each of the manuscript sections is as follows:

Title page

Title: Title should be less than 12 words.

Running title: A short running title of less than 6 words should be provided.

Authorship: Authorship credit should be in accordance with the standard proposed by International Committee of Medical Journal Editors, based on (1) substantial contributions to conception and design, acquisition of data, or analysis and interpretation of data; (2) drafting the article or revising it critically for important intellectual content; and (3) final approval of the version to be published. Authors should meet conditions 1, 2, and 3.

Institution: Author names should be given first, then the complete name of institution, city, province and postcode. For example, Xu-Chen Zhang, Li-Xin Mei, Department of Pathology, Chengde Medical College, Chengde 067000, Hebei Province, China. One author may be represented from two institutions, for example, George Sgourakis, Department of General, Visceral, and Transplantation Surgery, Essen 45122, Germany; George Sgourakis, 2nd Surgical Department, Korgialenio-Benakio Red Cross Hospital, Athens 15451, Greece

Author contributions: The format of this section should be: Author contributions: Wang CL and Liang L contributed equally to this work; Wang CL, Liang L, Fu JF, Zou CC, Hong F and Wu XM designed the research; Wang CL, Zou CC, Hong F and Wu XM performed the research; Xue JZ and Lu JR contributed new reagents/analytic tools; Wang CL, Liang L and Fu JF analyzed the data; and Wang CL, Liang L and Fu JF wrote the paper.

Supportive foundations: The complete name and number of supportive foundations should be provided, e.g., Supported by National Natural Science Foundation of China, No. 30224801

Correspondence to: Only one corresponding address should be provided. Author names should be given first, then author title, affiliation, the complete name of institution, city, postcode, province, country, and email. All the letters in the email should be in lower case. A space interval should be inserted between country name and email address. For example, Montgomery Bissell, MD, Professor of Medicine, Chief, Liver Center, Gastroenterology Division, University of California, Box 0538, San Francisco, CA 94143, United States. montgomery.bissell@ucsf.edu

Telephone and fax: Telephone and fax should consist of +, country number, district number and telephone or fax number, e.g., Telephone: +86-10-59080039 Fax: +86-10-85381893

Peer reviewers: All articles received are subject to peer review. Normally, three experts are invited for each article. Decision for acceptance is made only when at least two experts recommend an article for publication. Reviewers for accepted manuscripts are acknowledged in each manuscript, and reviewers of articles which were not accepted will be acknowledged at the end of each issue. To ensure the quality of the articles published in *WJR*, reviewers of accepted manuscripts will be announced by publishing the name, title/position and institution of the reviewer in the footnote accompanying the printed article. For example, reviewers: Professor Jing-Yuan Fang, Shanghai Institute of Digestive Disease, Shanghai, Affiliated Renji Hospital, Medical Faculty, Shanghai Jiaotong University, Shanghai, China; Professor Xin-Wei Han, Department of Radiology, The First Affiliated Hospital, Zhengzhou University, Zhengzhou, Henan Province, China; and Professor Anren Kuang, Department of Nuclear Medicine, Huaxi Hospital, Sichuan University, Chengdu, Sichuan Province, China.

Abstract
There are unstructured abstracts (no more than 256 words) and structured abstracts (no more than 480). The specific requirements for structured abstracts are as follows:

An informative, structured abstracts of no more than 480 words should accompany each manuscript. Abstracts for original contributions should be structured into the following sections. AIM (no more than 20 words): Only the purpose should be included. Please write the aim as the form of "To investigate/study/…; MATERIALS AND METHODS (no more than 140 words); RESULTS (no more than 294 words): You should present *P* values where appropriate and must provide relevant data to illustrate how they were obtained, e.g. 6.92 ± 3.86 *vs* 3.61 ± 1.67, $P < 0.001$; CONCLUSION (no more than 26 words). Available from: http://www.wjgnet.com/wjg/help/8.doc

Key words
Please list 5-10 key words, selected mainly from *Index Medicus*, which reflect the content of the study.

Text
For articles of these sections, original articles, rapid communication and case reports, the main text should be structured into the following sections: INTRODUCTION, MATERIALS AND METHODS, RESULTS and DISCUSSION, and should include appropriate Figures and Tables. Data should be presented in the main text or in Figures and Tables, but not in both. The main text format of these sections, editorial, topic highlight, case report, letters to the editors, can be found at: http://www.wjgnet.com/wjg/help/instructions.jsp.

Illustrations
Figures should be numbered as 1, 2, 3, *etc.*, and mentioned clearly in the main text. Provide a brief title for each figure on a separate page. Detailed legends should not be provided under the figures. This part should be added into the text where the figures are applicable. Figures should be either Photoshop or Illustrator files (in tiff, eps, jpeg formats) at high-resolution. Examples can be found at: http://www.wjgnet.com/1007-9327/13/4520.pdf; http://www.wjgnet.com/1007-9327/13/4554.pdf; http://www.wjgnet.com/1007-9327/13/4891.pdf; http://www.wjgnet.com/1007-9327/13/4986.pdf; http://www.wjgnet.com/1007-9327/13/4498.pdf. Keeping all elements compiled is necessary in line-art image. Scale bars should be used rather than magnification factors, with the length of the bar defined in the legend rather than on the bar itself. File names should identify the figure and panel. Avoid layering type directly over shaded or textured areas. Please use uniform legends for the same subjects. For example: Figure 1 Pathological changes in atrophic gastritis after treatment. A: ...; B: ...; C: ...; D: ...; E: ...; F: ...; G: …*etc.* It is our principle to publish high resolution-figures for the printed and E-versions.

Tables
Three-line tables should be numbered 1, 2, 3, *etc.*, and mentioned clearly in the main text. Provide a brief title for each table. Detailed legends should not be included under tables, but rather added into the text where applicable. The information should complement, but not duplicate the text. Use one horizontal line under the title, a second under column heads, and a third below the Table, above any footnotes. Vertical and italic lines should be omitted.

Notes in tables and illustrations
Data that are not statistically significant should not be noted. $^{a}P < 0.05$, $^{b}P < 0.01$ should be noted ($P > 0.05$ should not be noted). If there are other series of *P* values, $^{c}P < 0.05$ and $^{d}P < 0.01$ are used. A third series of *P* values can be expressed as $^{e}P < 0.05$ and $^{f}P < 0.01$. Other notes in tables or under illustrations should be expressed as ^{1}F, ^{2}F, ^{3}F; or sometimes as other symbols with a superscript (Arabic numerals) in the upper left corner. In a multi-curve illustration, each curve should be labeled with ●, ○, ■, □, ▲, △, *etc.*, in a certain sequence.

Acknowledgments
Brief acknowledgments of persons who have made genuine contributions to the manuscript and who endorse the data and conclusions should be included. Authors are responsible for obtaining written permission to use any copyrighted text and/or illustrations.

REFERENCES
Coding system
The author should number the references in Arabic numerals according to the citation order in the text. Put reference numbers in square brackets in superscript at the end of citation content or after the cited author's name. For citation content which is part of the narration, the coding number and square brackets should be typeset normally. For example, "Crohn's disease (CD) is associated with increased intestinal permeability[1,2]". If references are cited directly in the text, they should be put together within the text, for example, "From references[19,22-24], we know that..."

When the authors write the references, please ensure that the order in text is the same as in the references section, and also ensure the spelling accuracy of the first author's name. Do not list the same citation twice.

PMID and DOI
Pleased provide PubMed citation numbers to the reference list, e.g. PMID and DOI, which can be found at http://www.ncbi.nlm.nih.gov/sites/entrez?db=pubmed and http://www.crossref.org/SimpleTextQuery/, respectively. The numbers will be used in E-version of this journal.

Style for journal references
Authors: the name of the first author should be typed in bold-faced letters. The family name of all authors should be typed with the initial letter capitalized, followed by their abbreviated first and middle initials. (For example, Lian-Sheng Ma is abbreviated as Ma LS, Bo-Rong Pan as Pan BR). The title of the cited article and italicized journal title (journal title should be in its abbreviated form as shown in PubMed), publication date, volume number (in black), start page, and end page [PMID: 11819634 DOI: 10.3748/wjg.13.5396].

Style for book references
Authors: the name of the first author should be typed in bold-faced letters. The surname of all authors should be typed with the initial letter capitalized, followed by their abbreviated middle and first initials. (For example, Lian-Sheng Ma is abbreviated as Ma LS, Bo-Rong Pan as Pan BR) Book title. Publication number. Publication place: Publication press, Year: start page and end page.

Format

Journals

English journal article (list all authors and include the PMID where applicable)

1 **Jung EM**, Clevert DA, Schreyer AG, Schmitt S, Rennert J, Kubale R, Feuerbach S, Jung F. Evaluation of quantitative contrast harmonic imaging to assess malignancy of liver tumors: A prospective controlled two-center study. *World J Gastroenterol* 2007; **13**: 6356-6364 [PMID: 18081224 DOI: 10.3748/wjg.13.6356]

Chinese journal article (list all authors and include the PMID where applicable)

2 **Lin GZ**, Wang XZ, Wang P, Lin J, Yang FD. Immunologic effect of Jianpi Yishen decoction in treatment of Pixu-diarrhoea. *Shijie Huaren Xiaohua Zazhi* 1999; **7**: 285-287

In press

3 **Tian D**, Araki H, Stahl E, Bergelson J, Kreitman M. Signature of balancing selection in Arabidopsis. *Proc Natl Acad Sci USA* 2006; In press

Organization as author

4 **Diabetes Prevention Program Research Group**. Hypertension, insulin, and proinsulin in participants with impaired glucose tolerance. *Hypertension* 2002; **40**: 679-686 [PMID: 12411462 PMCID:2516377 DOI:10.1161/01.HYP.0000035706.28494.09]

Both personal authors and an organization as author

5 **Vallancien G**, Emberton M, Harving N, van Moorselaar RJ; Alf-One Study Group. Sexual dysfunction in 1, 274 European men suffering from lower urinary tract symptoms. *J Urol* 2003; **169**: 2257-2261 [PMID: 12771764 DOI:10.1097/01.ju.0000067940.76090.73]

No author given

6 21st century heart solution may have a sting in the tail. *BMJ* 2002; **325**: 184 [PMID: 12142303 DOI:10.1136/bmj.325.7357.184]

Volume with supplement

7 **Geraud G**, Spierings EL, Keywood C. Tolerability and safety of frovatriptan with short- and long-term use for treatment of migraine and in comparison with sumatriptan. *Headache* 2002; **42** Suppl 2: S93-99 [PMID: 12028325 DOI:10.1046/j.1526-4610.42.s2.7.x]

Issue with no volume

8 **Banit DM**, Kaufer H, Hartford JM. Intraoperative frozen section analysis in revision total joint arthroplasty. *Clin Orthop Relat Res* 2002; (**401**): 230-238 [PMID: 12151900 DOI:10.1097/00003086-200208000-00026]

No volume or issue

9 Outreach: Bringing HIV-positive individuals into care. *HRSA Careaction* 2002; 1-6 [PMID: 12154804]

Books

Personal author(s)

10 **Sherlock S**, Dooley J. Diseases of the liver and billiary system. 9th ed. Oxford: Blackwell Sci Pub, 1993: 258-296

Chapter in a book (list all authors)

11 **Lam SK**. Academic investigator's perspectives of medical treatment for peptic ulcer. In: Swabb EA, Azabo S. Ulcer disease: investigation and basis for therapy. New York: Marcel Dekker, 1991: 431-450

Author(s) and editor(s)

12 **Breedlove GK**, Schorfheide AM. Adolescent pregnancy. 2nd ed. Wieczorek RR, editor. White Plains (NY): March of Dimes Education Services, 2001: 20-34

Conference proceedings

13 **Harnden P**, Joffe JK, Jones WG, editors. Germ cell tumours V. Proceedings of the 5th Germ cell tumours Conference; 2001 Sep 13-15; Leeds, UK. New York: Springer, 2002: 30-56

Conference paper

14 **Christensen S**, Oppacher F. An analysis of Koza's computational effort statistic for genetic programming. In: Foster JA, Lutton E, Miller J, Ryan C, Tettamanzi AG, editors. Genetic programming. EuroGP 2002: Proceedings of the 5th European Conference on Genetic Programming; 2002 Apr 3-5; Kinsdale, Ireland. Berlin: Springer, 2002: 182-191

Electronic journal (list all authors)

15 Morse SS. Factors in the emergence of infectious diseases. Emerg Infect Dis serial online, 1995-01-03, cited 1996-06-05; 1(1): 24 screens. Available from: URL: http//www.cdc.gov/ncidod/EID/eid.htm

Patent (list all authors)

16 **Pagedas AC**, inventor; Ancel Surgical R&D Inc., assignee. Flexible endoscopic grasping and cutting device and positioning tool assembly. United States patent US 20020103498. 2002 Aug 1

Statistical data

Write as mean ± SD or mean ± SE.

Statistical expression

Express *t* test as *t* (in italics), *F* test as *F* (in italics), chi square test as χ^2 (in Greek), related coefficient as *r* (in italics), degree of freedom as υ (in Greek), sample number as *n* (in italics), and probability as *P* (in italics).

Units

Use SI units. For example: body mass, m (B) = 78 kg; blood pressure, p (B) = 16.2/12.3 kPa; incubation time, t (incubation) = 96 h, blood glucose concentration, c (glucose) 6.4 ± 2.1 mmol/L; blood CEA mass concentration, p (CEA) = 8.6 24.5 μg/L; CO_2 volume fraction, 50 mL/L CO_2, not 5% CO_2; likewise for 40 g/L formaldehyde, not 10% formalin; and mass fraction, 8 ng/g, *etc.* Arabic numerals such as 23, 243, 641 should be read 23 243 641.

The format for how to accurately write common units and quantums can be found at: http://www.wjgnet.com/wjg/help/15.doc.

Abbreviations

Standard abbreviations should be defined in the abstract and on first mention in the text. In general, terms should not be abbreviated unless they are used repeatedly and the abbreviation is helpful to the reader. Permissible abbreviations are listed in Units, Symbols and Abbreviations: A Guide for Biological and Medical Editors and Authors (Ed. Baron DN, 1988) published by The Royal Society of Medicine, London. Certain commonly used abbreviations, such as DNA, RNA, HIV, LD50, PCR, HBV, ECG, WBC, RBC, CT, ESR, CSF, IgG, ELISA, PBS, ATP, EDTA, mAb, can be used directly without further explanation.

Italics

Quantities: *t* time or temperature, *c* concentration, *A* area, *l* length, *m* mass, *V* volume.

Genotypes: *gyrA*, *arg* 1, *c myc*, *c fos*, *etc.*

Restriction enzymes: *Eco*RI, *Hin*dI, *Bam*HI, *Kbo* I, *Kpn* I, *etc.*
Biology: *H. pylori*, *E coli*, *etc.*

RE-SUBMISSION OF THE REVISED PAPER

Please revise your article according to the revision policies of *WJR*. The revised version including manuscript and high-resolution image figures (if any) should be re-submitted or uploaded online. The author should send copyright transfer letter, and responses to the reviewers and science news to us *via* email.

Editorial Office

World Journal of Radiology

Editorial Department: Room 903, Building D,
Ocean International Center,
No. 62 Dongsihuan Zhonglu,
Chaoyang District, Beijing 100025, China
E-mail: wjr@wjgnet.com
http://www.wjgnet.com
Telephone: +86-10-59080036
Fax: +86-10-85381893

Language evaluation

The language of a manuscript will be graded before it is sent for revision. (1) Grade A: priority publishing; (2) Grade B: minor language polishing; (3) Grade C: a great deal of language polishing needed; and (4) Grade D: rejected. Revised articles should reach Grade A or B.

Copyright assignment form

Please download a Copyright assignment form from http://www.wjgnet.com/1007-9327/news/10.doc.

Responses to reviewers

Please revise your article according to the comments/suggestions provided by the reviewers. The format for responses to the reviewers' comments can be found at: http://www.wjgnet.com/1007-9327/news/12.doc.

Proof of financial support

For paper supported by a foundation, authors should provide a copy of the document and serial number of the foundation.

Science news releases

Authors of accepted manuscripts are suggested to write a science news item to promote their articles. The news will be released rapidly at EurekAlert/AAAS (http://www.eurekalert.org). The title for news items should be less than 90 characters; the summary should be less than 75 words; and main body less than 500 words. Science news items should be lawful, ethical, and strictly based on your original content with an attractive title and interesting pictures.

Publication fee

Authors of accepted articles must pay a publication fee.
EDITORIAL, TOPIC HIGHLIGHTS, BOOK REVIEWS and LETTERS TO THE EDITOR are published free of charge.